

System Modeling, Graphical User Interface Development, and Sensors Testing for the Mars Oxygen In-Situ Resource Utilization Experiment (MOXIE)

Presented By

Eric Daniel Hinterman

B.S. Chemical Engineering
University of Notre Dame, 2013

*Submitted to the Department of Aeronautics and Astronautics
as a fulfillment of the requirement for a Master's Degree in Aeronautics and Astronautics
at the
Massachusetts Institute of Technology*

June 2018

© 2018 Massachusetts Institute of Technology. All rights reserved.


Signature redacted

Signature of the Author _____

Eric D. Hinterman
Graduate Student
Department of Aeronautics and Astronautics

Signature redacted

Signature of Faculty Advisor _____

 Jeffrey A. Hoffman
Professor of the Practice
Department of Aeronautics and Astronautics

Signature redacted

Signature of Graduate Chair _____

Hamsa Balakrishnan
Associate Professor of Aeronautics and Astronautics
Chair, Graduate Program Committee



System Modeling, Graphical User Interface Development, and Sensors Testing for the Mars Oxygen In-Situ Resource Utilization Experiment (MOXIE)

Presented By
Eric Daniel Hinterman

*Submitted to the Department of Aeronautics and Astronautics
on May 18, 2019 in partial fulfillment of the
requirements for the Degree of Master of Science in
Aeronautics and Astronautics*

Abstract

The Mars Oxygen In-Situ Resource Utilization Experiment (MOXIE) represents the first time that NASA is demonstrating In-Situ Resource Utilization (ISRU) on the surface of another planetary body. MOXIE will produce oxygen from atmospheric CO₂ on Mars. It is being developed for NASA's 2020 Mars Rover and will produce greater than 99.6% pure oxygen through solid oxide electrolysis. MOXIE is roughly 0.5% of the scale that would be necessary to produce oxygen for breathing and use as a propellant for a human Mars mission.

Tests are being performed on MOXIE in the laboratory at NASA's Jet Propulsion Laboratory (JPL) and the Massachusetts Institute of Technology (MIT). At the same time, a model is being developed to simulate and predict the performance of MOXIE. The ability to predict the performance of MOXIE on Mars is a critical step in preparation for surface operations. Without the ability to estimate inefficient or unsafe operating conditions, MOXIE operations on Mars run a spectrum of risk ranging from loss of efficiency to the loss of the entire mission. Therefore, to predict performance and thus avoid subjecting flight hardware to unsafe conditions, a dynamic model has been developed that simulates MOXIE's operation. Simulink, a package contained within the MATLAB programming language, was chosen as a convenient way to build a dynamic representation of MOXIE. The model was built as a combination of theoretical and empirical values regarding the gas flows, thermal transfers, electrochemistry, and control loops that are representative of the true MOXIE system. The results of this model have been validated against data from JPL's MOXIE testbed laboratory. Continued model validation will occur as JPL acquires new data throughout 2018.

This thesis gives an overview of how MOXIE works and how it has been modeled. MOXIE is the first instrument of its kind to leave the Earth, and the modeling of this instrument is similarly unique. As the dynamic model continues to evolve with new data, it becomes a fast and inexpensive way to test MOXIE without subjecting expensive hardware to hazardous conditions. In addition, this thesis covers the development of a Graphical User Interface (GUI) that allows users to easily control the model and view its outputs. Finally, the design and results of construction of a vacuum chamber for testing of MOXIE components are presented. These tests will help to further validate the model and will pave the way for extensibility studies of the MOXIE system.

Thesis Supervisor: Jeffrey Hoffman
Title: Professor of the Practice, Aeronautics and Astronautics

Acknowledgements

I am very fortunate for the support I have received over the course of the past two years. My career goal is to become the Director of Mars Missions for Human Spaceflight, and working on an actual instrument that is going to Mars to pave the way for human exploration has been a dream come true. I owe a lot to the people that made this possible, and I would like to take a moment to acknowledge them.

First, I would like to thank my advisor, Professor Jeff Hoffman, for bringing me to MIT to work on MOXIE. I hope that I haven't made you question your decision too many times. You have been exactly the type of advisor I would have hoped for. Thank you for the guidance you have given me in my research, the advice you have provided me with for life, and the trust you put in me to manage my time effectively and get my work done. I wish every graduate student could have the advisor experience that I have been fortunate enough to receive with you.

Thank you to the MOXIE Principle Investigator, Mike Hecht, for providing me with additional direction in my research. I hope to have many more productive years serving under your leadership.

Thank you to the folks at JPL that have helped me during my time in Pasadena and from afar in Cambridge. This includes my internship supervisor and mentor at JPL, Carl Guernsey. Also, thanks to Jeff Mellstrom, Gerald Voecks, and Richard Kidd for their support and time.

Thank you to Forrest Meyen for the mentorship and material he provided me during the transition between our times on MOXIE.

Thank you to Marianne Gonzalez and Piyush Khopkar for all the work they have done with me on the modeling and GUI development.

Thank you to my UROP, Maya Nasr, who has played a central role in the latter half of the research covered in this thesis. We will continue to work together as she begins her graduate studies here at MIT next year.

My parents have listened to my progress and continuously encouraged me throughout my studies. They are the reason I was able to attend MIT and realize my passion. Thank you for doing what you do.

Thank you to my fiancée, Maria, for joining me on this adventure. Your support has driven me to accomplish more and I couldn't have done it without you.

I would also like to thank my funding sources. This includes NASA for supporting me with the NASA Space Technology Research Fellowship, the Aero/Astro department, and the MOXIE team. MOXIE is supported by three NASA directorates: the Human Exploration and Operations Mission Directorate (HEOMD), the Space Technology Mission Directorate (STMD), and the Science Mission Directorate (SMD).

Table of Contents

ABSTRACT.....	3
ACKNOWLEDGEMENTS	5
LIST OF FIGURES.....	9
LIST OF TABLES.....	10
CHAPTER 1: INTRODUCTION	11
1.1 MARS EXPLORATION OVERVIEW	11
1.2 IN-SITU RESOURCE UTILIZATION.....	12
1.2.1 MARS ISRU.....	12
1.3 MOXIE	13
1.3.1 SYSTEM OVERVIEW.....	15
1.3.2 COMPRESSOR SYSTEM.....	16
1.3.3 SOXE.....	17
CHAPTER 2: SYSTEM MODEL CONSOLIDATION AND IMPROVEMENT	21
2.1 ESTABLISHING THE NEED FOR A SINGLE MODEL.....	21
2.2 INTEGRATING THE STRENGTHS OF EACH INTO A SINGLE, CENTRALIZED MODEL	21
2.2.1 SOXE ELECTROCHEMISTRY EQUATIONS.....	21
2.2.1.1 THE NERNST POTENTIAL.....	22
2.2.1.2 THE ACTIVATION POTENTIAL	23
2.2.1.3 THE INTRINSIC ASR.....	24
2.2.1.4 INTEGRATING THE ELECTROCHEMISTRY EQUATIONS INTO THE MODEL.....	25
2.2.2 THERMAL MODEL.....	25
2.3 VALIDATING THE OUTPUTS AND UPDATING THE MODEL WITH GREY FACTORS	26
2.3.1 MODELING RESULTS.....	26
2.3.2 VALIDATING THE OUTPUTS WITH DATA	28
2.3.3 ADDING GREY FACTORS TO UPDATE THE MODEL	30
2.4 NEW UPDATES TO THE MODEL.....	30
2.4.1 ELECTRICAL LOOP.....	30
2.4.2 THERMAL LOOP UPDATES.....	32
2.4.3 HEATER CONTROLLER.....	38
2.4.5 PRESSURE CONTROLLER.....	42
2.5 FAULT DETECTION.....	43
CHAPTER 3: GRAPHICAL USER INTERFACE (GUI).....	47
3.1 MOTIVATION.....	47

3.2 MICROSOFT EXCEL DESIGN	47
3.3 MATLAB APP DEVELOPER DESIGN	48
3.4 GUI INPUT PARAMETERS.....	51
3.4.1 MARS PARAMETERS	51
3.4.2 MOXIE AND SOXE PARAMETERS.....	53
3.4.3 ADDITIONAL INPUTS.....	53
3.5 GUI OUTPUTS.....	54
3.6 GUI EXTRAS	55
3.7 RUN CONTROL TABLE.....	56
3.8 GUI IMPLEMENTATION WITH THE MOXIE TEAM	57
CHAPTER 4: VACUUM CHAMBER DESIGN AND DEVELOPMENT	59
4.1 THE NEED FOR VACUUM CHAMBERS	59
4.2 SENSORS VACUUM CHAMBER DESIGN.....	59
4.3 FLAT-SAT AND EM VACUUM CHAMBER DESIGN	64
4.4 VACUUM CHAMBER FACILITIES DESIGN	65
CHAPTER 5: SENSORS	67
5.1 INTRODUCTION TO THE SENSORS.....	67
5.1.1 ANODE AND CATHODE COMPOSITION SENSORS	68
5.1.2 IR AND LUMINESCENCE SENSORS	68
5.2 MOTIVATION FOR CHARACTERIZATION AND CALIBRATION	69
5.2.1 MODIFIED BEER'S LAW.....	70
5.2.2 CALIBRATION.....	71
5.2.3 CHARACTERIZATION.....	71
5.3 METHODS	72
5.3.1 STANDARD OPERATION PROCEDURE.....	72
5.3.2 EXPERIMENTAL TESTING PLAN.....	75
5.4 PATH FORWARD	78
REFERENCES	79

List of Figures

FIGURE 1: MARS 2020 ROVER	14
FIGURE 2: MOXIE SCHEMATIC	15
FIGURE 3: MOXIE CONFIGURATION	16
FIGURE 4: SCROLL COMPRESSOR SECTIONAL VIEW. CREDIT: JPL	17
FIGURE 5: INLET HEPA FILTER ASSEMBLY. CREDIT: JPL	17
FIGURE 6: SCHEMATIC OF SOXE CELL AND THE CHEMICAL REACTION THAT IT DRIVES	18
FIGURE 7: MOLECULAR STRUCTURE OF CO ₂	18
FIGURE 8: VISUALIZED STRUCTURE OF CO ₂	18
FIGURE 9: CO ₂ DISSOCIATION INTO CO AND O ⁻	19
FIGURE 10: SOXE STACK EXPLODED VIEW	19
FIGURE 11: STACKED VIEW OF SOXE	20
FIGURE 12: DEMONSTRATION OF ACTIVATION POTENTIAL. THE ACTIVATION POTENTIAL, OR "ADDITIONAL POTENTIAL", IS THE DIFFERENCE IN THE OPEN-CIRCUIT VOLTAGE (OCV) AND THE VALUE OF THE EXTRAPOLATED LINE AT ZERO CURRENT DENSITY. THE EXTRAPOLATED LINE RESULTS FROM A LINEAR BEST FIT OF THE DATA POINTS RECORDED AT VARIOUS CURRENT DENSITIES.	23
FIGURE 13: SIMULINK EQUATIONS TO REPRESENT INTRINSIC ASR (TOP BOX), ACTIVATION POTENTIAL (MIDDLE BOX), AND NERNST POTENTIAL (BOTTOM BOX) FOR EACH SOXE CELL IN MOXIE.	25
FIGURE 14: SECTION OF SIMULINK THERMAL LOOP THAT REPRESENTS THE HEAT CONDUCTION AROUND CELL #1 IN THE SOXE STACK	26
FIGURE 15: RELATIONSHIP BETWEEN OXYGEN PARTIAL PRESSURE (LEFT) AND NERNST POTENTIAL (RIGHT)	27
FIGURE 16: SIMULATED (LEFT) AND EXPERIMENTAL (RIGHT) RESULTS COMPARED FOR SOXE TEMPERATURES	28
FIGURE 17: SIMULATED (LEFT) AND EXPERIMENTAL (RIGHT) RESULTS COMPARED FOR STACK CURRENT	28
FIGURE 18: DEMONSTRATION OF THE SIMULINK BLOCK USED TO ADD NOISE INTO THE CURRENT CONTROL LOOPS OF THE MOXIE DYNAMIC MODEL	29
FIGURE 19: SIMULATED (LEFT) AND EXPERIMENTAL (RIGHT) RESULTS COMPARED FOR STACK HEATERS	29
FIGURE 20: SIMSCAPE ELECTRICAL LOOP OF MOXIE	31
FIGURE 21: SIMSCAPE ELECTRICAL LOOP OF CELL 10 AND CELL 9 IN SOXE	32
FIGURE 22: CONSOLIDATED THERMAL MODEL	34
FIGURE 23: CONSOLIDATED VIEW OF DETAILED THERMAL MODEL	34
FIGURE 24: HEAT CALCULATIONS FOR CELL 1, REPRESENTING THE EXO- OR ENDO-THERMIC PROPERTIES OF THE ELECTROCHEMICAL REACTION.	35
FIGURE 25: THERMAL PI CONTROLLER	35
FIGURE 26: ALTERNATIVE THERMAL MODEL. INCLUDES RAMP FUNCTION TO SIMULATE TEMPERATURE RISE OF SOXE AND TEN INDIVIDUAL GAINS TO ALTER EACH CELL'S TEMPERATURE TO MATCH DATA.	36
FIGURE 27: RESULTS OF SOXE TEMPERATURE RAMP-UP WITH ALTERNATE THERMAL MODEL	37
FIGURE 28: JSA-003 SOXE PACKAGING TEST 8 DATA FROM JPL REPRESENTING TEMPERATURE OF THE SOXE STACK OVER TIME	38
FIGURE 29: EXPLODED VIEW OF SOXE STACK	39
FIGURE 30: CONTROLLER FOR BOTTOM HEATER, WITH TEMPERATURE INPUT, PI CONTROLLER, CONVERSION TO DN, AND HEATER COMMAND OUTPUT.	39
FIGURE 31: CURRENT CONTROLLER FOR TOP STACK. THE CONTROLLER FOR THE BOTTOM STACK IS IDENTICAL.	40
FIGURE 32: DETAILED EXPLANATION OF INPUTS TO CURRENT CONTROL SYSTEM	40
FIGURE 33: DETAILED EXPLANATION OF SWITCHES IN CURRENT CONTROL SYSTEM	41
FIGURE 34: DETAILED EXPLANATION OF ALL COMPONENTS OF FLIGHT SEGMENT IN THE CURRENT CONTROL SYSTEM	41
FIGURE 35: PRESSURE CONTROL SYSTEM	42
FIGURE 36: FAULT DETECTION SYSTEM FOR P2 SENSOR	45
FIGURE 37: LEVEL 0 VIEW OF THE CONSOLIDATED, DYNAMIC MODEL OF MOXIE. NOTICE ITS COMPLEXITY AND PERCEIVED DIFFICULTY OF USE.	47
FIGURE 38: ORIGINAL MOXIE GUI DESIGN IN MICROSOFT EXCEL	48
FIGURE 39: GRAPHICAL USER INTERFACE (GUI) THAT CONTROLS THE MOXIE DYNAMIC SIMULINK MODEL IN AN EASY-TO-USE FORMAT	49
FIGURE 40: GUI INTERFACE AFTER SELECTING INPUTS (ON THE LEFT HALF), RUNNING IT, AND DISPLAYING THE OUTPUTS (ON THE RIGHT HALF)	50
FIGURE 41: PROCESS FLOW OF GUI AND ITS INTERACTIONS WITH THE MATLAB SCRIPT AND ASSOCIATED SIMULINK MODEL.	50

FIGURE 42: SELECTING A LOCATION ON MARS	51
FIGURE 43: DEMONSTRATION OF THE PROCESS USED TO SELECT ATMOSPHERIC CONDITIONS ON MARS	52
FIGURE 44: ADDITIONAL INPUTS INTERFACE FOR CHANGING SECONDARY VARIABLE VALUES	54
FIGURE 45: TOOLBAR OF THE GUI WITH EXTRA USER OPTIONS	55
FIGURE 46: DEMONSTRATION OF THE "HIDE INPUT PARAMETERS" BUTTON	55
FIGURE 47: RUN CONTROL TABLE EXAMPLE FOR MOXIE	56
FIGURE 48: DESIGN OF SENSORS VACUUM CHAMBER	60
FIGURE 49: SENSOR VACUUM CHAMBER INTERNAL DESIGN	61
FIGURE 50: SENSORS VACUUM CHAMBER SETUP WITH VACUUM CHAMBER, PUMP, AND PUMP CONTROLLER VISIBLE. AN INCH RULER IS ADDED FOR SCALE.	62
FIGURE 51: DESIGN OF SENSORS VACUUM CHAMBER LID (TOP-DOWN VIEW)	63
FIGURE 52: TOP VIEW OF SENSORS VACUUM CHAMBER LID WITH BOTH VALVING MANIFOLDS VISIBLE	63
FIGURE 53: ELECTRICAL FEEDTHROUGHS FOR THE SENSORS VACUUM CHAMBER	64
FIGURE 54: INTEGRATED DESIGN WHERE BOTH VACUUM CHAMBERS UTILIZE THE SAME GASES, VACUUM PUMP, AND PUMP CONTROLLER	65
FIGURE 55: TEMPERATURE, PRESSURE, AND COMPOSITION SENSORS OF MOXIE	67
FIGURE 56: ABSORPTION SPECTRA FOR CO AND CO ₂ . SOURCE: HTTP://WEBBOOK.NIST.GOV/CHEMISTRY	69

List of Tables

TABLE 1: FAULT DETECTION LIMITS	43
TABLE 2: REQUIREMENTS FOR SENSOR VACUUM CHAMBER	60
TABLE 3: REQUIREMENTS FOR VACUUM CHAMBER TEST FACILITY	66
TABLE 4: CATHODE TESTING PLAN; COVERS A RANGE OF COMPOSITIONS AND PRESSURES THAT MAY BE SEEN BY THE CATHODE SENSORS ON MOXIE.	77
TABLE 5: CO ₂ AND N ₂ MIX TESTS THAT WILL PROVIDE A CONTROL THAT ENABLES THE QUANTIFICATION CROSS-TALK BETWEEN CO AND CO ₂	78

Chapter 1: Introduction

1.1 Mars Exploration Overview

Mars has fascinated humankind for centuries. Detailed observation of Mars began telescopically with Galileo Galilei in 1610. Over the next century, features such as the polar ice caps and tilt of the planet were documented. It was in the 19th century that the first map of Mars was published, and Percival Lowell mistakenly believed he could see a series of canals constructed on the planet. This gave rise to the widespread imagination of intelligent life on the planet. While the canals were later proven to be nothing more than an illusion, the idea blossomed into the multi-faceted appeal of Mars that we see today; it is a place that has an intriguing past similar to Earth, it may have or have had life, and it is seen by some as a place to settle humankind in the future.

The scientific appeal of Mars can be largely attributed to data returned from the multitude of robotic exploration missions of the planet over the past 55 years. The first successful spacecraft to reach Mars and return data was Mariner 4, which was launched in November of 1964. It conducted a fly-by of Mars and returned 21 photos of the planet to Earth. Mariner 6 and Mariner 7 achieved similar feats later in the decade. By coincidence, all three spacecraft flew over cratered areas of Mars, leading to the false conclusion amongst some scientists that Mars resembles our Moon [1].

In 1971, Mariner 9 became the first spacecraft to orbit another planet. What it found was radically different from that which was expected of the supposedly cratered, Moon-like planet. Mars was engulfed in a planet-wide dust storm. While this obscured the orbiter's vision of the surface, it still was able to see the peaks of what would later be identified as several dormant volcanoes. Mariner 9 also discovered what we know today as Valles Marineris – the largest canyon in the Solar System [2].

The natural progression in a robotic planetary observation system begins with a fly-by mission, followed by an orbiter, a lander, and a rover. NASA moved into the third category of this progression in 1976 when it successfully landed Viking 1 and Viking 2 on the surface. The Viking landers searched for life and studied the surface and local atmosphere of Mars. Other landers since have contributed heavily to our knowledge of the planet. The Phoenix lander, for example, arrived in 2008 and discovered water ice under the surface of Mars [3].

In 1997, the Pathfinder lander and Sojourner rover touched down on Mars, marking humankind's first mobile mission to the planet's surface. Since the success of Sojourner, several rover missions have followed and have been larger and more advanced with each iteration. In 2004, NASA sent twin rovers, Spirit and Opportunity, to the planet. One of their many accomplishments was discovering evidence that water had once flowed on the surface of Mars [4]. In addition, Opportunity continues to explore the planet today, and has driven over 28 miles across the surface. In 2012, humankind's most advanced rover to date landed. The Curiosity rover has contributed a plethora of knowledge to our understanding of Mars, including the detection of methane from the surface [5], identification of areas where water had flowed in the past [6], and discovery of organic compounds [7].

Other countries have also contributed substantially to our understanding of Mars. The Soviet Union had a partial success with its Mars exploration campaign, and India and ESA have both successfully orbited the planet. In addition, the Curiosity rover from NASA has inspired the design for the Mars

2020 rover, which will conduct the first In-Situ Resource Utilization experiment to pave the way for human exploration of the planet.

1.2 In-Situ Resource Utilization

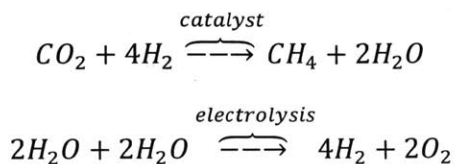
In-Situ Resource Utilization (ISRU), often considered the science of “living off the land”, is a concept that has been growing in momentum with humanity’s push towards developing a space economy and enabling space exploration. ISRU involves the use of technology to convert materials present at the destination site into useful resources. The early settlers of present-day nations used ISRU to construct their villages and survive, as they were often unable to bring everything they needed with them. In the case of space exploration, the resources that are derived from ISRU are useful for life support systems that keep astronauts alive, construction of space structures, generation of propellants, and as energy sources for missions. By obtaining these functionalities with materials found in space, one no longer needs to bring the materials with them from Earth, thus significantly reducing the mass, cost, and risk associated with spaceflight. For these reasons, development of ISRU technology is critical to the enablement of manned missions into the solar system.

1.2.1 Mars ISRU

ISRU for Mars has been a topic under discussion for decades. Analog experiments have been carried out on Earth to test various ISRU strategies for construction of dwellings, use of perchlorates, water purification, and production of oxygen, among others. This thesis will focus on the last-mentioned use, as the current lack of oxygen on Mars is an important barrier that needs to be overcome in order to send humans to Mars.

Many different forms of oxygen production have been studied. Before detailing the method that is explored in this thesis, it is useful to conduct a trade space analysis of previous oxygen-production proposals.

Perhaps the first credible study of Mars ISRU came from the Viking program of the late 1970s. The primary scientific objectives of the Viking missions were to obtain high-resolution images of Mars, characterize its atmospheric and surface composition, and search for life [8]. Using data from the orbiters and landers, scientists and engineers were able to begin exploring concepts for ISRU. Ash et al. focused on the potential to produce rocket propellant on Mars in 1978 [9]. Their findings were that the atmospheric carbon dioxide was the most useful resource, in combination with water, to produce both fuel and oxidizer to propel a Mars Ascent Vehicle off the surface. In order to achieve this goal, they proposed the following methanation reaction, which would produce rocket fuel in the form of methane along with the oxygen needed to combust it:

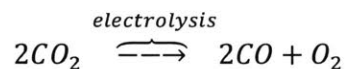


Their drive to produce propellant on Mars, rather than send it from Earth, was based on an analysis done by Hill and Peterson that showed that propellant mass typically represents between 80% and

90% of ascent vehicle mass. [10] When looking at modern launch vehicles, these numbers still hold true and may be even higher due to improvements in materials science and manufacturing processes. For example, the Falcon Heavy from SpaceX has a gross weight of 1.42 million kg and a propellant weight of 1.28 million kg, yielding a propellant percentage of 90.1% [11]. With these numbers in mind, Ash et al. determined that it would be economically advantageous to produce rocket propellant on Mars as opposed to bringing it from Earth. This is the same principle that motivates the MOXIE project.

Ramohalli et al. accepted the above conclusion and expanded on it to lay out a preliminary ISRU framework for a manned mission in 1989 [12]. While a methane-oxygen propellant system was still employed in this architecture, they determined that the methane should be carried from Earth as opposed to being produced on Mars. Instead, only the oxygen would be produced on Mars. This would still represent substantial cost savings, as the majority of rocket propellant in a methane-oxygen system is oxygen but would eliminate some of the complexity of producing methane on the surface.

Robert Zubrin, president of the Mars Society, has also put forth substantial literature that detail various ISRU avenues that one might take when working on Mars. In his book from 1996 “The Case for Mars”, he devotes multiple chapters to defining the specific ISRU that would be beneficial to employ on a manned mission to the planet. He refers to this ISRU as “known and practiced chemical engineering”, saying that all we need to do to land humans on Mars is “present-day technology mixed with some nineteenth-century chemical engineering, a dose of common sense, and a little bit of moxie” [13]. He proposes the same methanation system as Ash et al. [14] to build a methane – oxygen propellant system on Mars from the atmospheric CO₂ and ground-based H₂O. However, Zubrin realized that an additional source of oxygen may be necessary in order to run the MAV engine oxygen-rich, which would increase performance. In order to generate extra oxygen, he proposed using solid oxide electrolysis to drive the following chemical reaction [13]:



This is the very same process that MOXIE will employ in order to produce oxygen on Mars in 2021.

1.3 MOXIE

This thesis focuses on production of oxygen, which is the primary purpose of the Mars Oxygen In-Situ Resource Utilization Experiment (MOXIE). MOXIE is an instrument being developed for NASA’s Mars 2020 rover that will attempt to produce oxygen from the Martian atmosphere when it lands on the red planet in 2021. The Mars atmosphere is an example of a useful resource that can be processed with ISRU technology like MOXIE. It is primarily composed of carbon dioxide, which accounts for 96% of its volume. When converted to oxygen, it can be used as the oxidizer for a Mars Ascent Vehicle (MAV) that will lift astronauts off the surface of Mars to begin their journey back to Earth. In addition, some of the oxygen can be used for breathing and for rover and habitation pressure. For context, an image of the Mars 2020 Rover is shown below.

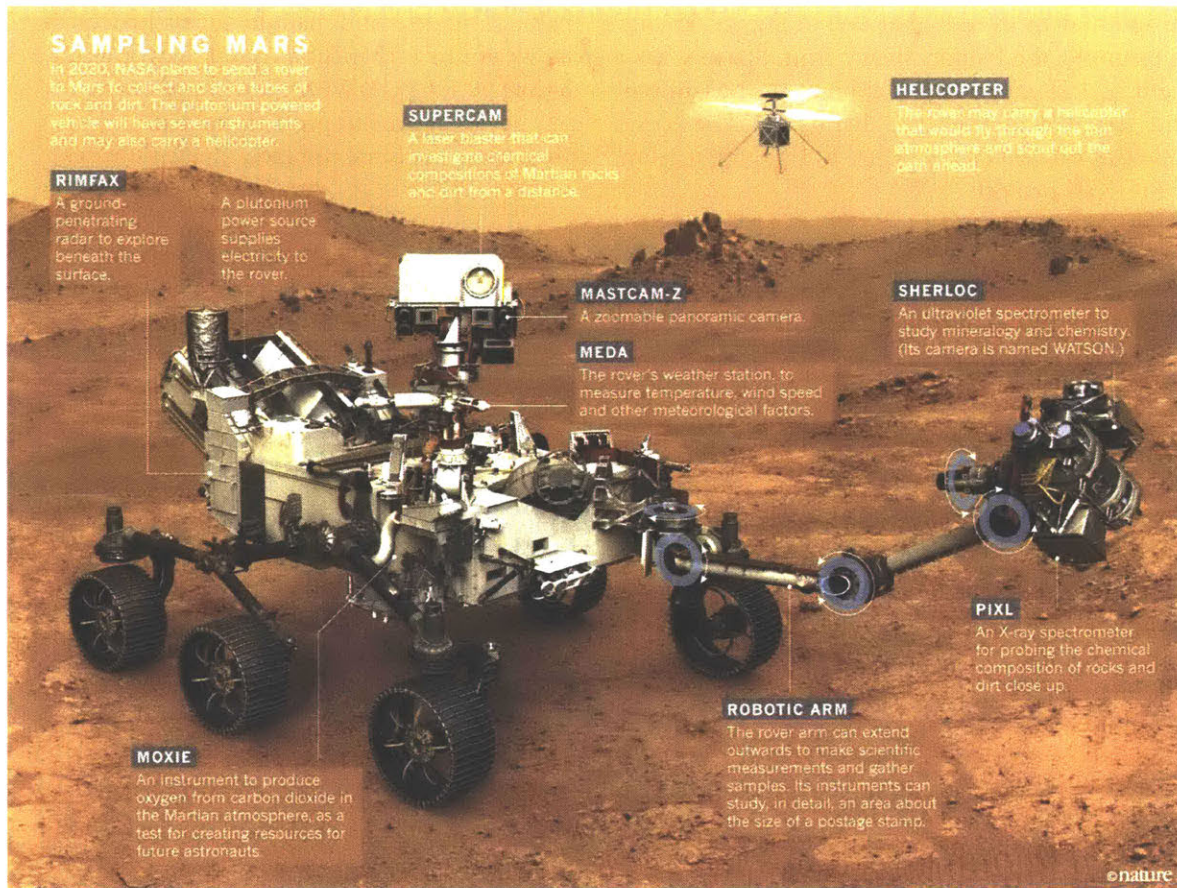


Figure 1: Mars 2020 Rover with payloads labeled. Image credit: NASA.

As Figure 1 shows, there are many payloads being sent onboard the next Mars rover from NASA. These will attempt to tackle a number of science objectives, including the continued study of Martian geology and the search for life. MOXIE, which will attempt to produce oxygen, is shown in greater detail in Figure 2.

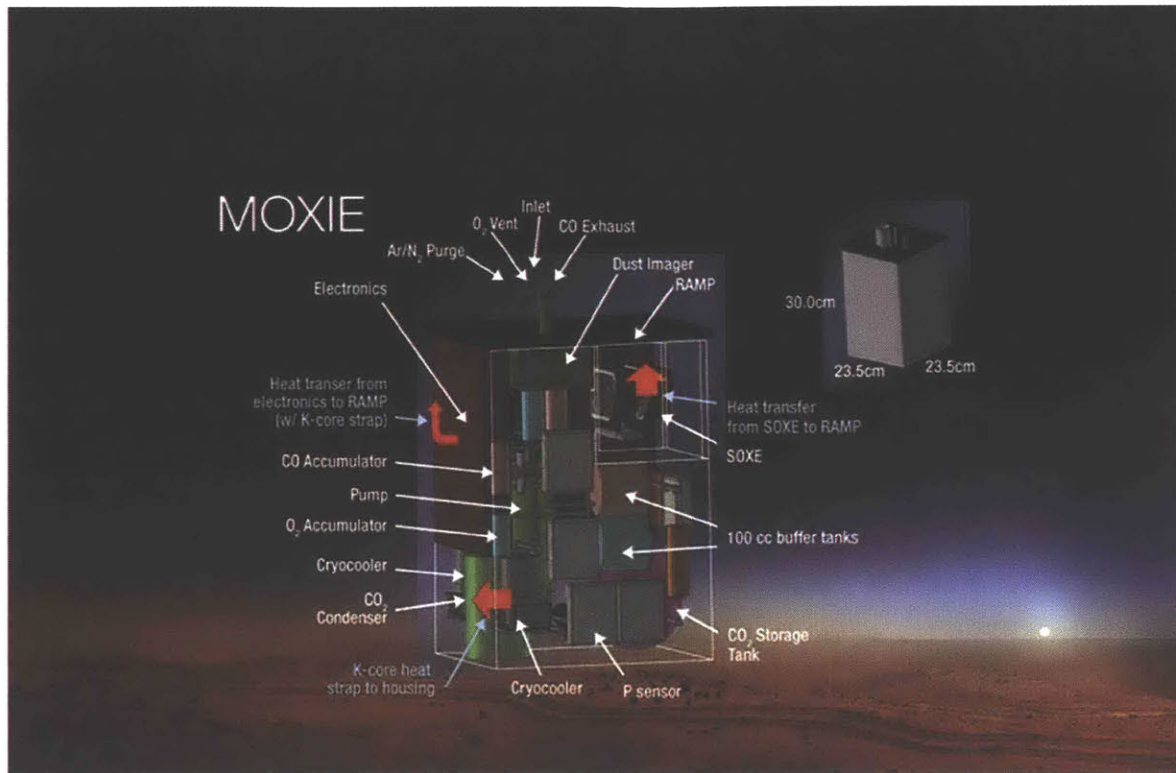


Figure 2: MOXIE Schematic

As you can see, MOXIE itself is a complicated piece of hardware. The following sections will give an overview of MOXIE from a systems level, and then will explore the major components of MOXIE in more detail.

1.3.1 System Overview

MOXIE is primarily composed of three subsystems: the compressor system, the solid oxide electrolysis (SOXE) system, and the process monitoring and control system. These systems, when functioning together, combine to pull in atmospheric gas on Mars, compress it, convert it to oxygen, measure its composition and production rate, and release the products back into the atmosphere. An expanded view of MOXIE is shown below.

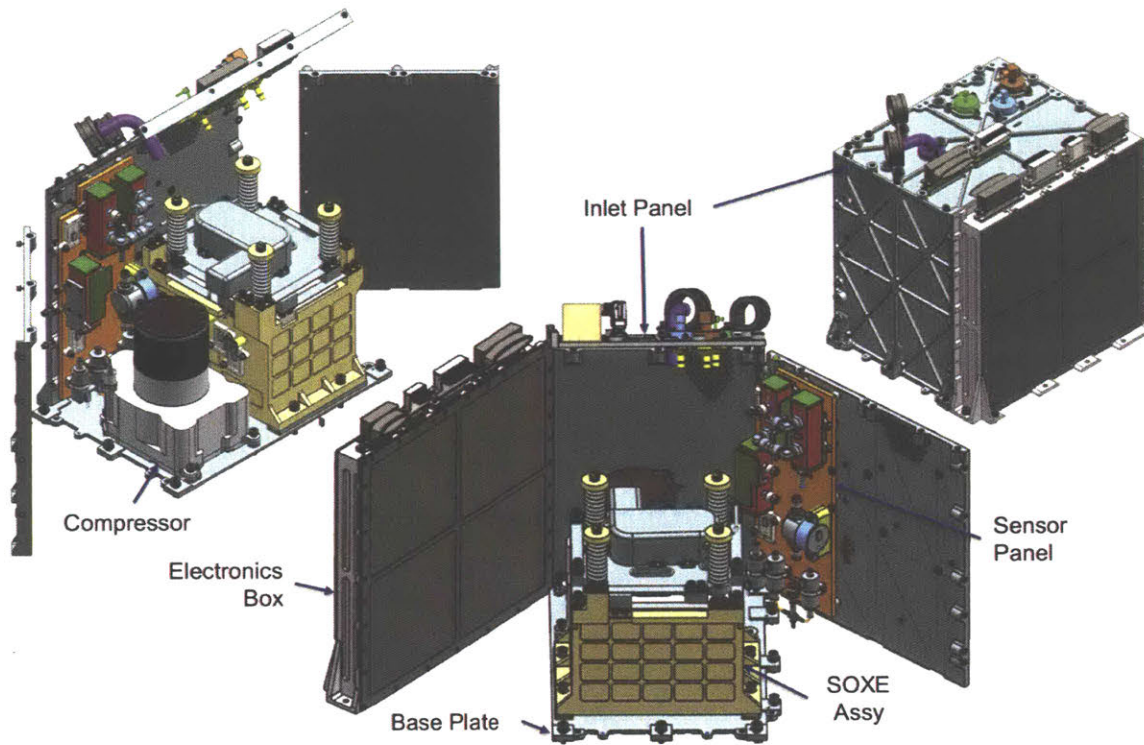


Figure 3: MOXIE Configuration

Figure 3 shows a broken-out view of the MOXIE assembly. The compressor takes up most of one side of the assembly while the SOXE assy takes up the majority of the other side. In addition, the electronics and sensors are fitted on the walls of the box in order to optimize space. When closed up, the MOXIE assembly becomes a comprehensive tool that can acquire, convert, and measure the Mars atmosphere and the resulting oxygen that is produced.

1.3.2 Compressor System

The compressor system acquires and compresses the Martian atmosphere by way of a scroll pump. A scroll pump is composed of two spiral-like structures superimposed on top of one another. In the case of MOXIE, one of the scrolls is fixed while the other orbits within it. This orbiting motion results in small pockets of air being compressed and pumped into the system. A cut-away view of a scroll pump is shown in Figure 4.

The Martian atmosphere is drawn first through a HEPA filter by the scroll compressor in order to remove dust and particulates that could damage the internals of MOXIE. The housing for this is shown in Figure 5. As the atmosphere passes through the scroll pump, it is compressed from around 7 mbar - the ambient pressure on Mars - to 700 mbar. SOXE is designed to operate at 700 mbar, and as such, the majority of testing and characterization work were done at this pressure.

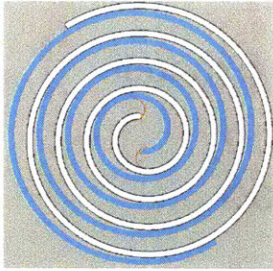


Figure 4: Scroll compressor sectional view. Credit: JPL

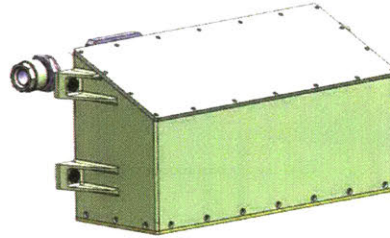


Figure 5: Inlet HEPA filter assembly. Credit: JPL

In addition, the scroll compressor is designed to move around 60 g/hr of gas through the MOXIE system. This occurs when the pump speed is set to roughly 3500 RPM. It was of some concern that pressure oscillations would occur during operation due to the fact that the compressor moves discrete packets of air into the system, one after the other. However, current testing at JPL has demonstrated that the pressure oscillations from the compressor are minimal. The compressor for MOXIE was developed by Air Squared, a company with an extensive background in scroll pumps. While this compressor was developed specifically for MOXIE, scroll pumps in general are well-established in the vacuum and HVAC industries.

1.3.3 SOXE

Solid oxide electrolysis (SOXE) is a heritage chemical engineering technology. It has been used in the nuclear industry, for example, to generate hydrogen gas from water [15]. However, the SOXE used on MOXIE takes a relatively new and unexplored approach: creating oxygen from carbon dioxide without the assistance of water. This is called “dry” electrolysis and has been studied and developed for MOXIE in recent years.

SOXE is the key technology that drives oxygen production in MOXIE. A SOXE cell consists of an Yttria-Stabilized Zirconia (YSZ) electrolyte membrane that is sandwiched between a cathode and an anode. This is shown in more detail in Figure 6.

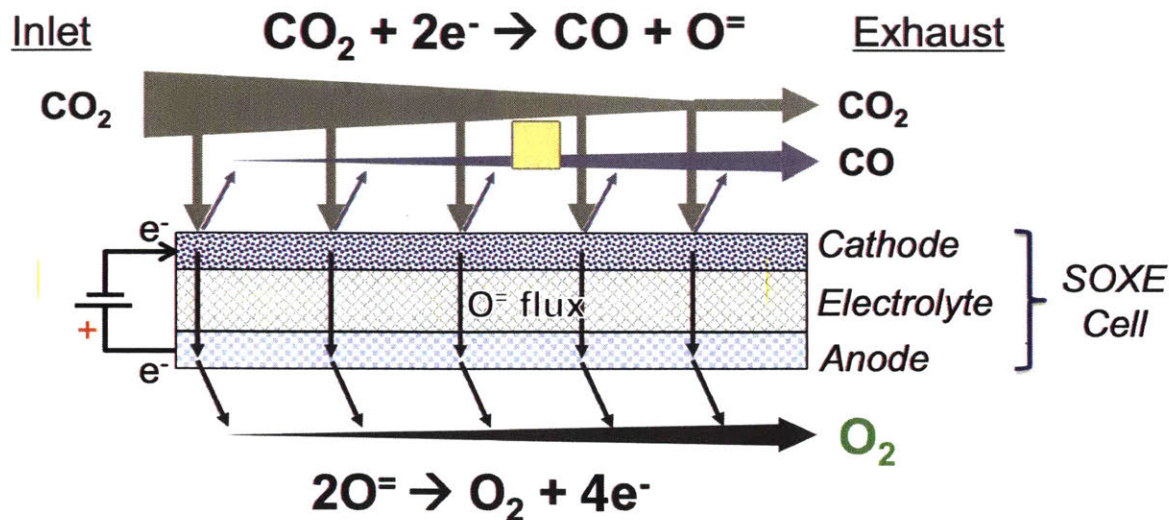
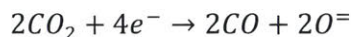


Figure 6: Schematic of SOXE cell and the chemical reaction that it drives

The cathode has a nickel coating that initiates the chemical reaction. Both the cathode and the anode are porous materials that allow diffusion of oxygen ions. Therefore, when a voltage is applied to the electrolyte and carbon dioxide is flowed over the cathode, the following net reaction takes place.



This reaction takes place over the entire surface of the cathode, as demonstrated in Figure 6. In order to better understand the chemistry that occurs, it is necessary to identify the intermediate reactions that lead to the net reaction above. First, as the CO_2 enters the porous cathode, it pulls free electrons from the cathode and is reduced to CO and oxygen ions.



This is easier to visualize if given the molecular structure of CO_2 , shown in two different formats below.



Figure 7: Molecular Structure of CO_2



Figure 8: Visualized Structure of CO_2

The nickel coating on the cathode allows one of the oxygen molecules (but not both) to be separated from its original molecule, thus forming a carbon monoxide (CO) molecule and a free oxygen ion. This is depicted below.

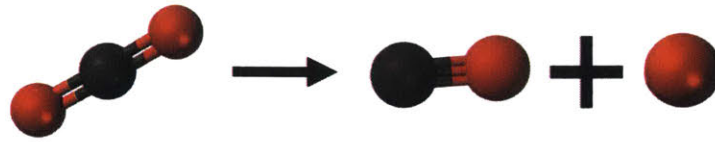
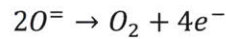


Figure 9: CO₂ dissociation into CO and O-

The carbon monoxide molecule continues to travel along the cathode and is either exhausted or captured on the other side. However, the oxygen ions begin to diffuse through the electrolyte. The anode provides a site for the oxygen ions to reconnect with each other in the following reaction.



As you can see, the net reaction becomes that which was presented earlier. The electrons are recycled back into the SOXE cell system and oxygen is produced on the anode side of the cell. The oxygen in MOXIE is measured and vented to the atmosphere. However, on a scaled-up version of the system, the oxygen would be stored and used for life support systems and rocket propellant.

The SOXE system on MOXIE consists of 10 cells arranged in two stacks of 5 cells. The two stacks are separated by an Inconel interconnect. An exploded view of the SOXE stack is shown in Figure 10, followed by a depiction of the stacked SOXE configuration in Figure 11.

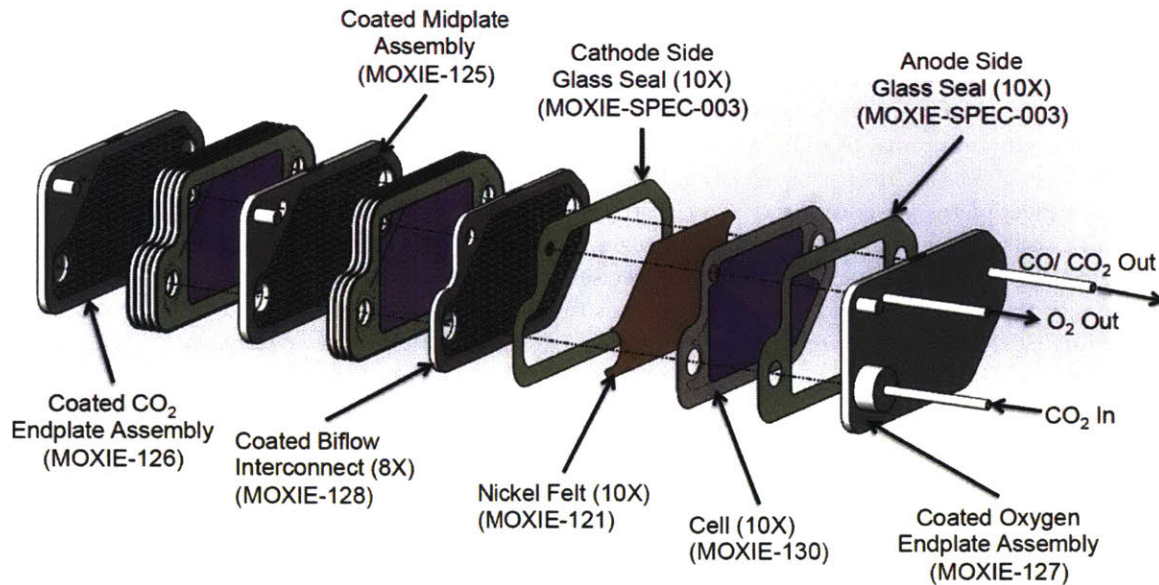


Figure 10: SOXE stack exploded view

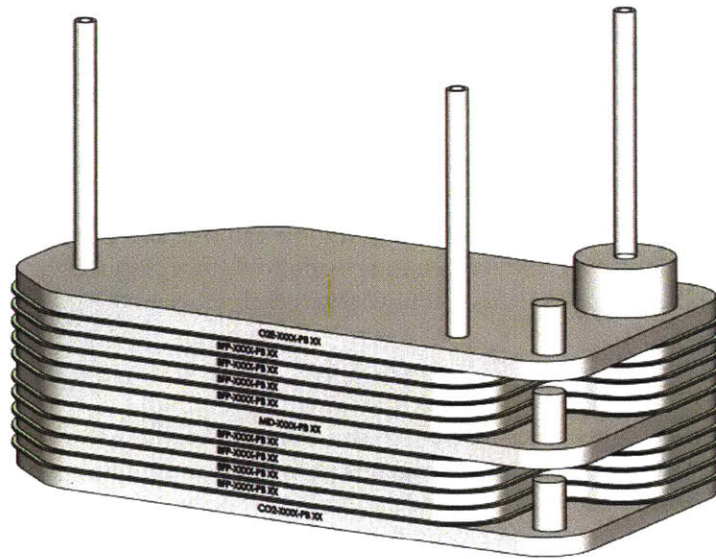


Figure 11: Stacked view of SOXE

Starting from the right side of Figure 10, take note of the endplate assembly that forms the top of the SOXE stack. Underneath the endplate lies the first glass seal, used to separate cells. Directly beneath the glass seal is the first cell, which consists of the anode, YSZ electrolyte, and cathode. As mentioned earlier, the cathode is coated with nickel to enhance the chemical reaction, and so a nickel felt lies beneath the cathode side of each cell. This is separated from the next cell by another glass seal and an interconnect plate. This setup repeats itself five times on each stack, yielding the final 10-cell configuration of SOXE.

The interconnect plates are composed of a chromium-iron-yttrium (CFY) alloy. CFY plates are commonly used as interconnects in fuel cells because – among other beneficial material properties – their coefficient of expansion can be tuned to precisely match that of the electrolyte [16]. This results in uniform expansion and contraction across the SOXE stack, preventing leaks or structural fatigue. Since SOXE cells operate as a fuel cell in reverse, CFY is the primary choice for interconnect material.

It is also important to recognize the gas flow in and out of the SOXE cell as depicted by Figure 10. The CO_2 flows in the top of each stack and follows a tube that allows it to reach every cell in the stack. As the CO_2 passes over each cell in a parallel configuration, it is converted into CO on the cathode and O_2 on the anode. It is neither practical nor advantageous to achieve a 100% conversion of CO_2 into product gases, so the outlet composition of the cathode will be a mixture of CO and unreacted CO_2 . After the CO_2 has passed over each cell, the O_2 and CO/CO_2 reaction products are exhausted through a similar tube on the other end of each cell.

Chapter 2: System Model Consolidation and Improvement

2.1 Establishing the Need for a Single Model

Simulink, a package contained within the MATLAB programming language, is a convenient way to build a dynamic representation of MOXIE. It allows a user to place blocks corresponding to a range of things, including pumps, resistors, PID controllers, and more generically, variables defined in an associated MATLAB file. In addition, Simulink allows connections to be made between these blocks, which can represent electrical cables, thermal contacts, or general passages of information, among others. As such, a time-domain model of MOXIE could be built in Simulink that simulates how MOXIE might operate when turned on.

At the onset of my graduate studies, two such models existed. Forrest Meyen, a former graduate student at MIT, built a model of MOXIE that had great detail about the operation of SOXE and the electrochemistry that goes into it. Marianne Gonzalez, a graduate student at USC and a JPL part-time employee, built a dynamic model that simulated the flow of gas through MOXIE and the process, monitoring, and control (PMC) system controlling it. Where Forrest's model lacked detailed modeling of flow through the system, Marianne's made up for it. Conversely, where Marianne's model lacked the detailed electrochemistry that occurs in SOXE, Forrest's had it. Given the strengths and weaknesses of both models, my goal was to combine them into a single Simulink model that could be used by the entire team.

The research objectives that drove this phase were:

1. Take the strengths of each model and integrate them into a single, centralized Simulink model
2. Validate the outputs of the model with theory and data, and update it accordingly
3. Make the model easy to use, as it is intended to be shared with the MOXIE team

The results of the first two research objectives will be explored in greater detail in the following sections. The latter research objective drove the need for a GUI, which will be addressed in Chapter 3.

2.2 Integrating the Strengths of Each into a Single, Centralized Model

Once the strengths of each model were realized, it was fairly straightforward to integrate the two. The original dynamic model developed by Marianne Gonzalez was chosen to be the platform, and pieces from Forrest Meyen's model were added to it. The reason Marianne's model was chosen is because it provided a better comprehensive view of MOXIE as a system, while Forrest's was very specific and had great detail of SOXE but left out other major components of the MOXIE hardware.

2.2.1 SOXE Electrochemistry Equations

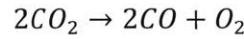
The two major pieces of Forrest's model that were taken and integrated into the dynamic model were the SOXE electrochemistry equations and Simscape thermal model. The electrochemistry in SOXE is driven by the following equation:

$$V_{op} = V_{Nernst} + V_{Act} + I * \frac{ASR_i}{A}$$

where V_{op} is the operating voltage that represents the voltage actually seen by the SOXE cell, V_{Nernst} is the Nernst potential, V_{Act} is the activation voltage, I is the current in the cell, ASR_i is the intrinsic Area Specific Resistance (ASR) of each cell, and A is the area of each cell that is exposed to electrochemistry. In order to understand this equation, and thus its implementation into the dynamic model, each component must first be explained in its own right.

2.2.1.1 The Nernst Potential

The Nernst potential is a quantity that represents the voltage at which a particular electrochemical reaction will take place. For a given set of input parameters (temperature, pressure, and chemical composition), each chemical reaction has its own particular Nernst potential. In order to achieve conversion of carbon dioxide to oxygen, for example, the Nernst potential of the following reaction must be surpassed.



The Nernst potential for this reaction is given by the following equation [17]:

$$V_{Nernst} = \frac{1}{x_{CO,out} - x_{CO,in}} \int_{x_{CO,in}}^{x_{CO,out}} \left(E_0 + \frac{RT}{4F} \ln \left[\frac{(P_c x_{CO})^2 P_{O_2}}{(P_c (1 - x_{CO}))^2} \right] \right) dx_{CO}$$

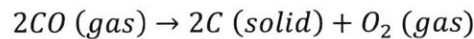
where x is the fraction of CO in the air, $x_{CO,in}$ represents the fraction of CO at the inlet of each SOXE cell, $x_{CO,out}$ represents the fraction of CO at the outlet of each SOXE cell, E_0 is the free energy potential at standard pressure, R is the universal gas constant, T is the operating temperature, F is Faraday's constant, P_c is the operating pressure of the cathode, and P_{O_2} is the partial pressure of oxygen on the anode.

For the operating conditions of MOXIE, which are taken nominally to be 800 °C, 1 bar, and an initial composition of gas equal to that found on Mars, the Nernst potential turns out to be:

$$V_{Nernst} = 0.9208 V$$

for each cell. The key takeaway from this is that if the voltage applied to each cell surpasses 0.9208 V under these conditions, carbon dioxide will begin to decompose into carbon monoxide and oxygen ions. This is what MOXIE aims to do, as its goal is to produce oxygen.

Importantly, there is also a Nernst potential for an unwanted side reaction that can occur in MOXIE: the decomposition of carbon monoxide into solid carbon and oxygen ions. This is shown below:



The ramifications of surpassing the Nernst voltage for this reaction will be explored in further detail later in this chapter. As a summary, this reaction causes solid carbon deposition on the cathode of each SOXE cell, which increases its resistance and ultimately leads to performance-reducing

degradation. Therefore, it is critical that SOXE is operated above the Nernst potential for CO₂ decomposition but below the Nernst potential for CO decomposition. In this way, oxygen will be produced and the cell will not experience significant degradation from carbon deposition.

2.2.1.2 The Activation Potential

The second component of the operating voltage equation is the activation potential. This is a quantity that represents the difference in theoretical open-circuit voltage and that which was seen experimentally. Open-circuit voltage refers to the difference in electrical potential between the cathode and anode when disconnected from the circuit. Another way to describe it is the potential between the terminals when no current is flowing between them. The experimental open-circuit voltage refers to the difference in potentials that would be expected if the data points were extrapolated to zero current density. This extrapolation is shown as the line connecting the data points in Figure 12. The activation potential is shown most clearly during start-up conditions, when the current initially is near zero. After the startup transient has occurred, the effect of activation voltage is masked by other components of the electrical circuit, such as the Nernst potential.

The value of the activation potential varies with temperature and flowrate, but for typical MOXIE conditions, it is roughly 0.4-0.8 V [17]. This is shown more clearly in Figure 12:

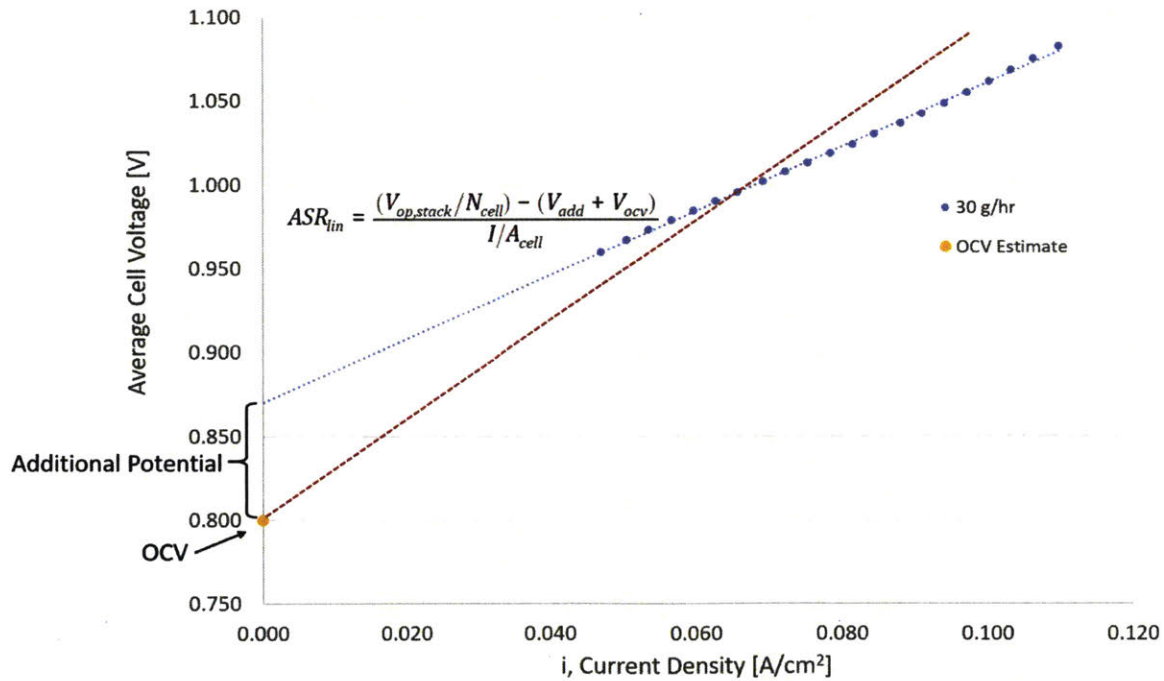


Figure 12: Demonstration of activation potential. The activation potential, or “additional potential”, is the difference in the Open-Circuit Voltage (OCV) and the value of the extrapolated line at zero current density. The extrapolated line results from a linear best fit of the data points recorded at various current densities [17].

where the activation potential is the difference between the open-circuit voltage (OCV) and the intercept of the line drawn using experimental data that measured the current flow for

corresponding voltages across the cell. In this case, where the stack was run at 800 °C and a flowrate of 30 g/hr, the activation potential had a value of roughly 0.07 V per cell.

2.2.1.3 The Intrinsic ASR

Intrinsic ASR represents the slope of the I-V curve after the Nernst Potential has been subtracted from the operating voltage. It is constant across flow rates, which is why it is an important metric to measure. The initial Dynamic Model of MOXIE used a simple linear approximation for Intrinsic ASR that was based solely on an initial ASR value and a rate of ASR change over time. This was changed to the more accurate, temperature-dependent formula for intrinsic ASR. This equation was characterized experimentally at 1073 K [17] and is corrected for temperature by the following equation:

$$ASR_{temp} = \frac{ASR_{Intrinsic@1073K}}{Ae^{-\frac{E_A}{RT}}}$$

where A is the pre-exponential term that represents the intercept of the linear fit of $\ln\left(\frac{k}{k_0}\right)$ vs. $-\frac{1}{T}$ and E_A is the activation energy of the reaction. k is the measured ionic conductivity per unit area in $\frac{S}{cm^2}$ and k_0 is the reference conductivity at 800 °C.

Based on observed data, the activation energy of these SOXE cells is $82.6 \frac{kJ}{mol}$ and the pre-exponential term has a value of 10,300. The baseline intrinsic ASR, measured at 1073 K from CSA 005, is equal to $0.9922 \text{ ohms} - cm^2$ [17].

2.2.1.4 Integrating the Electrochemistry Equations into the Model

Each of the electrochemistry equations described formerly were added into the Simulink model as shown below.

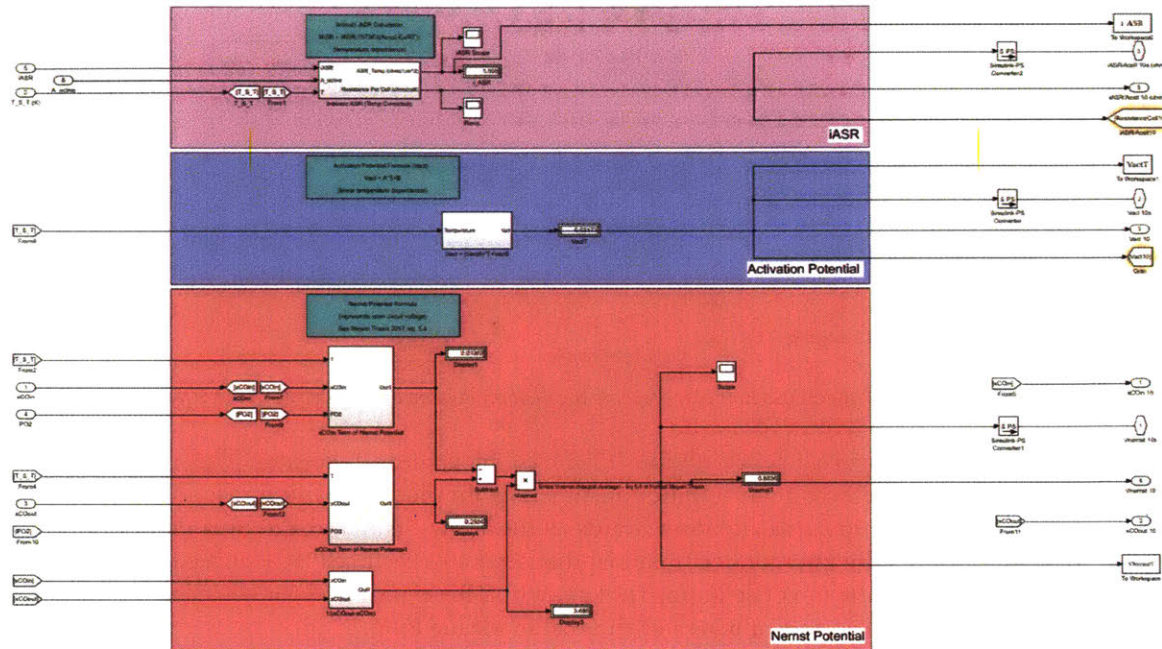


Figure 13: Simulink equations to represent intrinsic ASR (top box), Activation Potential (middle box), and Nernst Potential (bottom box) for each SOXE cell in MOXIE.

The top box contains input variables of a baseline intrinsic ASR value ($iASR$), active area of each SOXE cell (A_{active}), and temperature of the cell (T_{S_T}), the latter of which changes dynamically with time. These inputs are used to calculate the temperature-corrected intrinsic ASR value as described earlier, which is output on the right side of the top box. The activation potential and Nernst potential boxes have additional inputs that are used in their own calculations, and similar outputs on the right side of the figure. These values are all controlled for individual SOXE cells in the model, allowing for detailed investigation as to how each cell within the SOXE stacks performs over time. This is useful in determining the effects of degradation in the stacks and how to run at optimal oxygen-production conditions.

2.2.2 Thermal Model

In addition to the electrochemistry equations, the framework of the thermal loop in the MIT Simulink model was added. Its purpose is to model how the heat generated by the electrochemical reaction in SOXE, combined with the heat from the heaters on the top and bottom of SOXE, spreads throughout the stack. The profile of heat exchange within the stack is critical to model accuracy, as the temperature of the cells affects a wide range of other operating parameters, such as Nernst potential and activation potential. The thermal modeling of cell #1 of the SOXE stack is shown below.

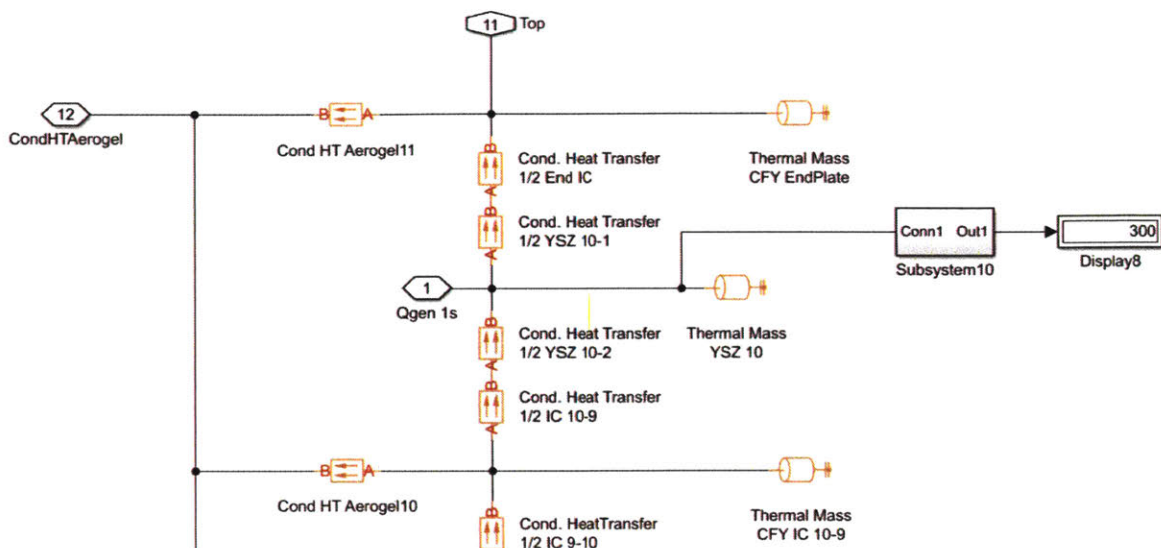


Figure 14: Section of Simulink thermal loop that represents the heat conduction around Cell #1 in the SOXE stack.

In order to understand the figure, begin with the “Qgen 1s” block near the center. This is an input parameter that represents the heat generated or consumed by the electrochemical reaction itself. From there, heat will spread upwards and downwards to the Ytria-Stabilized Zirconia (YSZ) electrode material, through the interconnect material that separates each cell (IC), and either out the top of the stack or down to the next cell in line (not shown). This is modeled for all cells and was added to the Simulink model as part of a greater thermal modeling loop.

2.3 Validating the Outputs and Updating the Model with Grey Factors

In order to ensure that the integration of the two models was a success, it was necessary to validate the outputs of the model first with theory, and then with data. When the outputs, such as the Nernst potential and cell current, of a sample run of MOXIE were confirmed to at least theoretically be on the right track, they could then be lined up next to actual data and compared. As the model did not incorporate many “grey” factors, meaning factors added to the variables to make them match reality, from the start, it was necessary to add these to the model after comparing its outputs with experimental data.

2.3.1 Modeling Results

The outputs of the model mirror what would be expected from theory. For example, as the pressure of oxygen increases on the anode side of SOXE, the model predicts an increase in Nernst Potential. This is expected, as the formula for Nernst potential given in section 2.2.1.1 contains a dependence on the partial pressure of oxygen. The model’s prediction of these two variables is shown in Figure 15.

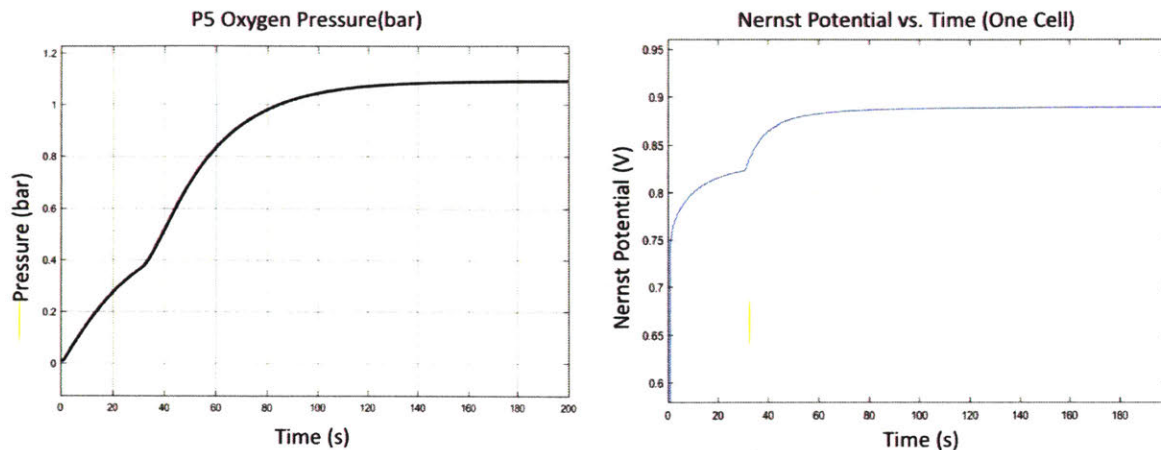


Figure 15: Relationship between oxygen partial pressure (left) and Nernst potential (right)

Indeed, the two exhibit similar shapes over time. The partial pressure of oxygen has a slower rise time, owing to the volume of space that must be filled with oxygen in order to increase the volume to its steady state value.

In addition to the example above, the model includes many other important variables, including:

1. Pressure at inlet of compressor (P1)
2. Pressure before flow sensor (P2)
3. Pressure after flow sensor (P3)
4. Pressure of cathode (P4)
5. RPM of the compressor
6. Current of the compressor motor
7. Voltage of the compressor motor
8. Voltage of the top stack (VT_OUT)
9. Voltage of the bottom stack (VB_OUT)
10. Nernst potential of each cell
11. Activation potential of each cell
12. Intrinsic ASR of each cell
13. Current of the top stack (IT)
14. Current of the bottom stack (IB)
15. Utilization Rate of inlet carbon dioxide (U)
16. Inlet flow rate
17. Recycle flow rate
18. Cathode flow rate
19. Anode flow rate
20. Composition of CO in recycle stream (xCOR)
21. Power supplied to the top heater
22. Power supplied to the bottom heater
23. Heat consumed or generated by each cell during electrolysis
24. Temperature at many points throughout the MOXIE system

By running a simulation that generates plots of all these variables, the model provides valuable insight into the operation of MOXIE and the interdependence of these variables.

2.3.2 Validating the Outputs with Data

It is important to validate the model with real data. Fortunately, JPL has recently been taking data that can be used to validate this model. A subset of data called “JSA-006” was recently compared to the outputs predicted by the model. Both the modeled data and experimental data agreed on all major factors. Two examples will be shown below: cell temperature and stack current.

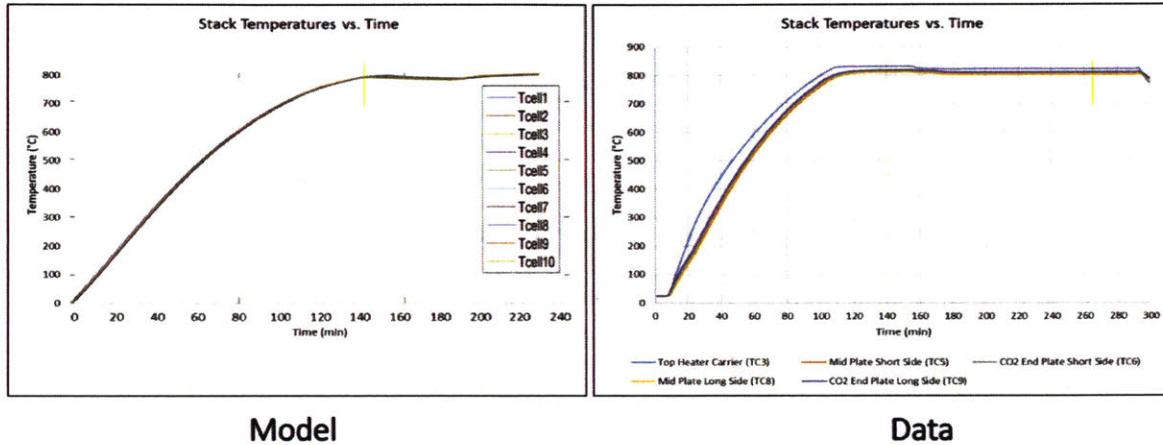


Figure 16: Simulated (left) and experimental (right) results compared for SOXE temperatures

Both the model and experimental data show the ramp up required to bring the SOXE stack from 300 K to the operational temperature of 1073 K in Figure 16. The curves mirror each other well, with both reaching steady-state temperature at roughly two hours. The model predicts a slight oscillation in temperature after reaching steady state, due to time constants in the thermal controller. The experimental stack performed better than predicted, maintaining temperature with very little fluctuations.

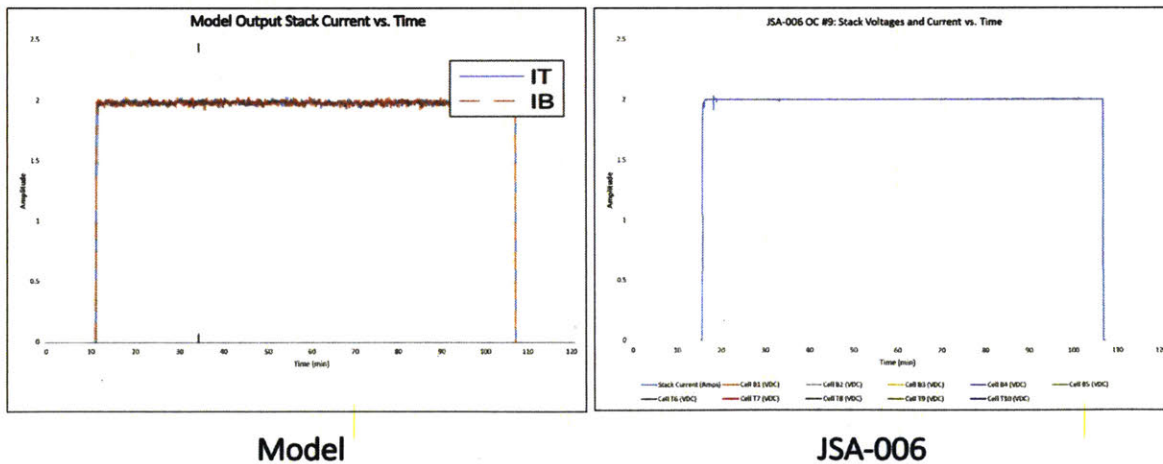


Figure 17: Simulated (left) and experimental (right) results compared for stack current

As Figure 17 indicates, the stack current is also very similar between the modeled and experimental results. Both the model and JSA-006 data have a fast ramp-up time once the stack is turned on, and

both maintain their setpoint value of 2 amps without any major oscillations. The one major difference is that the model shows more noise during steady-state operation than the data; this is intentional, as more noise is expected in the flight model on Mars than was generated from JSA-006 in the lab at JPL. Noise is modeled using one of Simulink's built-in blocks called *Band-Limited White Noise*, shown in the current control loop in Figure 18.

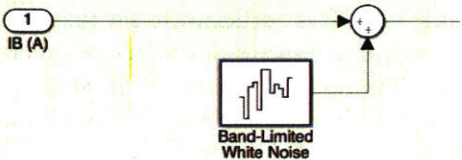


Figure 18: Demonstration of the Simulink block used to add noise into the current control loops of the MOXIE dynamic model.

The input values to the noise block are Noise Power and Sample Time. These have values of 0.0015 and 1 Hz, respectively, and were obtained from JPL's controls team.

There was one variable that had a major difference between modeled results and those seen in JSA-006: heater power. The results are shown in Figure 19.

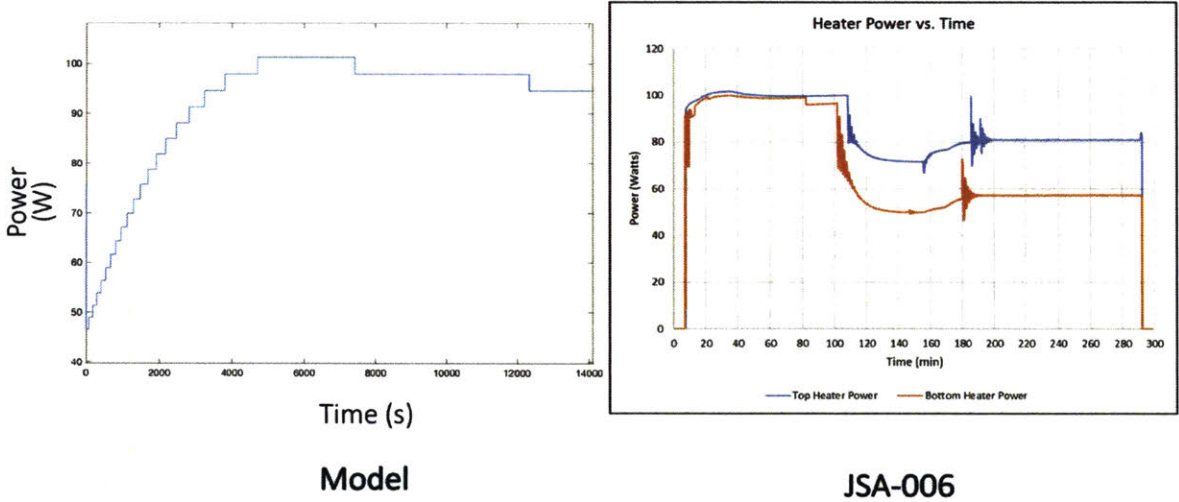


Figure 19: Simulated (left) and experimental (right) results compared for stack heaters

While these curves appear very different, there is an explanation. The heater configuration in the MOXIE lab at JPL was very different from what is expected with the MOXIE flight model. Instead of using a fully packaged MOXIE for JSA-006, the team used a flat-sat configuration. A flat-sat is essentially an unfolded version of MOXIE. All components, including the compressor, SOXE stack, and VFCD board, are laid out and connected on a flat surface inside the chamber. This has major implications for thermal transfer, as it varies significantly between packaged and open configurations. Additionally, JPL had an operator manually control the heater for JSA-006 instead of relying on the thermal control loops that the model – and eventually, MOXIE – uses. Therefore, this difference is not a cause for concern and the model is still properly validated by JSA-006.

Additional testing is occurring at JPL in the coming months and the resulting data will be used to further validate the model.

2.3.3 Adding Grey Factors to Update the Model

Grey factors represent variables that are added to the model in order to tune it to match what is seen experimentally. There are many reasons that theory may not match experiments, the details of which would be too extensive to include here. It is sufficient to say that things like manufacturing defects, unexpected flow perturbations, instrument noise, and a lack of precision mapping of various components of MOXIE are a few examples of variables that affect performance but may not be represented fully in a simulation. In order to attempt to represent them, grey factors are added.

The first variable that has been adjusted is in the thermal control loop. Originally, the cell-to-cell temperature variation depicted by the model resulted in a temperature gradient of roughly 2 degrees from the top and bottom of the stack (warmer) to the middle of the stack (cooler). In the lab at JPL, however, a temperature difference of about 5 degrees Celsius was observed. In order to match these, various gain values of up to 1.0045 were incorporated to adjust the temperature of each cell. These multiplicative grey factors allow the predicted model to match the experimental data from the lab.

Another variable that has been adjusted is the pressure drop across SOXE. Since SOXE provides resistance to gas flow, there will be a loss in pressure from gas entering SOXE to gas exiting it. This drop in pressure is the direct result of the mechanical structure of SOXE, but is difficult to model. Therefore, a gray factor was added to model the drop as a fixed percentage of the inlet pressure to SOXE.

Certain variables that contribute to the electrochemistry of SOXE are also represented as gray factors. These include the activation energy of the conversion of CO₂ to CO and O, the pre-exponential factor, A, the Activation Potential Coefficients, A and B, and the intrinsic ASR of the cells. All were derived using data from Ceramtec, the primary contractor for the development and testing of SOXE cells [17]. Ceramtec is a company that specializes in advanced ceramics materials.

Finally, it should be noted that various gray factors are being added and removed within the thermal subsystem of the model as new data from JPL arrive. Up to now, all tests at JPL have been conducted in an open, flat-sat configuration. From a thermal perspective, this is vastly different than what is expected with a fully packaged flight-like configuration. Therefore, as more data arrive from JPL, gray factors are being edited to account for insulation gaps, imperfect surface-to-surface contacts, and radiative heat transfer, which are difficult to model.

2.4 New Updates to the Model

In addition to the grey factors that were used to modify the outputs of the model, several entirely new systems were added to the model framework. These will be explored in this section.

2.4.1 Electrical Loop

One of the major updates to the model was the inclusion of a fully functional electrical loop. MOXIE's core function – producing oxygen – is enabled by the electrical circuit that runs through

SOXE. The sequence is as follows. First, a voltage is commanded to MOXIE. The amount of voltage is chosen on the basis of enabling production of at least 6 g/hr of oxygen while staying under the Nernst potential for carbon formation. As the voltage is applied to the stack, it passes through the individual cells, which have their own resistance specified by their intrinsic ASR. The current that results from this circuit is representative of the flow of oxygen ions through the cells. This current is measured and fed back through a PI controller, which compares its signal to a target current and adjusts the commanded voltage accordingly for each stack.

Simscape is a tool that allows for the rapid development of physical systems within Simulink. It was chosen as a means to represent the electrical system of MOXIE because of its visual appeal. The process described above is modeled via Simscape. A view of the electrical system as a whole is detailed in Figure 20.

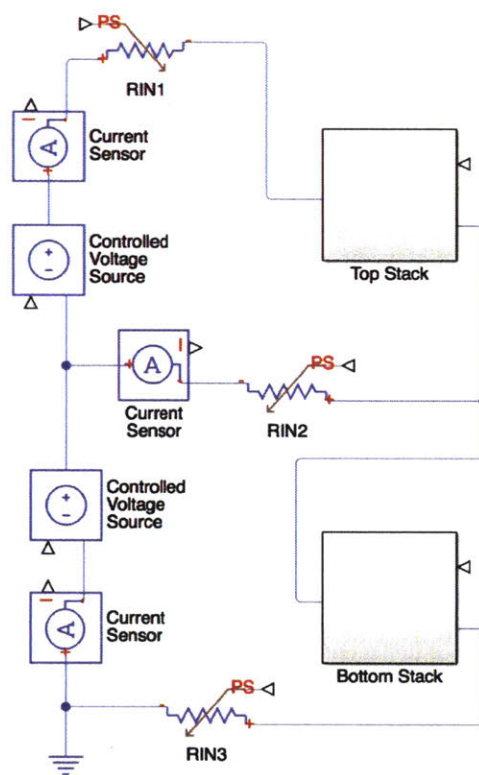


Figure 20: Simscape Electrical Loop of MOXIE

As can be seen from the image, the electrical loop model on the top half begins with a controlled voltage source and passes through a current sensor and a resistor before entering the stack of SOXE cells. It then either passes to the bottom stack or through the middle wire that exists between stacks, which is represented as an additional resistor. The bottom stack has a similar loop, which is shown in the bottom half of the image. It is important to note that the voltage commanded to the top and bottom voltage sources, referred to throughout this paper as V_{T_OUT} and V_{B_OUT} , are generated with two identical PI controllers. For simplicity, neither the controllers nor the V_{T_OUT} and V_{B_OUT} inputs are shown in Figure 20, although they do exist in the model and will be covered in other parts of this thesis.

In order to gain a better understanding of the circuit within the top and bottom stacks, an expanded view of two of the cells in the top stack is shown in Figure 21. Note that the top and bottom stacks, while individually controlled, have the same Simscape and Simulink architecture.

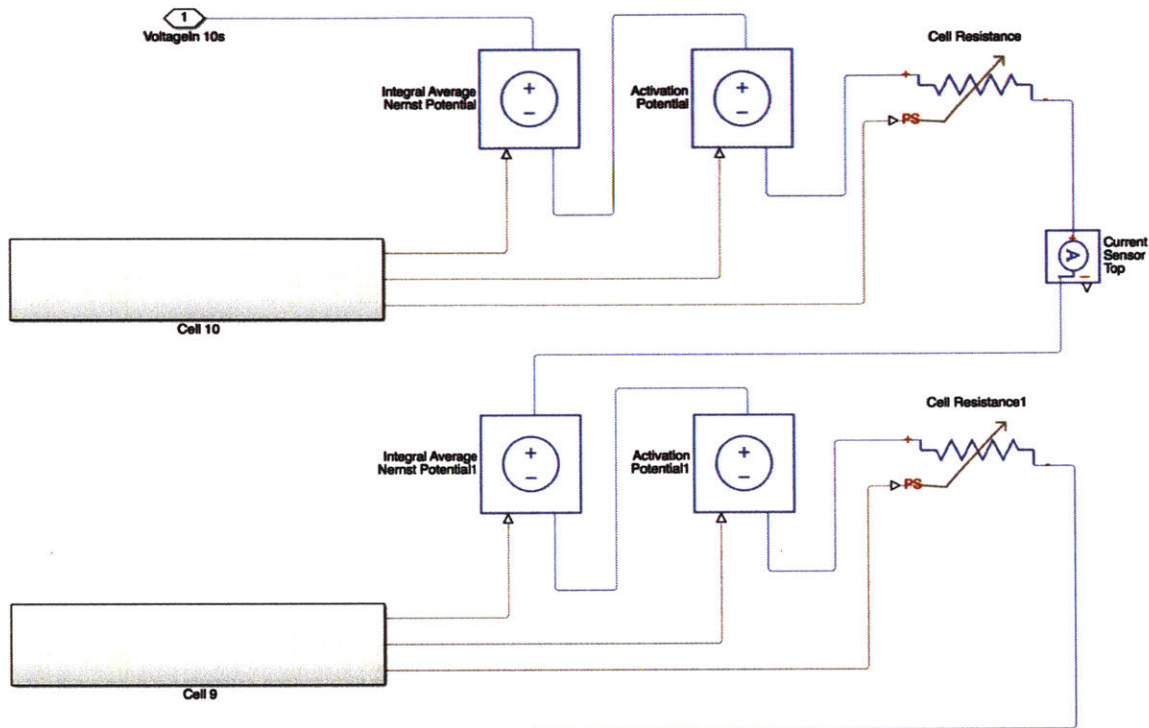


Figure 21: Simscape Electrical Loop of Cell 10 and Cell 9 in SOXE

Only two of the five cells in the top stack were shown here, as showing all five would make the image needlessly complex and difficult to read. Starting from the top of the image, the voltage in is representative of the line into the Top Stack box in Figure 20. From there, it is affected by voltage drops in the form of Nernst potential and activation potential, which are described in other sections of this thesis. It then passes through the calculated intrinsic ASR, or cell resistance, of the cell before passing on to the next cell. The complex calculations for each of these values occur within the Cell 10 box. Each cell undergoes this process, and the electrical loop flows through each in series in order to accurately capture the entire electrical output of each stack. This electrical loop is a key component in the simulation of MOXIE’s performance, as it dictates the rate at which the electrochemistry within SOXE occurs.

2.4.2 Thermal Loop Updates

As described earlier, the thermal loop framework put forth by the MIT model was used as a baseline for the new, consolidated model. The goal of the thermal loop is to demonstrate how heat passes through the SOXE stack, thereby yielding time-sensitive temperatures for each SOXE cell. The temperature of each cell is important for parameters that affect cell performance, such as Nernst Potential and Activation Voltage.

The existing thermal model mimics heat conduction among the stacks. Effects of radiation and convection are ignored, as they are expected to be insignificant for the scope of this model [18]. In addition, the model assumes a uniform thermal mass in the planar direction on each SOXE cell. This means that the temperature is assumed to be the same at all points on the same plane on each cell, interconnect, and endplate. The temperature varies between cells and interconnects, but not across the cell itself. This assumption was validated by an experiment conducted by JPL where several thermocouples were attached to different parts of the surface of a cell. When the stack was turned on, the temperature was consistent at each point on the cell's surface [19].

2.4.2.1 Updating Thermal and Mass Properties

While the existing thermal model provided a good framework, many of the values it assumed were either outdated or unconfirmed. These include the specific heats of the materials, the thermal conductivities of the materials, the thickness of the segments of SOXE, the masses of the components of SOXE, and the cross-sectional areas across which heat would be transported.

The specific heats and thermal conductivities of the materials were updated with data from Hua et al [18]. For the sake of uniformity and simplicity, the values of these temperature-dependent variables were taken at 400 °C, the approximate half-way point during the heating phase of MOXIE. This is a more accurate way of modeling heat conduction than using the endpoint temperature, 800 °C, because by the time it reaches the endpoint, the heat has mostly reached equilibrium throughout the entire stack. The model is more useful if it can demonstrate what is happening to heat distribution *during* the startup phase because the warm-up period of SOXE is a significant portion of a MOXIE experimental run. It is advantageous to model this as closely to reality as possible in order to understand the rate of heating that should be expected across the stack; therefore, 400 °C was chosen as the baseline temperature for temperature-sensitive variables.

The thicknesses, masses, and cross-sectional area within SOXE were validated with data from the SOXE CAD model. These data were provided by JPL and were current as of August 5, 2017. The majority of these values are expected to remain static for the remainder of the MOXIE project.

2.4.2.2 Consolidating Existing Thermal Modeling

In addition to updating the values within the model, the framework itself required reorganization. The main issue with the existing framework was that it slowed the model's simulation speed by a factor of five. While the improved accuracy of the modeling was well worth the additional time for detailed analysis, it was desirable to have an option to turn down the accuracy in favor of speeding the simulation back up for other purposes. The high accuracy of the thermal loop was not required for, say, investigations into the effects of tuning the PID controller in the pressure loop. Therefore, it became practical to develop a less accurate but much faster thermal model that could be toggled on or off depending on the purpose of the user running the model.

In order to allow this toggling action between the detailed thermal model and the faster thermal model, it first became necessary to consolidate all thermal activity in the model within a single block. As it stood at the time, thermal properties and calculations were scattered throughout several areas of the model. It would have required a large manual effort to toggle all of these components on or off every time the model was run. To improve the efficiency, the calculations were moved to a single

block in the thermal section of the model, and the thermal pathways were universally rerouted to this central location. The “Detailed Thermal Model” block in Figure 22 contains all heat-related information and calculations that were previously scattered throughout the model.

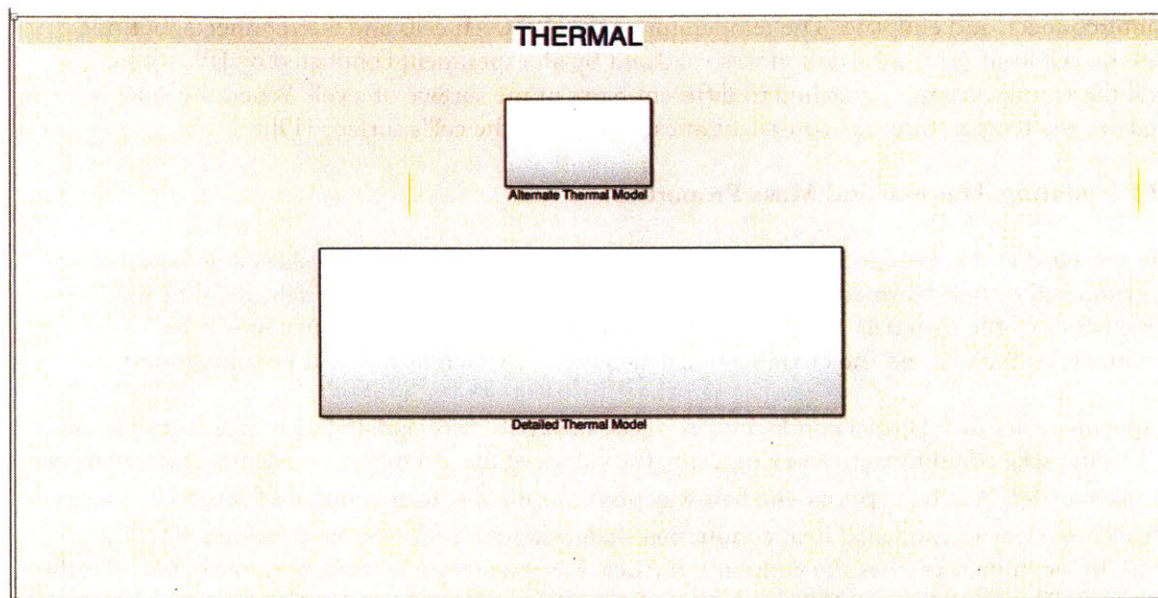


Figure 22: Consolidated thermal model

The framework mentioned earlier from the MIT model is contained inside of this Detailed Thermal Model block. However, consolidated calculations for each individual cell were also added. These can be seen as the ten blocks on the left-hand side of Figure 23, which is the sublevel view of the Detailed Thermal Model block from Figure 22.

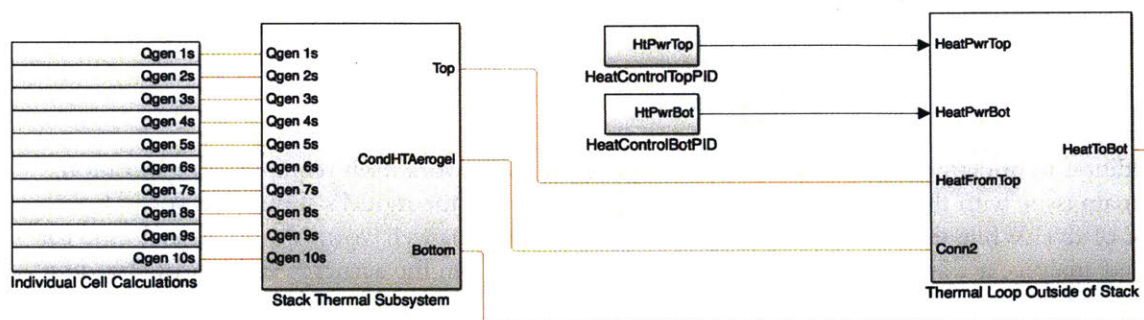


Figure 23: Consolidated view of detailed thermal model

The Stack Thermal Subsystem, Heat Controllers, and Thermal Loop Outside of the Stack are all similar in framework to those in the MIT model. However, the Individual Cell Calculations are a new addition to the model and are an efficient way to represent the heat generated during the electrochemical reaction for each cell. These calculations are shown in Figure 24.

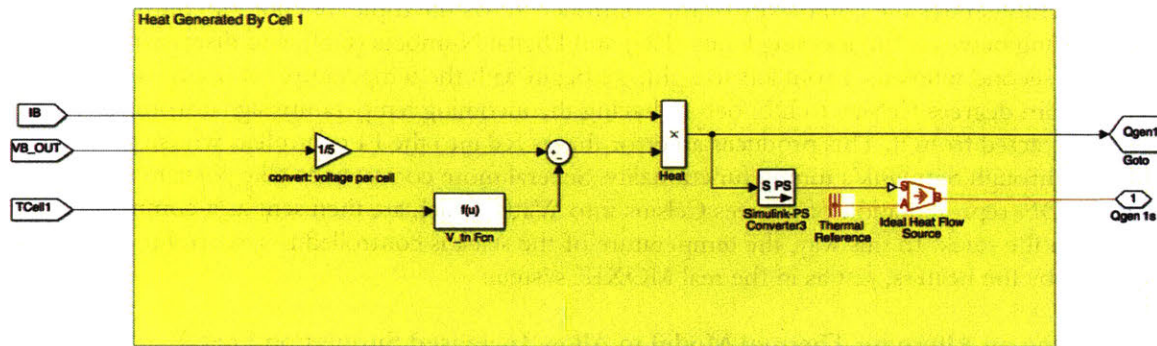


Figure 24: Heat calculations for Cell 1, representing the exo- or endo-thermic properties of the electrochemical reaction.

Each of the ten cells has a unique heat generation calculation that is dependent on its temperature, the stack current, and the stack voltage being supplied to each cell. These inputs are viewable on the left side of Figure 24. They feed into a function that calculates heat generation or consumption, which is primarily based upon the selected voltage of the cell. The reason for this has to do with the reaction's thermoneutral potential, which refers to the crossover point between endothermic and exothermic reactions in electrochemistry. If the cell is running at a higher voltage than its thermoneutral potential, it will create an exothermic reaction, while if it is running at a lower voltage than its thermoneutral potential, it will create an endothermic reaction. Finally, on the right side of Figure 24 are the output values of the heat generated or consumed by the stack, which are fed into the rest of the thermal subsystem, as viewed by the connecting lines from the cell blocks to the Stack Thermal Subsystem in Figure 23.

2.4.2.3 Thermal Control

Developing controllers for the thermal subsystem was both challenging and important. From the Flight Software (FSW) team's requirements, a PI controller was chosen with a sample rate of 1 Hz. The thermal stack system was found to have a time constant of approximately 14,400 seconds, or 4 hours (CITE). As such, the PI controller had to be developed and tuned to match these parameters. The thermal controller for the bottom stack is shown below in Figure 25 and is identical to the controller for the top stack.

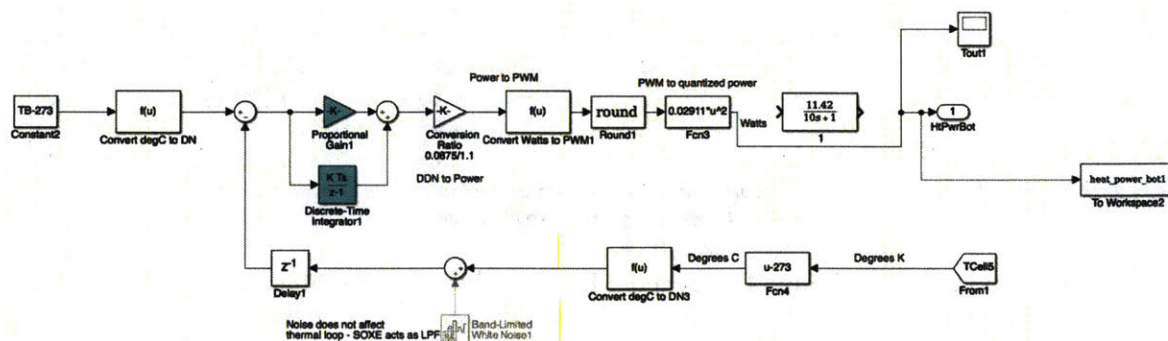


Figure 25: Thermal PI Controller

The figure demonstrates the complexity of the controller. It has the triple function of controlling the heat, converting between Engineering Units (EU) and Digital Numbers (DN), and discretizing the signal into 1-second intervals. From left to right, we begin with the temperature set point. It is converted from degrees Celsius to DN before having the incoming temperature signal from the stack be subtracted from it. This produces an error that is fed into the PI controller, whose gains were found through Simulink’s tuning functionality. Several more conversions take place in order to convert the DN representation of degrees Celsius into Watts, which are then sent as a command to the heater on the stack. In this way, the temperature of the stack is controlled to a set point temperature by the heaters, just as in the real MOXIE system.

2.4.2.4 Adding an Alternate Thermal Model to Allow Increased Simulation Speed

As mentioned earlier, the purpose of consolidating the thermal modeling into one block was to allow that block to be turned off in favor of a faster, alternative thermal model. Several architectures were considered for development of an alternate thermal model, including a cell-by-cell piecewise function and a modified Simscape flow model. What was decided was to use a simple ramp function to simulate heat-up of the SOXE. In order to allow the flexibility to tune each cell’s individual temperature with what is seen experimentally, a gain value block was attached to the outlet of the ramp function for each cell. The ramp system with ten gain blocks is shown below in Figure 26. This is the subsystem view of the “Alternate Thermal Model” block shown earlier in Figure 22.

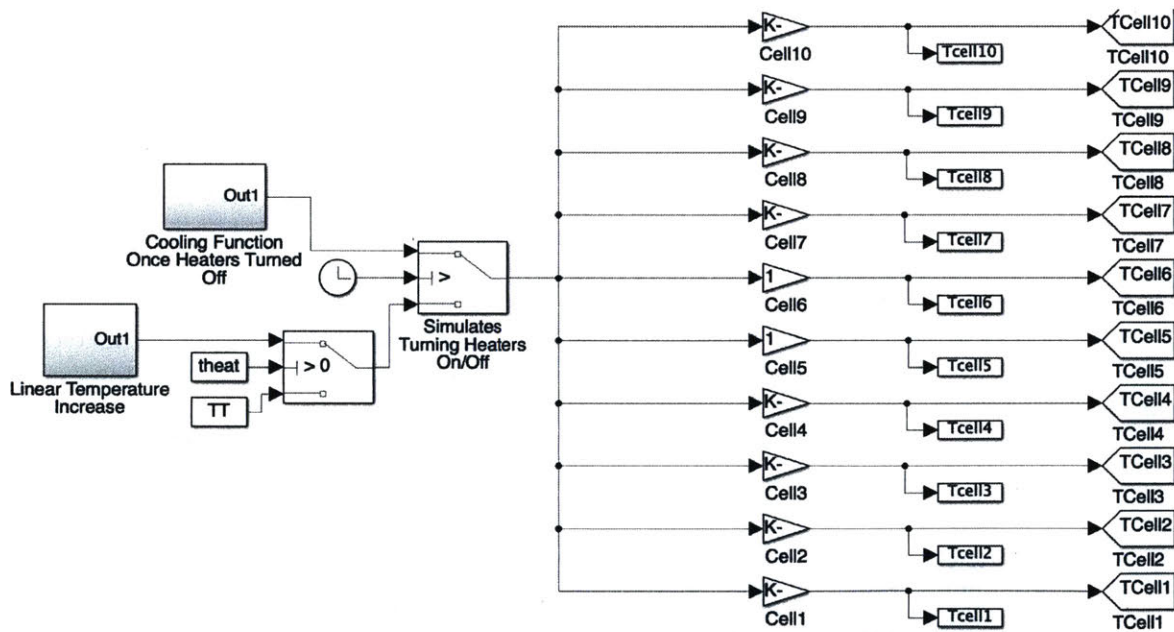


Figure 26: Alternative thermal model. Includes ramp function to simulate temperature rise of SOXE and ten individual gains to alter each cell's temperature to match data.

The ramp temperature in the “Linear Temperature Increase” block on the left side of Figure 26 is set to increase the temperature from ambient conditions (300 K) to the set-point temperature of SOXE (1073 K), given by TT, at a ramp rate of eight degrees per minute. This was found experimentally at JPL [20]. When it reaches the heating time setpoint given by “theat”, it sets the temperature to TT to mimic the PID controllers maintaining the setpoint temperature. Finally, the

value of each cell is passed through a gain block that alters the cell temperature to match what was seen experimentally before being passed to the rest of the Simulink model for use.

The ramp-up temperature profile of the 10 cells from the alternate thermal model, with appropriate gain values, is shown in Figure 27.

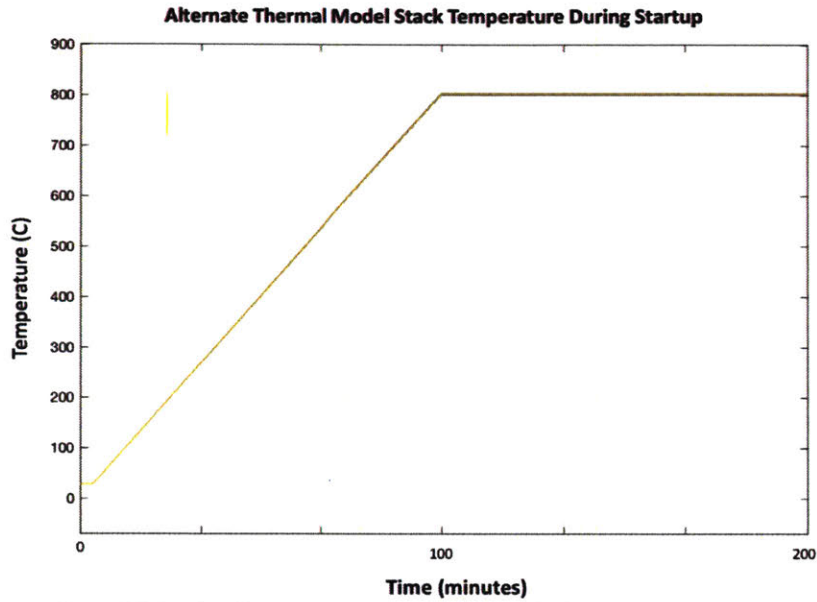


Figure 27: Results of SOXE temperature ramp-up with alternate thermal model

When comparing this with data from JPL, shown below in Figure 28, it is clear that a decent approximation has been made.

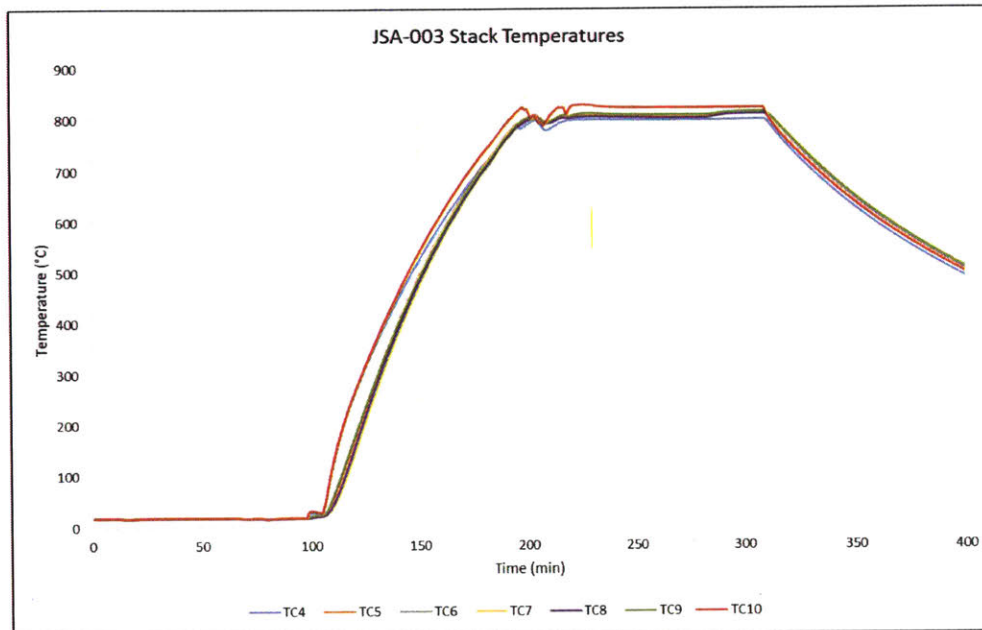


Figure 28: JSA-003 SOXE Packaging Test 8 Data from JPL representing temperature of the SOXE stack over time

In this experiment, individual cell temperatures could not be taken. However, measurements at the top, middle, and bottom of the stack were taken, as represented by TC6, TC7, and TC8 in the figure, respectively. Both models exhibit similar features, including an approximate linear ramp-up time of 90 minutes and equivalent differences between cell temperatures from the bottom to the top of the stack.

With the new values in the model, the thermal loop additions consolidated, and the alternative thermal model completed, the thermal model is complete and offers a highly accurate, slower option or a less accurate but much faster option.

2.4.3 Heater Controller

Several control systems exist within MOXIE to ensure safe operation of the instrument. One of these is the heater control system, which determines how much heat is output by the heaters on the top and bottom of the SOXE stack. The two heaters are labeled in the depiction of SOXE in Figure 29.

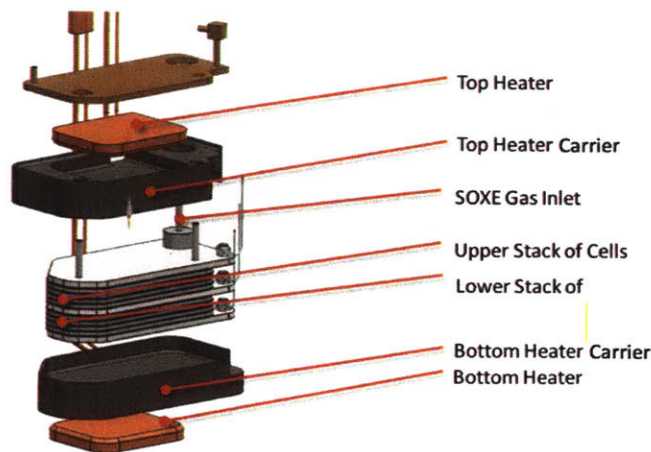


Figure 29: Exploded view of SOXE stack

As the diagram indicates, heat will conduct from the heater, through the heater carrier, and onto either the bottom or top of the stack. This is how the SOXE cells are heated. Bear in mind that in order for the electrochemical conversion of carbon dioxide to oxygen to occur within MOXIE, the cells must be heated to the vicinity of 800 °C. As a result, it is necessary to have a controller that can sense the current temperature, compare it to its desired set point, and adjust the output of the heaters accordingly.

The heater control loop, as modeled in Simulink, utilizes a Proportional-Integral (PI) controller. In addition, it converts the input temperature signals into Digital Numbers (DN), which are the units read by the MOXIE software. The PI controller and conversions to DN are shown in Figure 30, which shows the entire heater controller for the bottom heater.

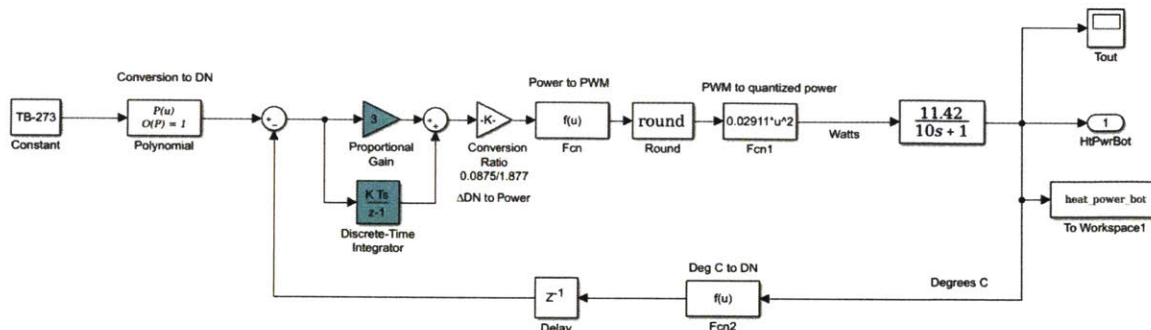


Figure 30: Controller for bottom heater, with temperature input, PI controller, conversion to DN, and heater command output.

2.4.4 Current Controller

A second control system in MOXIE is the current controller. In order to produce oxygen, a voltage must be applied to the SOXE stack. The value of this voltage is determined by comparing the system's current with the desired current. If the system's current is lower than the current set point, the voltage being applied to the stack will increase. If it is higher than the set point, the voltage being applied will decrease. This change in voltage is determined by the current controller.

Figure 31 shows the Simulink model of the current controller.

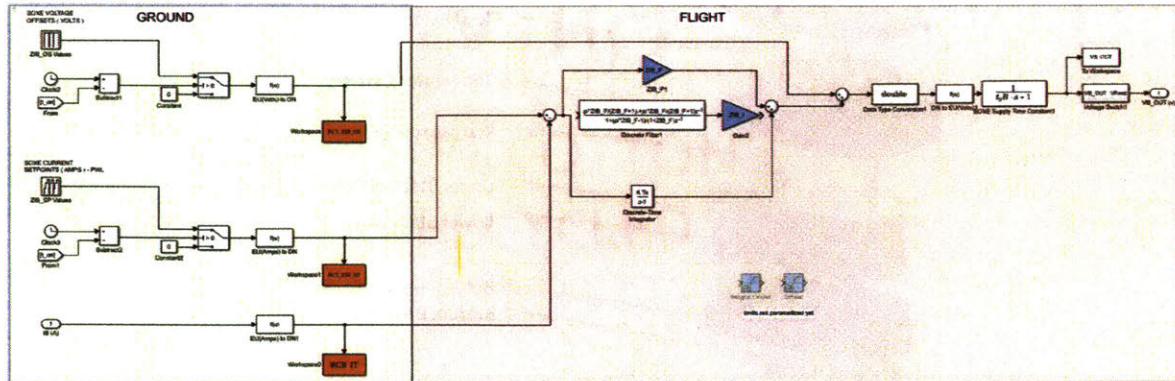


Figure 31: Current controller for top stack. The controller for the bottom stack is identical.

From the image, it is clear that the controller is segmented into two parts. The left side is the “Ground” segment, which takes input values in Engineering Units (EU), such as amps and volts, and converts them into Digital Numbers (DN) for the equipment to read. The right side is the “Flight” segment, which takes the inputs in DN, runs them through a PI controller, time-delay transfer function, and DN-EU converter, and outputs a voltage signal. This voltage signal, labeled VT_OUT for the top stack and VB_OUT for the bottom stack, is what commands the stack voltage in an attempt to match the current with its set point.

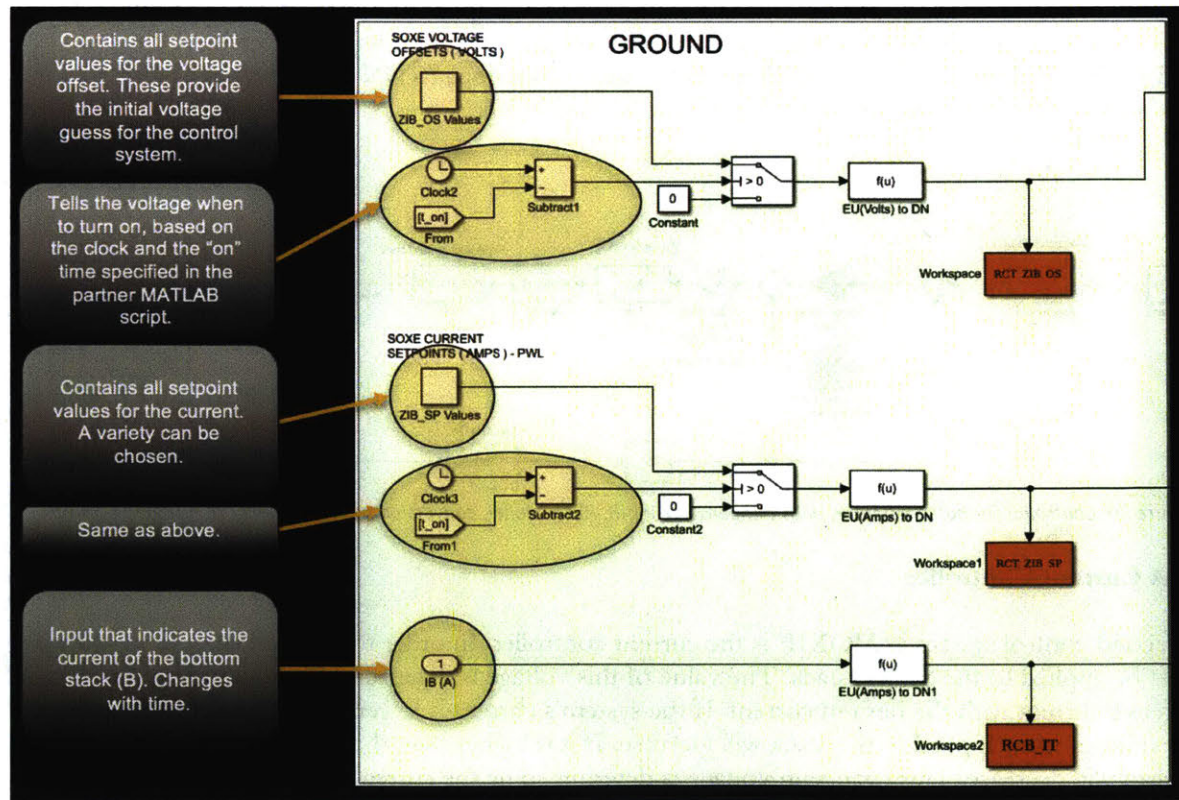


Figure 32: Detailed explanation of inputs to current control system

Figure 32 gives a detailed look at the various inputs to the Ground Segment of the current controller, with explanations in the left margin. Similarly, Figure 33 gives a detailed explanation of the right-hand side of the Ground Segment of the current controller with explanations in the right margin.

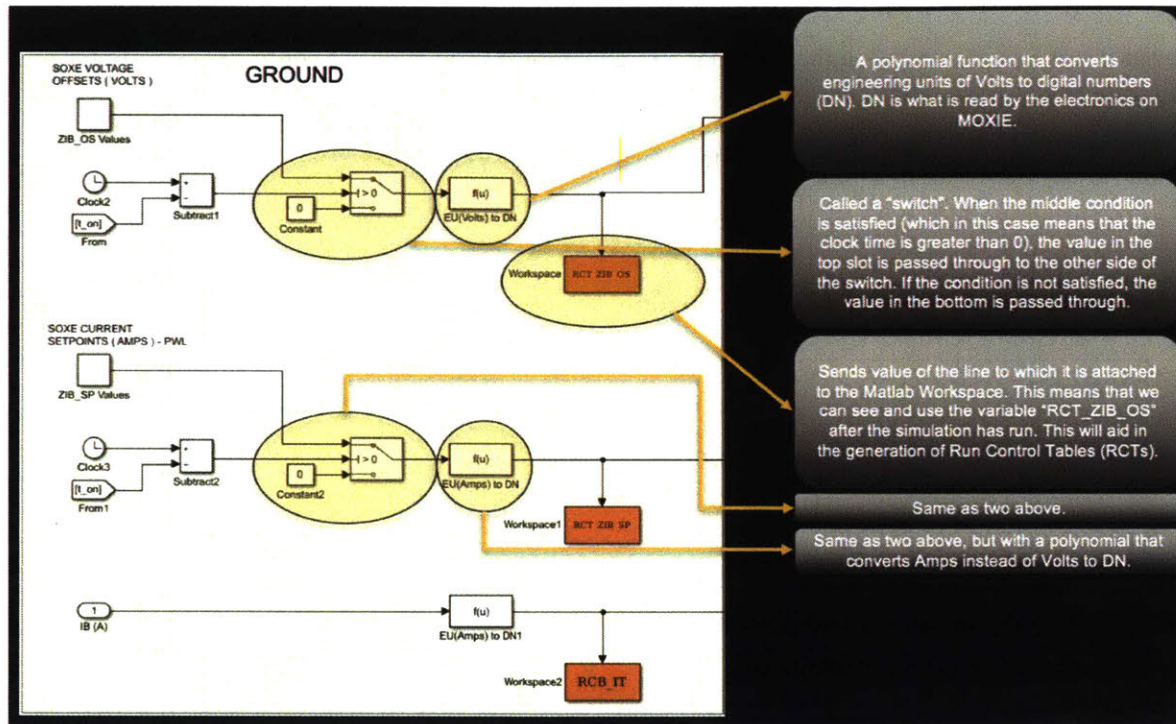


Figure 33: Detailed explanation of switches in current control system

Finally, Figure 34 gives a detailed explanation of the Flight Segment of the current controller.

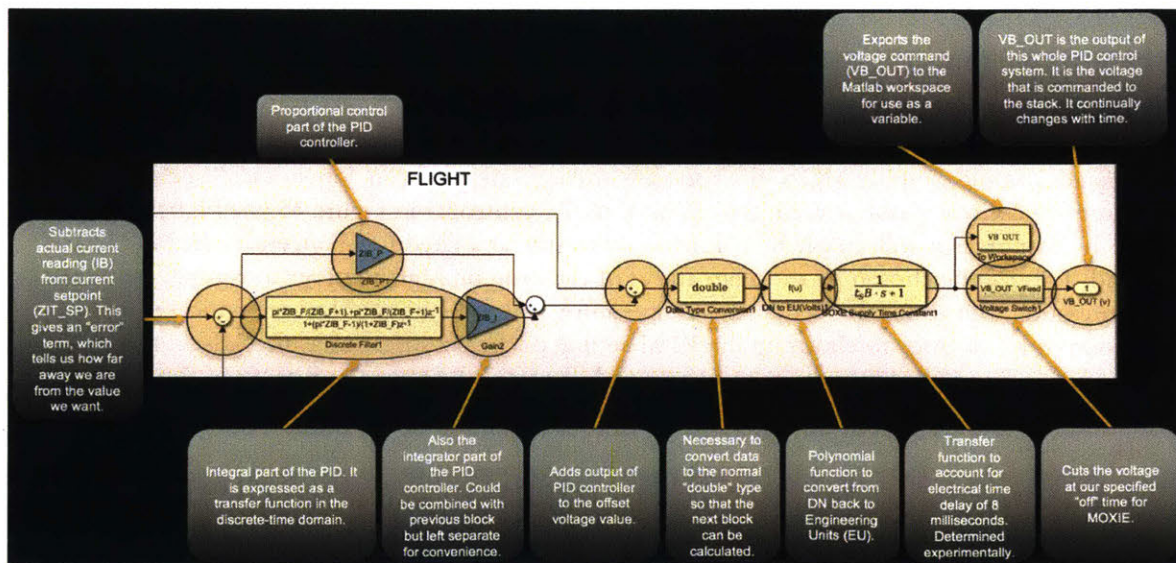


Figure 34: Detailed explanation of all components of Flight Segment in the current control system

Together, these segments make up the complete current control system that enables safe and efficient electrochemistry to occur within SOXE.

2.4.5 Pressure Controller

The third and final controller in the MOXIE Simulink model is the pressure controller. The user is able to specify a desired input pressure, and the model will adjust the compressor speed to reach and maintain this pressure. An image of the pressure controller is shown in Figure 35, as created by Marianne Gonzalez at JPL and integrated into the Dynamic Model.

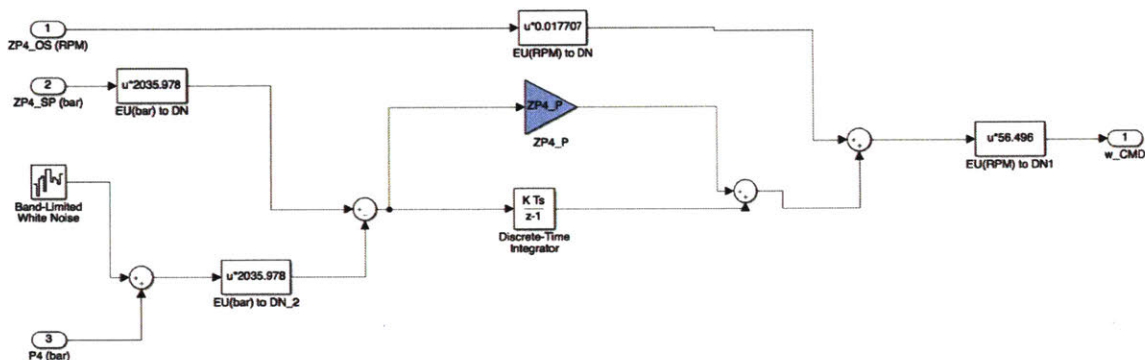


Figure 35: Pressure Control System

This controller is similar to the current controller. It consists of an RPM offset that gives the controller its initial value. Then, the pressure is computed downstream in the model and fed back into the controller as P4. This is subtracted from the actual pressure set point chosen by the user, and the resulting error is fed through a PI controller to tune it. The outlet of the system is w_CMD, which commands (CMD) the rotational rate (ω) of the compressor. A higher rotational rate for the compressor will result in higher internal pressure for MOXIE, as the only exit points for the gas are fixed orifices at the end of the system.

It is currently under debate within the MOXIE team whether or not the pressure controller will be used in the flight system. The possible reasons for running without pressure control are that pressure does not affect system performance as much as previously thought, and the removal of this control system would simplify MOXIE's software and operations. In an "open-loop" scenario where pressure control is not desired, the majority of the controller in Figure 35 will be bypassed. Instead, the compressor will simply be commanded to spin at a fixed RPM, given by the "ZP4_OS" command. This can be chosen by the team ahead of each run on Mars in order to roughly generate a desired pressure. The atmospheric density, temperature, and pressure on Mars are critical pieces of information to know prior to choosing the RPM setting of the compressor, as they affect the amount of gas being pulled into the compressor and therefore the internal pressure of the system. MEDA, another science instrument on the Mars 2020 rover, can provide these data to the MOXIE team ahead of schedule, thereby enabling proper RPM selection for each run.

2.5 Fault Detection

It is desirable for the model to be able to identify and flag when certain values are exceeded for critical parameters. For example, if the temperature of the top stack of SOXE exceeds the safe operating limit before coking begins to occur when running a simulation, it would be advantageous to have the model notify the user that a safe operating limit has been exceeded. This way, setpoints that lead to dangerous operating conditions can be caught before sending the commands to MOXIE on Mars.

A fault detection system that accomplishes this goal was successfully implemented into the dynamic model. It affords the user two different ways to use it:

1. Immediate Notification: if a value of any parameter exceeds a limit that was set, the entire simulation stops and MATLAB displays an informative error.
2. Delayed Notification: if a value of any parameter exceeds a limit that was set, the simulation continues running as usual but displays an informative error when the simulation has completed. In addition, it logs all errors that occurred during the simulation in a .txt file for review.

2.5.1 Fault Detection Limits

The JPL MOXIE team provided a list of faults that should be identified in the aforementioned system. These include exceeding minimum and maximum values for various pressures, temperatures, voltages, and currents, among others. The majority of the fault limit requirements are displayed in Table 1.

Table 1: Fault Detection Limits

ID	Rationale	Variable Name	Max Allowed Value	Min Allowed Value
599809	Protects against overvoltage that could damage the SOXE.	VB_OUT	7.1	-
599807	Protects against overpressure that could rupture or otherwise damage the gas system.	P4	1.2	-
599819	Protects against over temperature that could damage the ELX.	T22	70° C	-
600705	Protects against damaging the SOXE due to specific operational conditions associated with excessive CO ₂ conversion (coking). The default limit value should not risk terminating an experiment unintentionally.	IT/P4	10	-
599811	Protects against overcurrent that could damage the SOXE.	IB	4	-
600765	Protects against overpressure that could rupture or otherwise damage the gas system.	P5	1.2	-
599804	Prevents sustained overcurrent condition which could damage 3.3 V regulator, by disabling power to the Composition Sensors if the current draw is too high for an extended period.	-	0.4	-

600707	Protects against damaging the SOXE due to specific operational conditions associated with excessive CO ₂ conversion (coking). The default limit value should not risk terminating an experiment unintentionally.	IB/P4	10	-
599785	Supports artifact 599796 CAS Current Limiting, by disabling power to the Composition Sensors if the current draw is too high for an extended period	-	2	-
600704	Protects against damaging the SOXE due to specific operational conditions associated with excessive CO ₂ feed rates (oxidation). The default limit value should not risk terminating an experiment unintentionally.	P4	2	-
599815	Protects against overtemperature that could damage the Composition Sensors.	T1	50° C	-
599805	Protects against overpressure that could rupture or otherwise damage the gas system. P2 is expected to be the highest measured system pressure, and therefore could be the limiting pressure safety limit for the MOXIE system.	P2	1.2	-
599823	Protects against overcurrent on the 10A switch due to high supply voltage into the resistive loads.	-	33	-
599808	Protects against overvoltage that could damage the SOXE.	VT_OUT	7.1	-
599822	Protects against overcurrent on the 10A switch due to low supply voltage into the DC-DC Converters. Also protects against excessively draining the Rover battery.	-	-	28
599814	Protects against overtemperature that could damage the Compressor Motor.	T4	105° C	-
599803	ELX must prevent overloading the 3.3 V regulator such that it is damaged, or such that the 5 V supply is affected in a way that results in the Control Board not operating properly.	-	2	-
599821	Protects against overtemperature due to operation of MOXIE above its AFT.	T7	50° C	-
599812	Protects against overtemperature that could damage the SOXE.	TBot	850° C	-
599810	Protects against overcurrent that could damage the SOXE.	IT	4	-
599813	Protects against over temperature that could damage the Compressor.	T3	70° C	-
599806	Protects against overpressure that could rupture or otherwise damage the gas system.	P3	1.2	-
600708	Protects against damaging the SOXE due to specific operational conditions associated with insufficient CO ₂ conversion (oxidation). The default limit value should not risk terminating an experiment unintentionally.	IB/P4	-	0
600701	Protects against damaging the SOXE due to specific operational conditions associated with low SOXE temperature. The default limit value should not risk terminating an experiment unintentionally.	TTop	-	-60° C

600702	Protects against damaging the SOXE due to specific operational conditions associated with high SOXE temperature. The default limit value should not risk terminating an experiment unintentionally.	TBot	1000° C	-
600699	Protects against damaging the SOXE due to specific operational conditions associated with high SOXE temperature. The default limit value should not risk terminating an experiment unintentionally.	TTop	1000° C	-
600703	Protects against damaging the SOXE due to specific operational conditions associated with low SOXE temperature. The default limit value should not risk terminating an experiment unintentionally.	TBot	-	-60° C
600697	Protects against overcurrent on the 10A switch due to low supply voltage into the DC-DC Converters. Also protects against excessively draining the Rover battery.	-	-	28
600698	Protects against overcurrent on the 10A switch due to high supply voltage into the resistive loads.	-	33	-
600706	Protects against damaging the SOXE due to specific operational conditions associated with insufficient CO ₂ conversion (oxidation). The default limit value should not risk terminating an experiment unintentionally.	IT/P4	-	0
600766	Protects against overtemperature that could damage the SOXE.	TTop	850° C	-
600767	Protects against damaging the SOXE due to specific operational conditions associated with insufficient CO ₂ feed rates (coking). The default limit value should not risk terminating an experiment unintentionally.	P4	-	0

2.5.2 Model Implementation

These fault limits were implemented into the model by way of a MATLAB function. Within Simulink, each fault detection block is similar to the example shown in Figure 36.

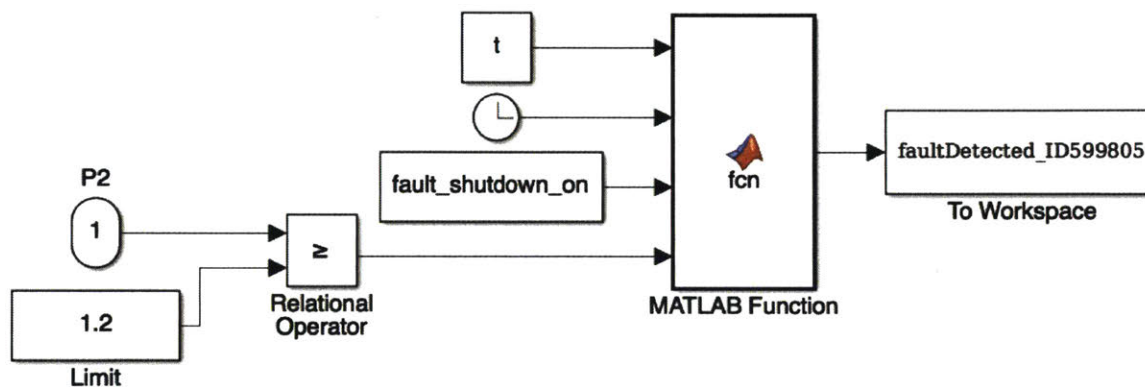


Figure 36: Fault Detection System for P2 Sensor

This block takes the input value of P2 from the simulation and compares it to its maximum allowable value of 1.2 bar. If it is greater than 1.2 bar, it feeds a value of “1” into the MATLAB function block; otherwise it is ignored. When the MATLAB function block sees a value of 1, it logs an error. The MATLAB function algorithm is shown below.

```

function faultDetected_ID599805 = fcn(Clock, t, fault_shutdown_on, u)
faultDetected_ID599805= 0;

if (u == 1)
    faultDetected_ID599805 = 1;
    if fault_shutdown_on == 1    %If fault detection is turned on by user
        error('P2 exceeded its allowable bounds');           %Display an error
    else
        if t >= Clock          %Display error after the simulation ends
            disp('P2 exceeded its allowable bounds');
        end
    end
end
end

```

As the code indicates, two different options are available to the user. These were mentioned earlier; the user can either have the simulation shut down immediately when a fault limit is exceeded, or else have the simulation run as normal and display the errors after. The user determines which option to use by changing the value of the “fault_shutdown_on” variable to either 0 or 1 in the MATLAB script.

The fault detection system is an important tool that will identify and prevent dangerous operating conditions before they are commanded to MOXIE. It acts as a gate between the software development team and the actual hardware on Mars and has the potential to catch and prevent a mission-ending setting in the commanded software.

Chapter 3: Graphical User Interface (GUI)

3.1 Motivation

As detailed earlier, design and development of a GUI was necessary in order to allow people other than the model developers to run the simulation and gain useful information from it. The complexity of the Simulink model is demonstrated below in an image of its Level 0 configuration.

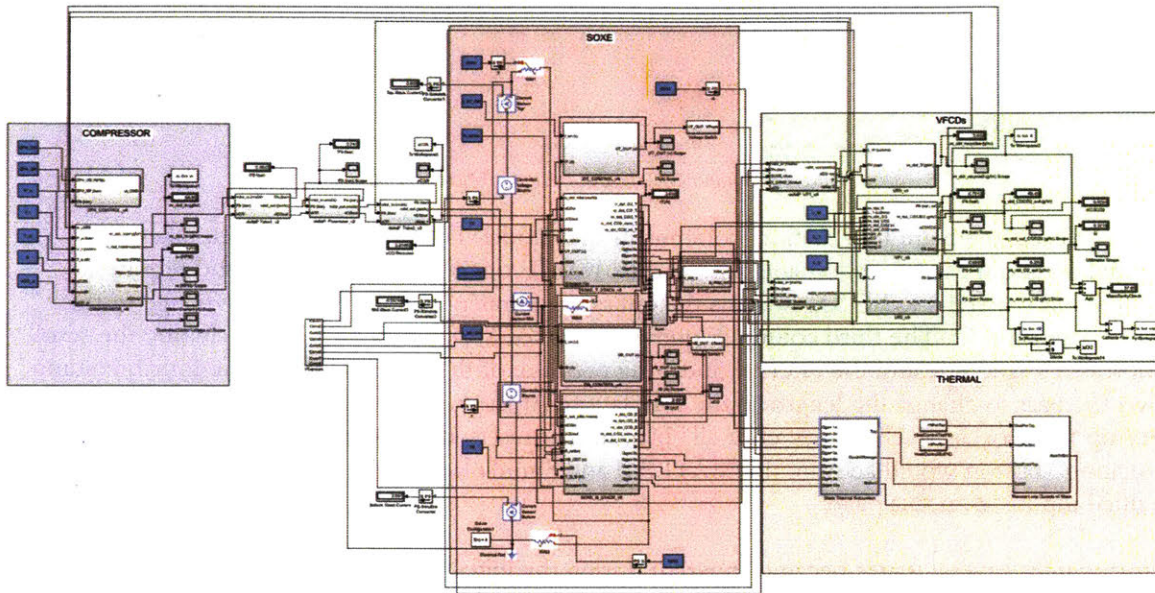


Figure 37: Level 0 view of the consolidated, dynamic model of MOXIE. Notice its complexity and perceived difficulty of use.

Note that within each gray box, another subsystem exists. This continues to partition up to five layers deep in some cases. While the model developers are comfortable altering variables and running simulations with this model, it would require significant training for others to do the same. This is what brought about the need for a simple-to-use GUI.

3.2 Microsoft Excel Design

The GUI design began as an Excel sheet. The idea was that the majority of people are familiar enough with Microsoft Excel that they would feel comfortable controlling a MATLAB and Simulink model with Excel. Preliminary designs were sketched, and the first implementation of these designs into Microsoft Excel is shown below in Figure 38.

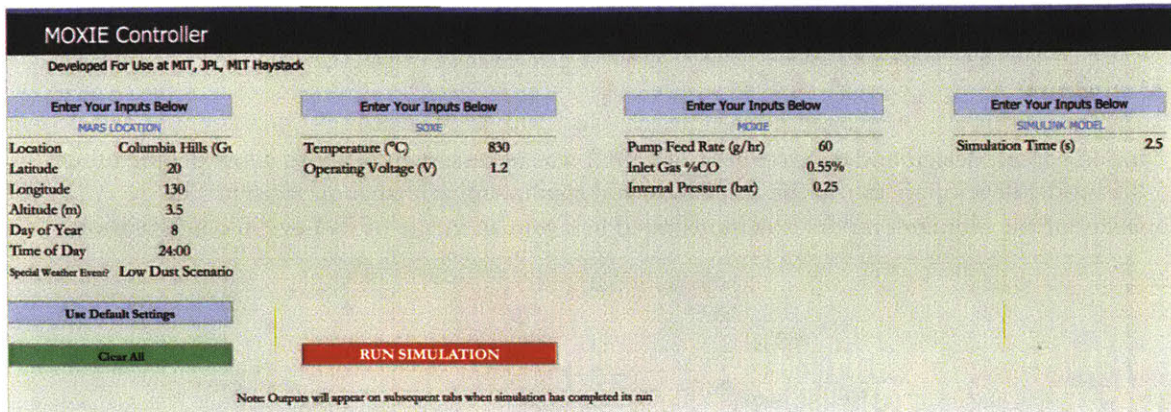


Figure 38: Original MOXIE GUI Design in Microsoft Excel

As you can see, there are four distinct columns in this model. The first is an area that takes information about Mars location and time at the MOXIE operations site. The second requires inputs that are specific to SOXE, such as the operating temperature and operating voltage of the electrochemical cells. The third column requires inputs for MOXIE as a system, including the scroll compressor's feed rate and the internal operating pressure of the system. Finally, the fourth column allows the user to change the length of the simulation. At the bottom of the GUI are buttons to help speed up the process, such as the "clear all" button that resets all variables. Finally, the "Run Simulation" button would activate the MATLAB and Simulink model in the background using the specified inputs from this page.

Unfortunately, several issues became apparent during the initial testing phases of this GUI. The first was that it was difficult to link excel to MATLAB on both Macintosh and Windows platforms. Commands existed in each operating system to allow variables to be drawn from Excel and placed into MATLAB, but they were not the same between platforms. This meant that at least two separate GUIs would have to be developed and maintained. Another issue was the lack of flexibility available from Excel. Every cell in Excel that was referenced by MATLAB had to be hard-coded. This meant that if a cell, row, or column was inserted that displaced any cells in the GUI, all displaced cells would have to be changed in the MATLAB code. This became a very manual and tedious process, forcing an alternative to be sought.

3.3 MATLAB App Developer Design

As it were, MATLAB has an app developer program that eliminates both of these issues. MATLAB's app developer, which outputs .mlapp files, runs equally well on Macintosh and Windows platforms, and is much easier to code than an Excel-MATLAB crosslink. An image of the final GUI is shown in Figure 39, and will be explored in more detail in the following sections.

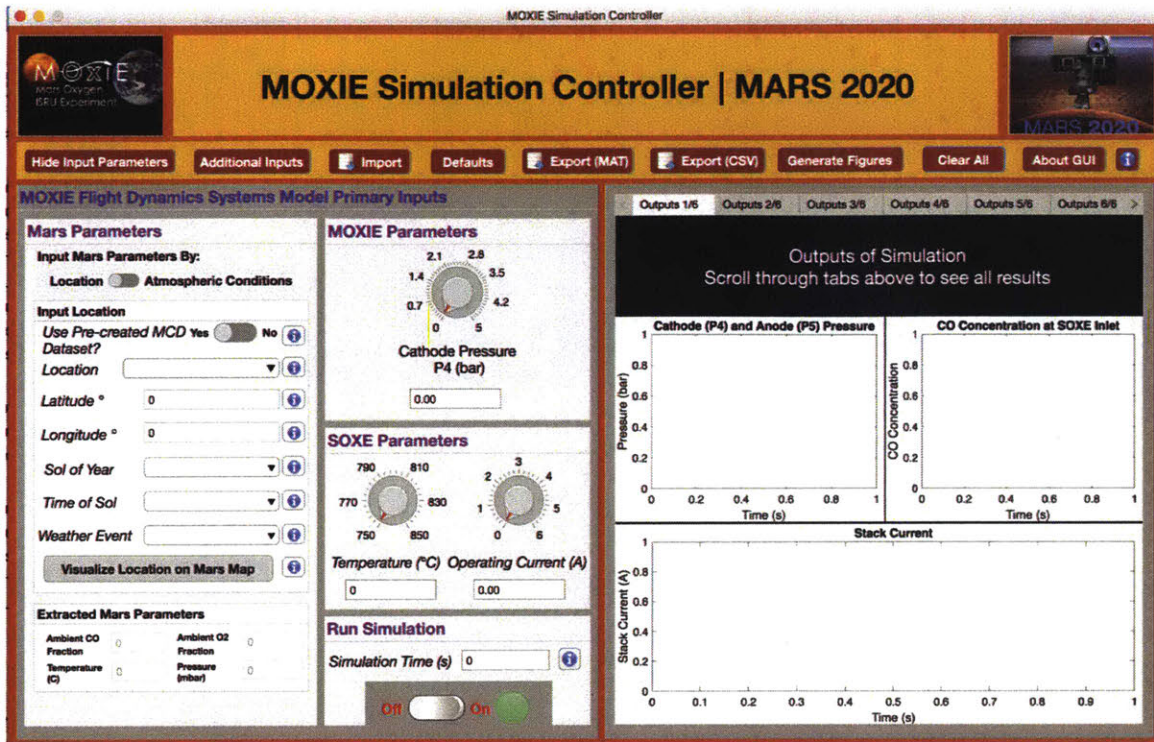


Figure 39: Graphical User Interface (GUI) that controls the MOXIE dynamic Simulink model in an easy-to-use format

On the left half of the GUI are the inputs that a user might want to change in order to see how they affect oxygen production performance of MOXIE. These include the physical location of MOXIE on Mars, whether or not there is a special weather event like a global dust storm, and the pressure and temperature set points of SOXE. The right half of the GUI contains several tabs of output figures that populate when the simulation is finished running. These show time-series plots of oxygen production, internal pressure, stack current, and gas composition, among others.

An example of the GUI after selecting inputs and running it is shown in Figure 40.

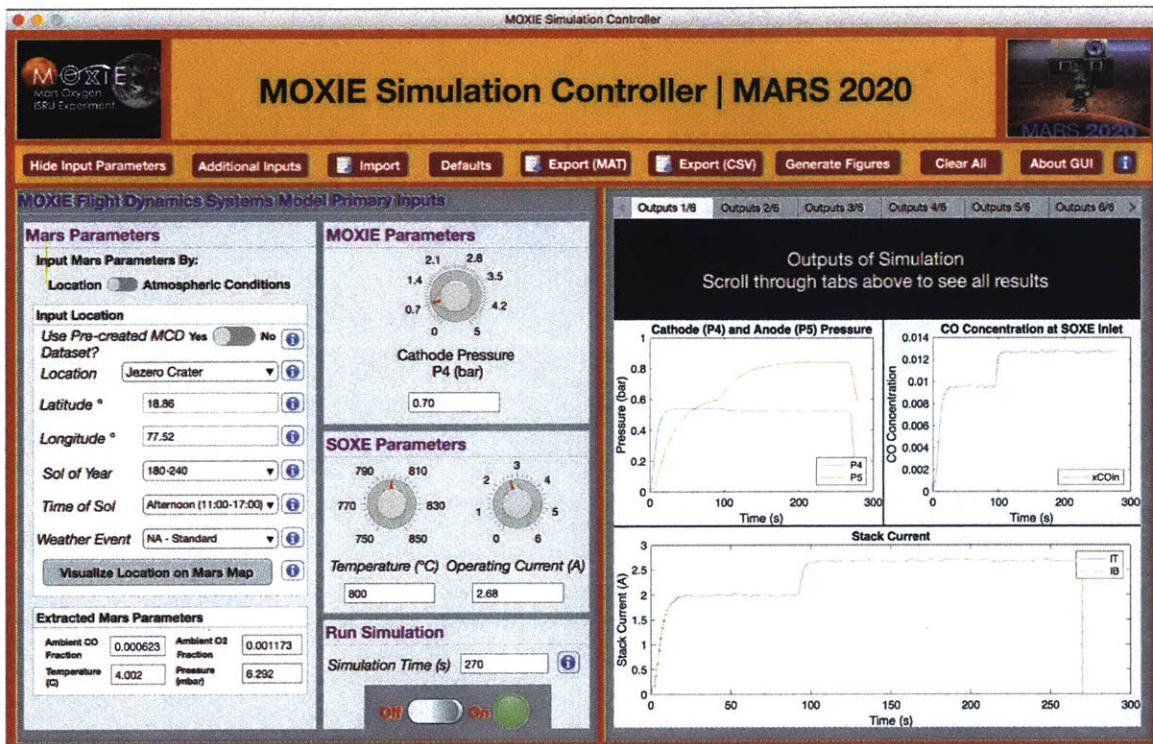


Figure 40: GUI interface after selecting inputs (on the left half), running it, and displaying the outputs (on the right half)

As can be seen, the user selected various inputs on the left half of the GUI, clicked the button below “Run Simulation”, and the simulation ran and yielded the output graphs on the right side of the GUI. The overall process flow of this system is:

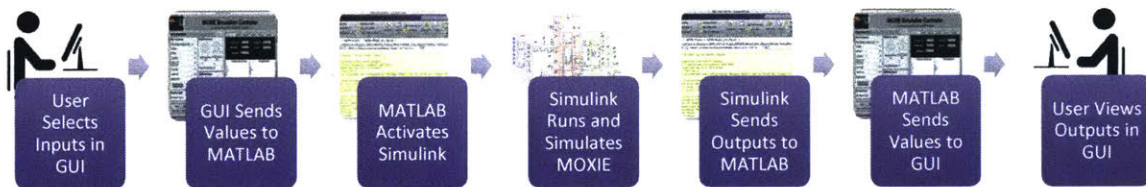


Figure 41: Process flow of GUI and its interactions with the MATLAB script and associated Simulink model.

The inputs and outputs will be described in more detail in the following sections.

3.4 GUI Input Parameters

Four distinct sections that control inputs to the model can be seen in Figure 40. These are the Mars Parameters, MOXIE Parameters, SOXE Parameters, and Run Simulation sections. The values chosen for all of these inputs change the way that the Simulink model is run. Each will now be looked at in more detail, with the exception of the Run Simulation section, as it is simply the simulation run time.

3.4.1 Mars Parameters

Figure 42 shows the various Mars parameters that can be changed by the user. The idea behind choosing these values is that the surface temperature, pressure, and atmospheric composition on Mars vary depending where you are on the planet, what sol of the year it is, and what time of that sol you decide to turn MOXIE on. For example, if you were to run MOXIE at Jezero Crater in the Martian winter and at night, you would see significantly different results than when running at Mawrth Vallis in the summer at high noon. For these reasons, the user is prompted to specify when and where they want to simulate running on Mars.

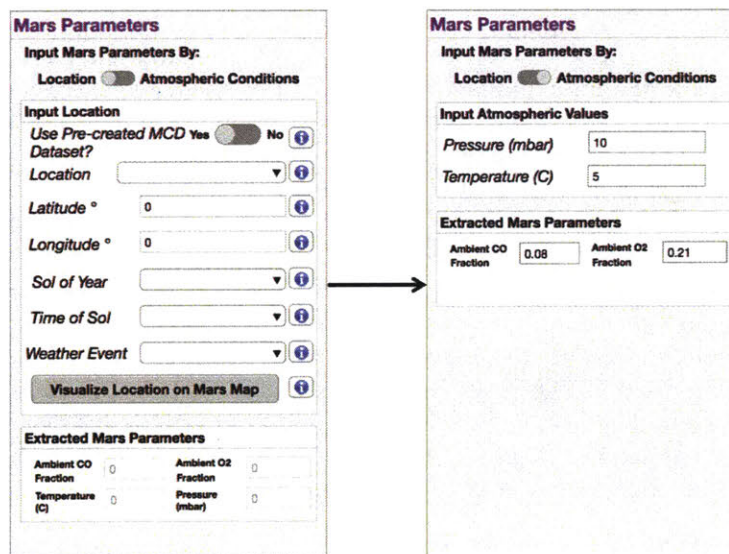


Figure 42: Selecting a location on Mars

The left side of Figure 42 demonstrates the default way in which a user will input Mars parameters. By choosing a location or a latitude and longitude, the GUI will import data for that position on Mars from the Mars Climate Database, a large atmospheric database for Mars built and maintained in Europe. After selecting a location, the user is then prompted to input a value for Sol of Year, Time of Sol, and optionally, a special Weather Event. With this information, the GUI is able to identify the average temperature, pressure, and composition of the atmosphere. If, however, the user wishes to simply input a pressure and temperature without worrying about the location or time on Mars, he or she is able to do that by selecting the “Atmospheric Conditions” options on the switch at the top of the box. This is shown in the right side of Figure 42.

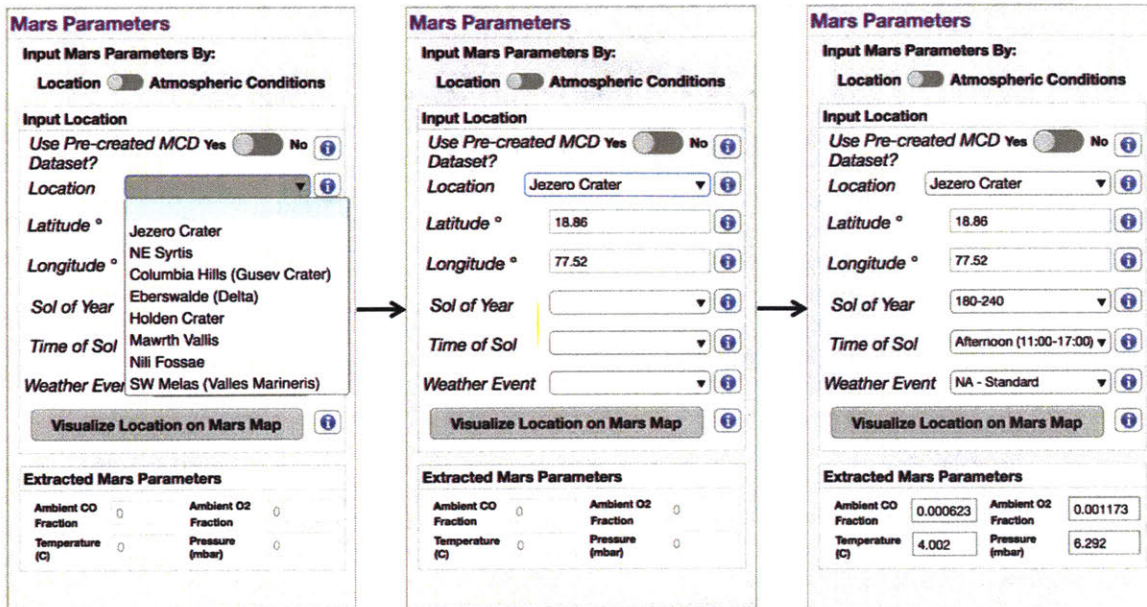


Figure 43: Demonstration of the process used to select atmospheric conditions on Mars

Figure 43 demonstrates the process a user would follow in order to import atmospheric data using the location method. The user can either define his or her own latitude and longitude coordinates for anywhere on the planet or choose from a drop-down list of preselected sites. When a preselected site like Jezero Crater is selected, it will automatically fill in the precise latitude and longitude of that location on Mars as shown in the middle box of Figure 43. Eight sites were pre-programmed into the GUI, and these eight were chosen from the top eight candidate landing sites for the Mars 2020 rover from NASA’s Jet Propulsion Laboratory. If the user wants to choose a location other than one of the preselected options, he or she may leave the “Location” drop-down menu blank and instead manually type in a latitude and longitude for the site. The next input is the Sol of Year, which ranges from 0 to 668. Just as the Earth has 365 days, Mars has 668 sols. Similarly, the user needs to specify the time during that sol that they wish to run MOXIE. The Martian day is slightly longer than an Earth day, and as such, the user can choose half-hour increments starting at 00:00 (midnight) and ending at 24:30 (just a few minutes before the next day’s midnight).

The last option for the user to specify is if they want a special weather event to be modeled. Mars is known for having global dust storms, but more importantly, the dust content and solar UV penetration into the atmosphere changes throughout the year in somewhat unpredictable ways. For this reason, the user can select from options like “Solar Minimum”, “Solar Maximum”, “Global Dust Storm”, and “Low Dust Scenario”. When selected, each of these options applies a specific multiplier to the set of data returned from the Mars Climate Database in order to reflect the effect of an unusual solar or dust situation. In the case of solar activity, increased UV penetration into the atmosphere will increase the average temperature near the surface of the planet. This is taken into account and represented with the temperature predictions put forth by the Mars Climate Database model. Using the same logic, when a global dust storm scenario is selected, the UV penetration to the surface is drastically reduced, resulting in a decrease in surface temperature. This is the net effect of the dust storm temporarily raising the albedo of Mars. The Mars Climate Database will adjust the

temperature of the chosen location on Mars in accordance with whatever weather effect is selected, which will ultimately affect the performance of MOXIE.

When all of the inputs are complete, the “Extracted Mars Parameters” box automatically populates with atmospheric composition, pressure, and temperature data from the Mars Climate Database, as shown in the right box of Figure 43. These values will then be sent to the model when the simulation is started.

3.4.2 MOXIE and SOXE Parameters

After specifying the Mars parameters, the user will need to enter a few MOXIE and SOXE parameters to complete the inputs section. As seen in Figure 39, the MOXIE parameters solely consist of internal pressure. Previously, the recycle flow rate was also available, but was removed due to the inability to change it once it is sent to Mars. The recycle flow rate value refers to the amount of the flow from the outlet of the cathode that is recycled to the beginning of MOXIE. The reason that a recycle loop is necessary in MOXIE is largely as a measure to prevent oxidation of the nickel cathode through the introduction of CO into the stream. The internal pressure, on the other hand, refers to the pressure of the gas on the cathode side of the electrode. Initially, MOXIE was intended to be run at an internal pressure of 1 bar, but that has since been reduced to 0.7 bar for a variety of reasons. A benefit of the GUI is that the user can easily run back-to-back simulations with different internal pressure set points in order to determine the difference in MOXIE performance between the two scenarios.

The SOXE parameters that can be altered on the front page of the GUI are the temperature and operating current. These are both critical values that have large effects on the performance of MOXIE. Increasing the temperature too much will cause coking to occur in the cell, which reduces performance. Lowering the temperature too much will cause the desired reaction to slow and oxygen production to fall. These effects can be observed by running simulations with different temperature set points. Similarly, the operating current is a critical parameter. Increasing the operating current set point will result in a higher level of oxygen production. However, increasing it too much could result in a blown fuse on MOXIE. It should be noted that this architecture assumes that MOXIE will be operated with current control. It is also possible for MOXIE to be operated with voltage control, where a voltage setpoint is commanded to the stack. In this case, the GUI would be altered to allow for the voltage setpoint to be chosen by the user instead of the current setpoint.

All of the SOXE and MOXIE inputs can be changed with the rotational knobs seen in Figure 39 or by typing an exact number into the box below the dials.

3.4.3 Additional Inputs

While the most critical inputs were included in the GUI, many more exist in the MATLAB file that is controlled by the GUI. To access and change these, the user should select the “Additional Inputs” button in the GUI toolbar. This opens a second interface that allows users to change any input value apart from those that are physical constants (i.e. thermal conductivity of materials, etc.). This secondary interface is shown in Figure 44.

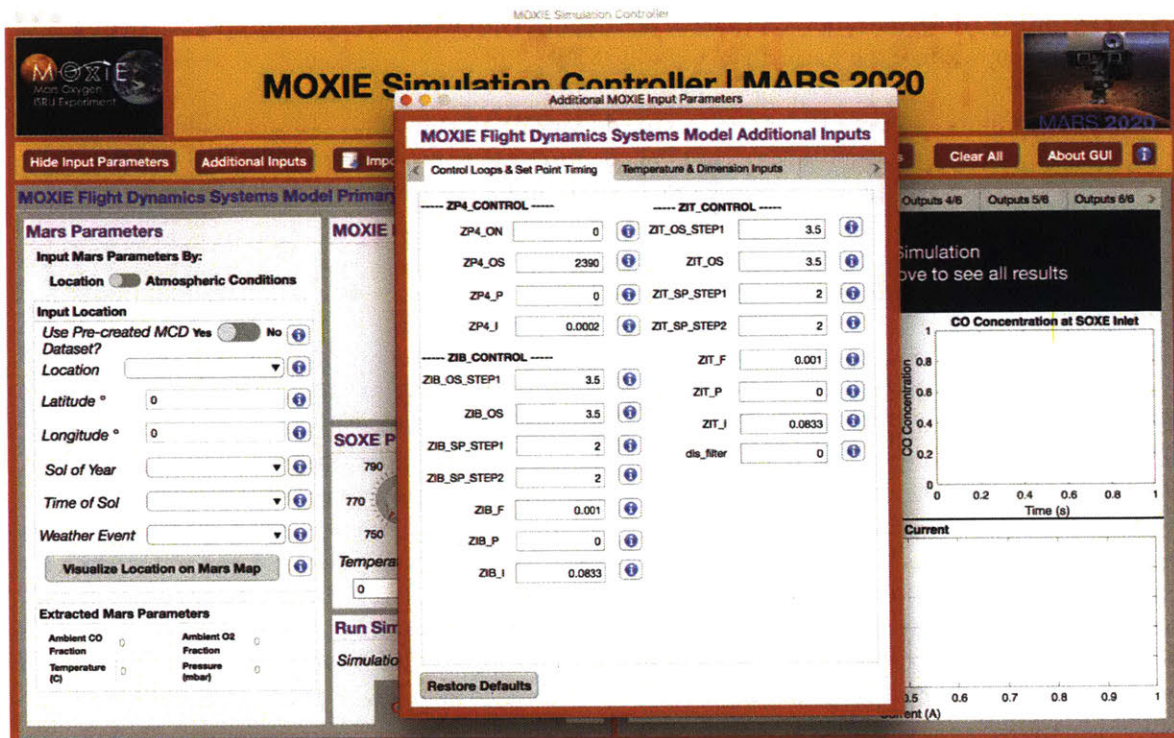


Figure 44: Additional Inputs interface for changing secondary variable values

This “Additional Inputs” GUI has several tabs that allow the user to change nearly every variable associated with the Simulink model. Additionally, should the user wish to return to the default values for the additional inputs, he or she simply needs to click the “Restore Defaults” button at the bottom of the window.

3.5 GUI Outputs

The right-hand side of the GUI displays outputs from the Simulink model after it has run. Several tabs are included, each displaying information valuable to the user. The following outputs are shown graphically versus time in the output tabs:

1. Cathode Pressure
2. Anode Pressure
3. CO Concentration at the Inlet of SOXE
4. Top Stack Current
5. Bottom Stack Current
6. Composition of Gas at the Cathode
7. Composition of Gas at the Anode
8. Utilization Rate of CO₂
9. RPM of Scroll Compressor Motor
10. Voltage Applied to SOXE Stacks
11. Activation Voltage for each cell
12. Nernst Potential for each cell
13. Intrinsic ASR for each cell
14. Temperature for each cell

In addition, a table displaying the maximum and average values for each of these variables is displayed in the final output tab. This offers a quick and easy way for the user to compare performance between different test runs. The first tab of the outputs can be referenced in Figure 40.

3.6 GUI Extras

In addition to the functionalities already described, the GUI offers some additional options to the user that are useful. These all lie in the toolbar on the GUI. A cut-away view of the toolbar by itself is shown in Figure 45.



Figure 45: Toolbar of the GUI with extra user options

Hide Input Parameters

Clicking the “Hide Input Parameters” button removes all of the input parameters from view. This allows the user to view larger output plots, as shown in Figure 46.

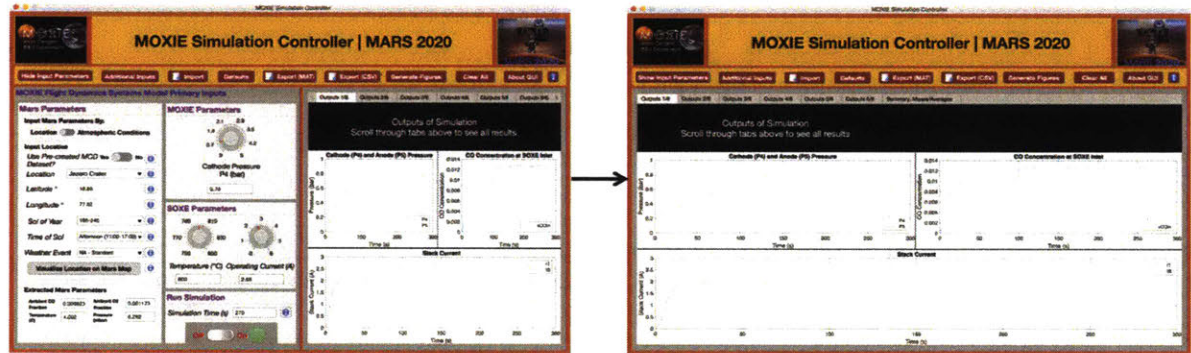


Figure 46: Demonstration of the “Hide Input Parameters” button

The inputs are still logged in the GUI and can be brought back into view by clicking the “Show Input Parameters” button that appears in the same location as the “Hide Input Parameters” button after the latter is clicked.

Additional Inputs

The “Additional Inputs” button has already been described. When clicked, it opens up a secondary GUI that gives the user total control over all variables that affect the MOXIE simulation, apart from physical constants.

Import

The “Import” button allows the user to import previous simulations. When a previous simulation file is loaded, it will import both the inputs and the outputs of that simulation.

Defaults

The “Defaults” button gives the user a quick way to run a standard simulation. It auto-fills all of the inputs with values that are expected for an average run of MOXIE on Mars. This saves the user time from entering all of the input values if they simply wish to view an average run or make adjustments to a small number of inputs.

Export (MAT)

The “Export (MAT)” button allows the user to export a simulation as a .mat file. This is a standard MATLAB file format and is therefore easy to import back into MATLAB. It will export both the inputs and the outputs of the simulation.

Export (CSV)

The “Export (CSV)” button has the same functionality as the “Export (MAT)” button but exports the file as a Comma-Separated Value file. This file format is easy to open in workbooks like Microsoft Excel.

Generate Figures

The “Generate Figures” button opens the output plots in a separate window so that they can be printed or saved.

Clear All

The “Clear All” button restores all input values in the main GUI to zero. This is useful when the user wants to reset the GUI template.

About GUI

The “About GUI” button gives information on the GUI, including an overview of GUI functions and developer contact information.

3.7 Run Control Table

Operational commands will be sent to MOXIE by a Run Control Table (RCT). This is a time series of commands, primarily composed of set points. An example of an RCT is shown in Figure 47.

Step	Control Loop Setpoints										Enable Flags (full names are *_*_en)	Time Transition	Condition	Cumulative Time	Comments
	ZIT_SP(°C)	ZTB	ZT1_SP(°C)	ZP3_SP(hbar)	ZP3_OS(RPM)	ZIT_SP(A)	ZIT_OS(V)	ZTB_SP(A)	ZTB_OS(V)	HT HB H1 CS ML VT VR					
0	0	0	0	0	0	0	0	0	0	0	0	1s		1s	Initialization
1	800°C	800°C	0	0	0	0	0	0	0	0	1100000	50min		1s	SOXE Warmup before CAS
2	800°C	800°C	25°C	0	0	0	0	0	0	0	1110000	10min		3001s	SOXE and CAS Warmup
3	800°C	800°C	25°C	0	0	0	0	0	0	0	1111000	30min		3601s	SOXE and CAS Warmup w/CAS enabled
4															Then enable operational SOXE temperature limits
5	800°C	800°C	25°C	1	3000	0	0	0	0	0	1111100	1s		5401s	Pump on
6															Then enable operational P3 limits
7	800°C	800°C	25°C	1	3000	1.70A	4.55V	1.70A	4.55V		1111111	30s		5411s	SOXE voltage step 1 of 4 (4.5V is the min voltage in the SLX requirements)
8	800°C	800°C	25°C	1	3000	3.5A	4.55V	3.5A	4.55V		1111111	10s		5421s	SOXE voltage step 4 of 4
9															Then enable operational SOXE current limits
10	800°C	800°C	25°C	1	3000	3.5A	4.55V	3.5A	4.55V		1111111	90min		5431s	Oxygen Production
11	800°C	800°C	25°C	1	3000	0	0	0	0	0	1111100	1s		10831s	SOXE voltage off, begin disabling operational limits
12	800°C	800°C	25°C	0	0	0	0	0	0	0	1111000	1s		10832s	Pump off
13	0	0	0	0	0	0	0	0	0	0	0	1s		10833s	Heaters and CAS off
END	0...														7 Special 'END' character (TBD)

Figure 47: Run Control Table example for MOXIE

The actual template for MOXIE RCTs is not yet finalized; however, this is the baseline that is currently being used by JPL and MIT. The first column represents the step in the sequence. Columns 2 through 10 represent the values of each variable that will be commanded at each step.

These variables include temperature, voltage, and current set points. Finally, columns 12 and 13 are the time duration of each step.

The process for an RCT to be uploaded and executed on Mars is as follows. First, an RCT will be developed at either JPL or MIT. Before being sent to Mars, it will be tested on the software model and the engineering model (EM) to ensure that it will not adversely affect the real unit on Mars. To run the RCT on the software model, it will be imported into the main GUI and act as an inputs source. This capability is currently under development. If the model determines that the RCT produces safe results and will not harm MOXIE, it will then be tested on the MOXIE EM in the test facility at MIT. If this also has positive results, it can begin the process of being sent to Mars for actual execution.

3.8 GUI Implementation with the MOXIE Team

The GUI will be a useful tool as the MOXIE team moves into the data analysis, integration and testing, and operations phases of its mission in the coming years. For this reason, in March, 2018, the GUI was sent to 20 members of the MOXIE Science Team and select members of the JPL MOXIE team. The goal was to have those members run the GUI on their own computers as beta testers. In addition, they were asked to provide feedback on the usability of the GUI and what they hoped to see in future versions.

The response from the team was positive. Small-scale suggestions were made, including changing the title of one of the graphs, adding an indicator to show that the model was running, and removing warnings from the command window of the MATLAB application. This feedback was taken into consideration and updated in the most recent version of the GUI. In terms of larger-scale attributes like functionality and performance, the team members were satisfied.

Chapter 4: Vacuum Chamber Design and Development

4.1 The Need for Vacuum Chambers

Part of the agreement between MIT and JPL for the MOXIE project was that a significant portion of testing would be conducted at MIT. In the end, this included testing of the following hardware components:

1. Flight-like gas sensors
2. SOXE stacks
3. “Flat-sat” Engineering Model
4. Flight Configuration Engineering Model

Only the first on this list, the flight-like gas sensors, is covered by this Master’s thesis and therefore has its own chapter. Testing on the other three pieces of hardware will be conducted in the future and covered in the subsequent Ph.D. dissertation.

In order to accurately test any of these systems, it is first necessary to have a Mars analogue environment to place them in. Sensors, SOXE stacks, and full-on MOXIE configurations behave differently at Mars pressure and temperature than they do at Earth ambient conditions. For this reason, a temperature-controlled vacuum chamber is the obvious testing apparatus choice to simulate the Mars environment.

It was decided that a minimum of two vacuum chambers would be built to test all of the hardware mentioned. The first vacuum chamber will be used to characterize the flight-like gas sensors, the need for which will be described in more detail in Chapter 5. The second vacuum chamber will be used to test SOXE stacks, the MOXIE flat-sat engineering model, and the MOXIE flight configuration engineering model (EM). A flat-sat is essentially an unfolded version of MOXIE. All components, including the compressor, SOXE stack, and VFCD board, are laid out and connected on a flat surface inside the chamber. The flight-like EM, on the other hand, is an identical copy of the MOXIE unit that is going to Mars. The vacuum chamber for the SOXE stacks and these two pieces of hardware could be shared. In addition, it will be substantially larger and will require a wider range of controls than the chamber used to characterize the gas sensors.

4.2 Sensors Vacuum Chamber Design

In order to test the flight-like gas sensors on a tight timescale, a small vacuum chamber had to be quickly designed and constructed. The sensors likely could have been tested in the full-scale flat-sat / EM vacuum chamber, but it would have delayed the timeline unacceptably.

Requirements for the sensors vacuum chamber were derived in order to inform its design. Table 2 shows the preliminary list of requirements.

Table 2: Requirements for Sensor Vacuum Chamber

Requirement #	Indicator	Description
VS-01	Pressure	The vacuum chamber shall be operable from Mars pressure (5 mbar) to slightly above Earth sea-level atmospheric pressure (1.2 bar).
VS-02	Temperature	The vacuum chamber shall be controllable from -25 °C to 70 °C.
VS-03	Gases	The testing setup shall allow for custom mixes of CO ₂ , CO, and N ₂ gases.
VS-04	Purging	The testing setup shall be designed with a nitrogen purging system.
VS-05	Extra Gases	The tubing and valving system shall be designed to accommodate up to four total gas tanks: CO, CO ₂ , N ₂ , and O ₂ .
VS-06	Regulation	Each gas tank shall have a regulator to reduce pressure of the gas to 0-15 PSI prior to it entering the vacuum chamber.
VS-07	Electronics	The system shall be capable of recording outputs of up to three sensors in the vacuum chamber at one time.
VS-08	Extensibility	The pump and pump controller should be extensible to the flat-sat vacuum chamber setup.

With these requirements in mind, it was possible to design the sensors vacuum chamber. It went through several iterations, and the final design of the chamber is shown in Figure 48.

MOXIE Sensors Vacuum Chamber

Created by Eric Hinterman
Modified Feb 7, 2018

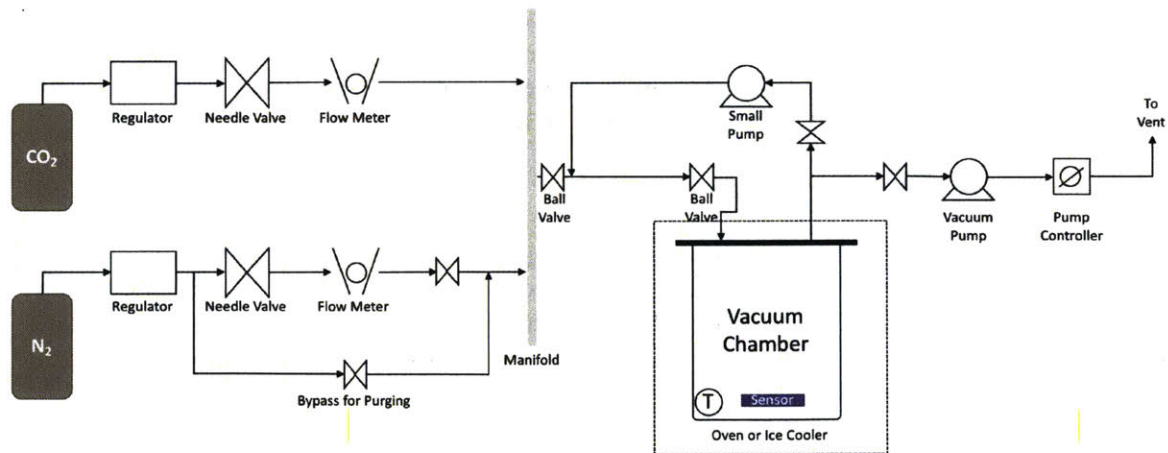


Figure 48: Design of Sensors Vacuum Chamber

Pressurized gas cylinders flow their contents through a regulator, needle valve, and flow meter and into the central gas manifold. The composition of gas flowing into the vacuum chamber can be controlled with these individual flow meters. The chamber itself is housed either in an ice box, if

cooling is desired, or wrapped in strip heaters, if heating is desired. When purging, the gas flows into the vacuum chamber, through the sensor(s), out of the vacuum chamber, and through the vacuum pump. From there, the gas is vented into an exhaust hood. When running a test, the gas inside the chamber is recirculated with the small pump shown in the top of Figure 48. The chamber will be filled with gas to the appropriate pressure, isolated by closing the ball valve just after the manifold and the ball valve just before the vacuum pump, and recirculated by turning on the small pump. Additionally, the outlet of the composition sensor is tied directly to the exhaust line out of the chamber lid with 1/8" inner diameter Tygon tubing (not shown). In this configuration, the gas inside the chamber is forced to flow through the sensor yet is not wasted by directly venting it to the exhaust hood. This conserves gas while still providing flow through the sensor, which is ideal for sensor operation.

A side view of the design of the vacuum chamber, showing the sensors and tubing alignment, is shown in Figure 49.

SENSOR VACUUM CHAMBER FLOW-THROUGH DESIGN

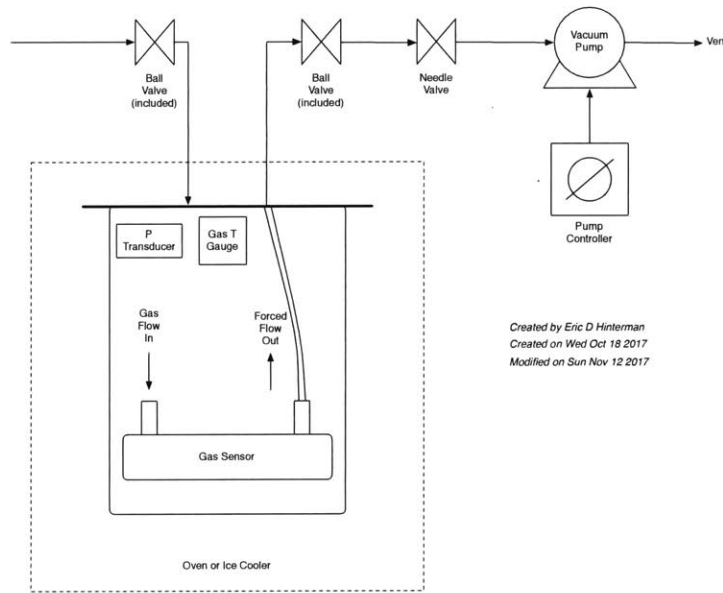


Figure 49: Sensor Vacuum Chamber Internal Design

It is important to note that the final design included this flow-through approach for the gas sensor. Rather than using a static approach, where the sensor would be placed in the chamber without any tubing and turned on, a tube is attached to the outlet of the gas sensor and directly tied into the recirculation line. This ensures that gas is pulled through the sensor when the pump is operating. As mentioned, this was a necessary step to take because the SmartGas sensors rely on flow in order to operate effectively.

An image of the actual chamber setup behind cleanroom curtains is shown in Figure 50.



Figure 50: Sensors vacuum chamber setup with vacuum chamber, pump, and pump controller visible. An inch ruler is added for scale.

The chamber is on the left side of the figure, the pump controller is in the middle, and the vacuum pump is on the right side. Tygon tubing of 1/4" inner diameter and 3/8" inner diameter was used to connect these systems in a series configuration.

The top of the chamber lid was another design challenge. Only two pre-drilled holes in the lid existed, and there was a minimum of four pieces of equipment that needed to be tied into these holes. To accommodate this design without drilling additional holes, two manifolds were ordered and installed that allowed all four pieces of equipment to operate with their intended functionality. A schematic of the design is shown in Figure 51 with an image of the finished product shown in Figure 52.

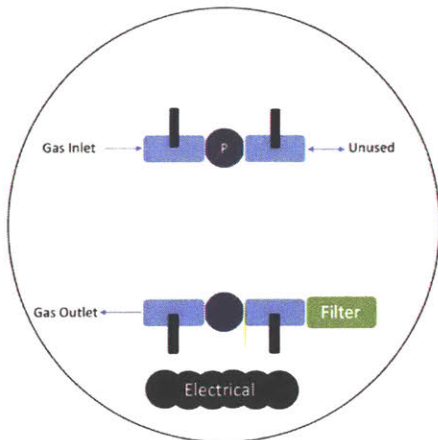


Figure 51: Design of sensors vacuum chamber lid (top-down view)

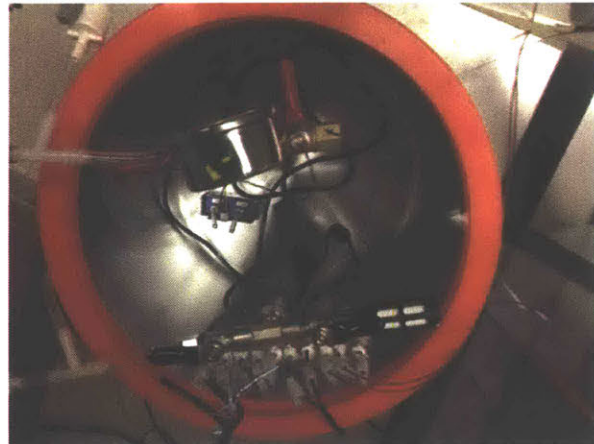


Figure 52: Top view of sensors vacuum chamber lid with both valving manifolds visible

As the figures indicate, five paths into or out of the chamber were actually accommodated with the dual-manifold system. In order from top-left to bottom-right of the figures, these are: the gas inlet line, the pressure gauge (denoted with a “P” in Figure 51 and rising vertically from the lid in Figure 52), an unused port, the gas outlet line, and an air filter. The gas inlet line allows gas to flow in from either the compressed gas cylinders or from the recirculation loop. The pressure gauge is used to read the level of vacuum currently being pulled in the system. The gas outlet line allows gas to either flow out of the system to the vent or into the recirculation loop. Finally, the filter allows the chamber to be re-pressurized with ambient air without allowing dust or other particulates to enter the chamber when its inline valve is opened.

Electrical feedthroughs were also a design challenge. In order to transmit information from each sensor to the computer, a minimum of 7 cables had to be passed through the lid of the vacuum chamber without causing any leaks. To do this, 1/4” holes were drilled in the lid and single-stranded, 18-gauge copper wire pieces were passed through. After applying a vacuum epoxy to fill the gaps around the wire in each hole, a leak-proof electrical contact was created that could be accessed from inside the chamber and outside. Next, the USB and power cables from the sensor were cut in half and partially stripped. They were affixed to the copper feedthroughs by way of standard AMP connectors [21]. A side view of the chamber that demonstrates these feedthroughs with their AMP connectors is shown in Figure 53.

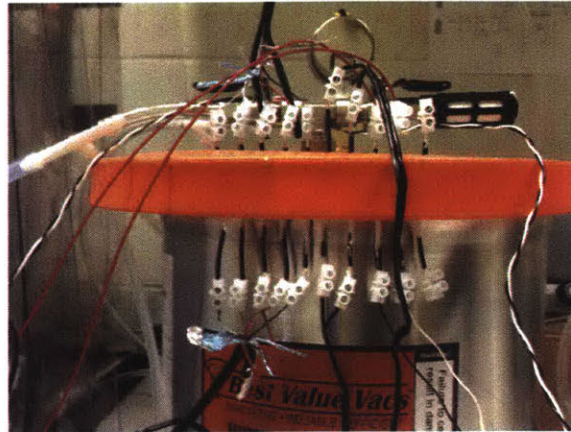


Figure 53: Electrical feedthroughs for the sensors vacuum chamber

In addition to the sensor feedthroughs, two lines were added for the thermocouple wiring. The thermocouple will be used to measure temperature inside the chamber for tests that require cooled or heated conditions.

The details and motivation for testing the gas sensors in this chamber are provided in Chapter 5.

4.3 Flat-sat and EM Vacuum Chamber Design

The flat-sat vacuum chamber design went through a similar design phase to the sensors vacuum chamber. At this point, it is unclear whether or not the vacuum chamber for the flat-sat and EM will be built by MIT or JPL. Initially the plan was to build it at MIT, and this brief section will show the designs for this chamber. However, recent talks have indicated that JPL might build a duplicate of their own planned vacuum chamber to send to MIT in order to cut down on design complexity and save time. This will also help ensure consistency between MIT and JPL results and allow the comparison of data taken at both locations.

The pump and pump controller that were purchased for the sensors vacuum chamber were intentionally oversized so that they could also be used for the larger flat-sat and EM vacuum chamber. Two options exist for the layout of the future MOXIE testbed laboratory at MIT with respect to the vacuum chambers. The first is to have the two vacuum chambers completely separate, so that both can run different experiments at the same time. A more integrated option also exists, which is to have both chambers linked to the same gases, vacuum pump, and pump controller. This latter option is shown in the following design.

DUAL VACUUM CHAMBER DESIGN

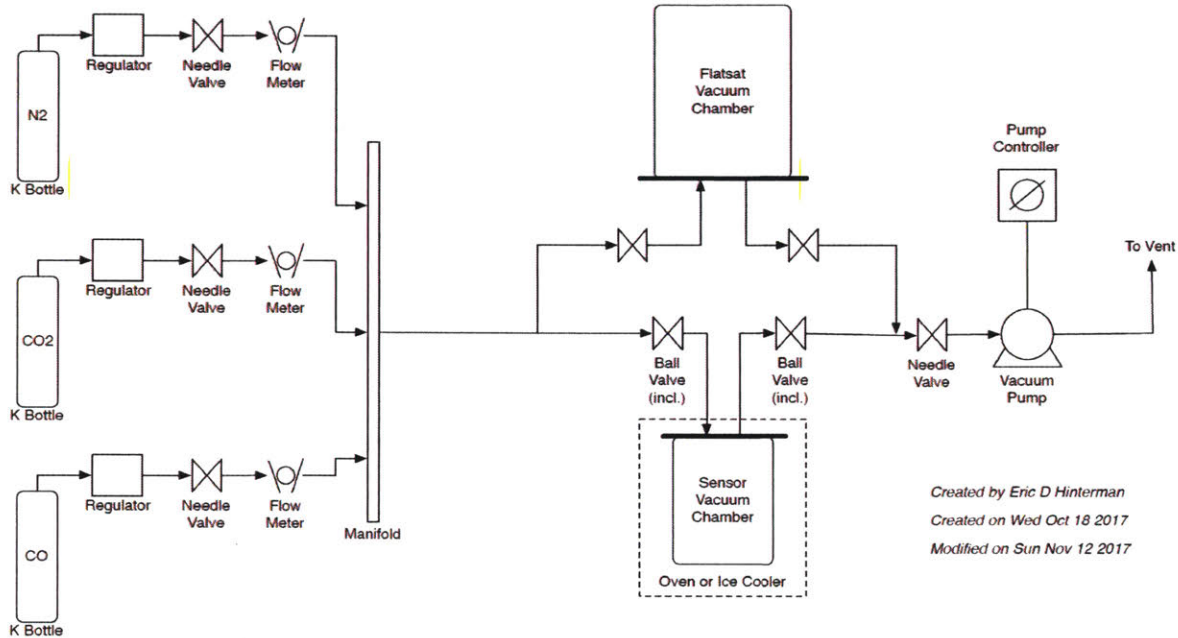


Figure 54: Integrated design where both vacuum chambers utilize the same gases, vacuum pump, and pump controller

As Figure 54 indicates, both vacuum chambers would use the same pump and pump controller, thus reducing overall cost and system complexity. In addition, they can use the same feed gases, manifold, and vent line. This design will significantly reduce the clutter in the MOXIE lab and save setup time for future experiments. In theory, both chambers could even be run at the same time if operating under the same pressure, although it may require some coordination to ensure that both chambers receive their desired mix of gases.

4.4 Vacuum Chamber Facilities Design

With requirements and designs in hand for the vacuum chambers, it was necessary to lay out the design for the laboratory that would house the chambers and its associated mission control center. Two adjacent rooms on the ground floor of Building 37 in MIT's Department of Aeronautics and Astronautics were selected as the future site for operations. One room will serve as the mission control center, and the other will hold the vacuum chambers. Additionally, an adjacent open space will be used as a conference room. The first step towards designing the rooms was to lay out the requirements of the facilities. A preliminary list of these requirements is detailed in Table 3.

Table 3: Requirements for Vacuum Chamber Test Facility

Requirement #	Indicator	Description
TF-01	Exhaust	The test facility shall have adequate exhaust (hood or direct exhaust lines) to remove N ₂ , CO ₂ , CO, O ₂ , and H ₂ from the vacuum chambers.
TF-02	Ventilation	The test facility shall include adequate air circulation to meet MIT safety's specifications.
TF-03	Power	The test facility shall provide AC 115 V / 60 Hz outlets for power.
TF-04	Cooling	The vacuum chamber room (VCR) test facility shall include a liquid nitrogen cooling system for the flat-sat vacuum chamber.
TF-05	Layout	The test facility shall include two adjacent rooms separated with a door: a vacuum chamber room (VCR) and a control center room (CCR).
TF-07	Sensors	The VCR shall include an oxygen sensor and a carbon monoxide sensor, with readouts of current levels of each gas on every entrance to the room.
TF-08	Sensors	The CCR shall have a panel with access to gas sensor readings from VCR.

These facilities requirements are just a start. The plan is continuously evolving and will be a coordinated effort among faculty, facilities personnel, MIT Haystack, graduate students, and JPL.

Chapter 5: Sensors

5.1 Introduction to the Sensors

MOXIE hosts a suite of sensors that track various aspects of its state. These include the temperature, pressure, and composition of the gas flowing through the system. The purpose of the sensors is to inform and control. For example, the temperature sensors near the heater carriers for the top and bottom stacks of SOXE are used as the signal for the thermal feedback control loop. A schematic displaying various sensors on MOXIE is shown in Figure 55.

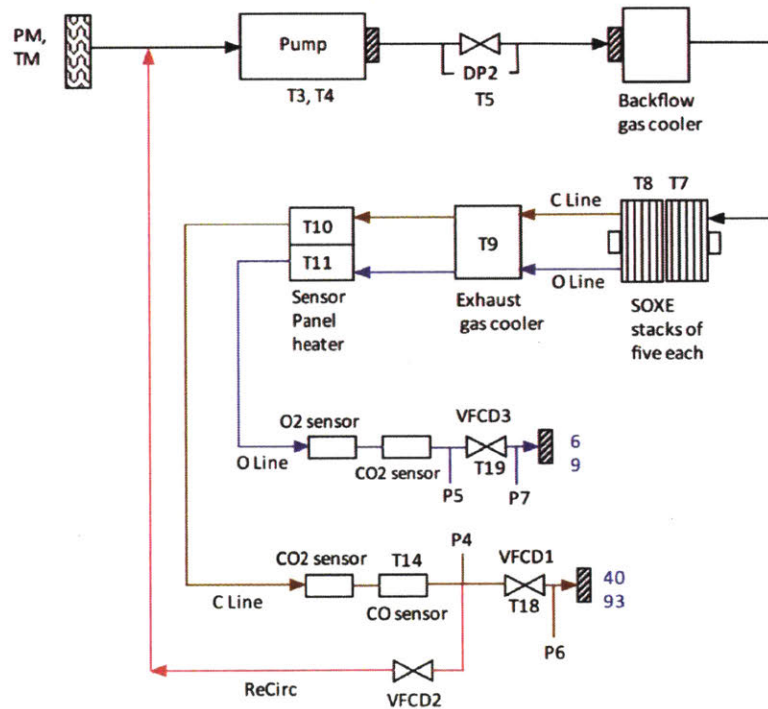


Figure 55: Temperature, pressure, and composition sensors of MOXIE

The schematic depicts the flow of gas through MOXIE, beginning from acquisition from the Mars atmosphere and ending with venting back to the Mars atmosphere. All sensors labeled “T” represent temperature sensors and those labeled “P” represent pressure gauges. “TM” refers to the temperature of Mars’ atmosphere and “PM” represents the pressure of Mars. In addition, the figure indicates the location of the various composition sensors, as labeled by “O₂ sensor”, “CO sensor”, and “CO₂ sensor”. Finally, “VFCD” refers to the Viscous Flow Control Devices used to control the flow rate of the gas through the system.

With an overview of the sensors and their locations now in mind, the following chapter will focus on the characterization and calibration testing plan for the composition sensors. While no data have yet been collected, the designs and planning leading up to data collection will be presented. Other sensors will not be covered here.

5.1.1 Anode and Cathode Composition Sensors

Four composition sensors are being flown on MOXIE:

1. Oxygen sensor, 0 – 100%
2. Carbon Dioxide sensor, 0 – 5%
3. Carbon Monoxide sensor, 0 – 100%
4. Carbon Dioxide sensor, 0 – 100%

The first two sensors are used to measure the output gas stream from the SOXE anode. This stream is expected to be nearly pure oxygen. However, there is the potential that some leaks may occur in the system, which would allow small amounts of carbon dioxide to pass through to the anode. This is why a sensor that measures 0 – 5% CO₂ is placed on the anode with the oxygen sensor. It is also worth noting why a carbon monoxide sensor is not needed on the anode. Even though carbon monoxide could leak through to the anode, it would immediately recombine with oxygen to produce carbon dioxide. Thus, an oxygen sensor and carbon dioxide sensor are sufficient to measure all expected gases of interest from the anode outlet.

The latter two sensors are used to measure the output gas stream from the SOXE cathode. This stream will have a higher variance in terms of composition than the anode stream for a couple of reasons. First, during the startup phase of each run, the composition of the cathode outlet will be nearly pure CO₂ from the Mars atmosphere. As the voltage in SOXE ramps up, the CO₂ will begin to react on the electrolyte and will break down into CO and O⁻, thus introducing CO into the sensors' stream. Second, the MOXIE team may choose to vary the “utilization rate”, or the amount of CO₂ that is converted into CO and O⁻, between runs. This would introduce even more variance in the composition of the cathode gas stream. For these reasons, two sensors will be placed at the outlet of the cathode stream that measure 0 – 100% composition for CO and CO₂. It is again worth noting that even though a leak could occur that allows oxygen to move from the anode to the cathode, it would quickly react with CO to make CO₂ before reaching the sensors. Thus, an oxygen sensor is not needed on the cathode side.

5.1.2 IR and Luminescence Sensors

All of the composition sensors, with the exception of the O₂ sensor, use the nondispersive infrared radiation (NDIR) method to detect concentration. The main components of the sensors are the infrared source, the chamber itself, and the infrared detector. In this method, infrared radiation is passed through the gas residing in the sensor's chamber, and the resulting spectrum is read at the detector. By analyzing the frequency bands that were attenuated in the chamber, it is possible to determine the composition of the gas.

The oxygen sensor is a luminescence sensor. Its purpose is to measure the concentration of oxygen in the gas stream coming from the anode of SOXE. It is expected that this stream will be greater than 99% pure oxygen, so the sensor should only see values between 99% and 100% oxygen. However, in the instance of a leak, for example, it may read lower values due to the presence of carbon dioxide.

5.2 Motivation for Characterization and Calibration

Several valid reasons exist to characterize and calibrate the sensors in the lab prior to their flight on the Mars 2020 rover. These include identifying the internal algorithms used by the SmartGas company to calculate composition, testing for cross-sensitivity between gases, measuring the response time of the sensors, and understanding the aging and degradation of the sensors.

During operation, the SmartGas sensors output results using proprietary algorithms that are hidden from the operator. These algorithms include a temperature correction and require occasional recalibration. Unfortunately, the team will not be able to recalibrate on Mars, and so understanding these algorithms is very important. In addition, the current algorithms from the manufacturer do not include any pressure correction factors. Since Mars pressure is just a fraction of Earth's ambient pressure, the algorithms will need to be modified in order to correct for this when Mars data are received.

Cross-sensitivity is another potential issue that needs to be addressed with laboratory testing prior to MOXIE being flown to Mars. SmartGas uses non-dispersive infrared sensors that determine the concentration of a particular gas by measuring the absorption of a light source over a specific frequency band. As a result, there is the potential for interference from a second gas with an overlapping IR absorption spectrum. The potential overlap between CO₂ and CO is shown in Figure 56.

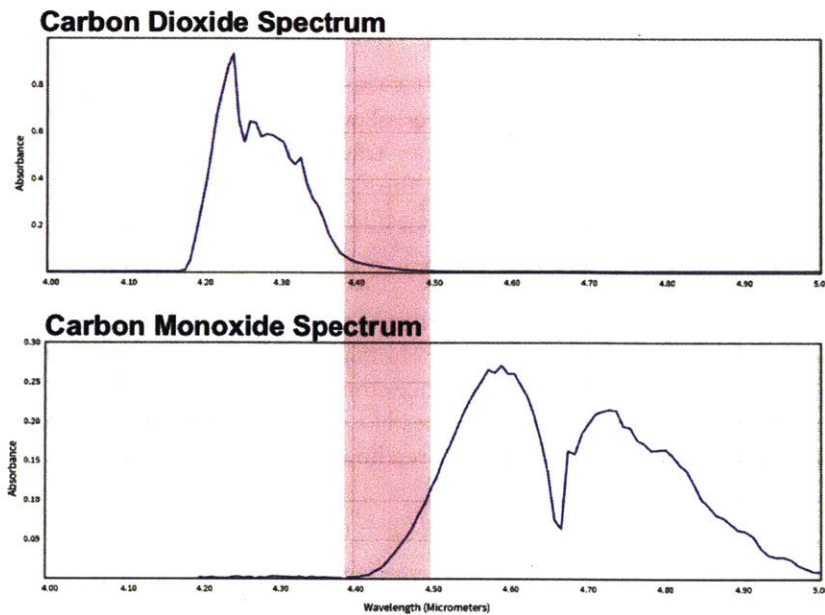


Figure 56: Absorption Spectra for CO and CO₂. Source: <http://webbook.nist.gov/chemistry>

As the shaded region of the figure indicates, a band of frequencies exists where both carbon dioxide and carbon monoxide would demonstrate IR absorption. Therefore, a CO sensor could “detect” CO even if the gas inside the sensor is pure CO₂ due to the false reading from these overlapping spectra. It is important to characterize this cross-sensitivity, as the MOXIE sensors will see both gases during operation. For this to happen, three series of tests will need to be run. First, both the

CO and CO₂ sensors will be placed in a chamber filled with 100% CO₂ and read at various pressures. Next, both sensors will be placed in a chamber filled with 100% CO and read at various pressures. Finally, a mixture of CO₂ and CO gases will be used in the chamber at various pressures. The scenarios with pure gas will indicate the level of cross sensitivity at each pressure tested. For example, the level of detection that the CO sensor reads in pure CO₂ will indicate the cross sensitivity of CO₂ with the CO sensor. The same is true for the CO₂ sensor in a pure CO environment. Then, when a mixture of gases is used, it will be possible to subtract out the levels of cross sensitivity from the true readings of each sensor in order to determine the true composition in the chamber.

The final two reasons for characterizing and calibrating the sensors is to measure the response time and to understand the aging and degradation of the hardware. For the former, it is currently unknown how quickly the sensors respond to a change in gas concentration. Relevant data to solve this unknown will be quick and easy to collect and is important for understanding MOXIE's operation on Mars. In addition, the sensors may be used in feedback control loops, which would require knowledge of their response times. For the latter of the final two reasons, the sensors will eventually degrade. In order to correctly interpret data from Mars, it will be necessary to understand the expected degradation and account for it. It is also important to know this to inform a future, scaled version of MOXIE to support a human mission. In this scenario, the sensors will be operating continuously for months or even years, and it will be very important to understand the expected degradation and its impact on the system.

5.2.1 Modified Beer's Law

The SmartGas sensors that will be used to measure CO and CO₂ from MOXIE are Non-Dispersive Infrared Radiation (NDIR) sensors. They utilize Beer's law to relate the attenuation of light to the composition of the medium through which the light is traveling. In this case, they relate the attenuation of light to the amount of CO or CO₂ in the flow stream. Beer's law is given below:

$$I = I_0 e^{-ktx}$$

where I is the intensity of the signal after it passes through the sample gas, I_0 is the initial intensity, k is the absorption coefficient for the gas and filter combination, l is the equivalent optical path length between the lamp and the detector, and x is the concentration of the gas. Unfortunately, this equation is too idealized to use for practical purposes like MOXIE. Therefore, a modified Beer's law must be employed to fully understand the sensors' readings. This is given below:

$$ABS_x = SPAN(1 - e^{-bx^n})$$

Where ABS is the absorbance and is also equal to $1 - \frac{I}{I_0}$, $SPAN$ is a factor introduced to realize the fact that not all of the IR radiation is absorbed by the gas as it passes through it, and b and n are both factors used to fit the equation to the actual absorption data [22]. A primary purpose driving the experimentation on these sensors is to determine these factors under a range of temperatures, pressures, and concentrations.

In order to fully understand how these gas composition sensors will work on Mars, it is necessary to calibrate and characterize them on Earth. All four sensors are produced with Earth-bound

applications in mind, and as a result, the manufacturers do not have data to show how they operate under Mars-like conditions. Without this information, it falls on the MOXIE team to experiment and provide a basis for calibration and characterization of the sensors.

5.2.2 Calibration

Calibration typically refers to the measurement of properties that vary from unit to unit and that vary with time. All flight, engineering, and flat-sat units should be calibrated, but it is especially important to calibrate the flight model. Calibration takes place throughout the integration, assembly, and testing process of a mission. For Mars 2020, it will also take place during the cruise phase to Mars and on the surface of Mars. For these sensors in particular, it will be necessary to calibrate the “Zero Offset” and the “Span” settings. Zero offset refers to a calibration with 0% of the target gas, while Span refers to one with 100% of the target gas (or in the case of the 0 – 5% sensor, 5% of the target gas). This way, the MOXIE team will understand how the sensors behave at their minimum and maximum expected values during operation. These sensors will be calibrated as a function of concentration, temperature, and total pressure.

Calibrations can take place by referencing an external standard, referencing a known environment, or referencing a well-characterized sensor. For the cruise and surface phases of the MOXIE mission, it is likely that these sensors will be calibrated by referencing a known environment. MEDA is an instrument that is also on the Mars 2020 rover and measures the atmospheric composition. Therefore, a MEDA measurement can be taken to provide known compositional values of the Mars atmosphere (on the surface). The composition sensors can then be turned on and calibrated to these values. This works because both the anode and cathode paths on MOXIE are exposed to the ambient environment from their exhaust ports and therefore should read the same concentrations as MEDA. A different method will have to take place with future, scaled iterations of MOXIE, since the outlets of such systems will likely be tied directly to a compression and storage system as opposed to the ambient environment.

It should also be noted that the sensors can be cross-calibrated during normal MOXIE operations. Several methods exist for determining the amount of oxygen produced, including values of the current, O₂ sensor, and anode pressure. All of these can be used to deduce values for the compositions of the anode and cathode, and therefore are useful as cross-calibration tools.

5.2.3 Characterization

Characterization differs from calibration in that it typically refers to the measurement of properties that capture the general behavior of a component or system, as opposed to the time-dependent individual properties that are measured in calibration. Characterization for MOXIE will be done by conducting a variety of tests in a variety of labs. It will take place before, during, and after the mission, and will be mainly done on the MOXIE engineering model. Characterization is important because it provides knowledge about the safe operating limits for MOXIE. In addition, it allows the team to refine and validate models, and gives insight into how to interpret data from Mars.

A major characterization question for the MOXIE gas composition sensors is whether or not the sensors have cross-sensitivity. For example, will the CO₂ sensor have sensitivity to CO or O₂, since all three have similar IR absorption characteristics? This will be tested in the lab by comparing measurements of a CO₂/CO gas mixture to a CO₂/N₂ mixture. Simply put, if there is a major

difference in how a known concentration of CO₂ is read in a CO environment versus in a N₂ environment, cross-sensitivity likely exists.

Another characterization goal is to determine the response time of the sensors. It is possible that the composition sensors could be used in feedback loops to control parameters like utilization fraction. In order for this to work, it would be necessary to know and characterize the response times of the sensors.

A third - and very important - characterization goal is to learn what amount of aging is expected for the sensors. By operating these units over repeated cycles and pushing them to their end of life, it is possible to determine and characterize the degradation in performance that is experienced by the sensors. These data are not only important for recognizing degradation in the MOXIE system, but are also critical in informing future, scaled versions of MOXIE that will operate continuously for months or years in order to support human missions. If the sensors exhibit significant loss in performance over time, it will be necessary to develop new sensors or provide redundancy on future Mars missions. The consequences of not doing so could be severe and result in scenarios such as rapid degradation of the SOXE from unsafe operating compositions or contaminated propellant that is unsafe to use in a launch vehicle.

5.3 Methods

Prior to running the first experiment in the vacuum chamber, an operating procedure and testing plan were put together, reviewed, and accepted by the MIT MOXIE team.

5.3.1 Standard Operation Procedure

To ensure the chamber is operated consistently and safely, a Standard Operating Procedure (SOP) was written in accordance with MIT policies. The SOP outlines a step-by-step approach to running an experiment with the sensors vacuum chamber. It also includes proper startup and shutdown procedures. Prior to running the first experiment, the SOP was presented to MIT Environment, Health, and Safety (EH&S) employees for their approval. After one revision, it was approved and the chamber was cleared for testing.

The SOP in its entirety is displayed below.

MOXIE Sensors Testing SOP

1. Purpose / Background

The purpose of this Standard Operating Procedure (SOP) is to describe the procedure that shall be followed when operating the MOXIE Sensors Vacuum Chamber in Lab 37-564.

2. Scope

This SOP is intended to inform MIT EHS employees and those operating the MOXIE Vacuum Chamber equipment of the proper procedures to follow when using the equipment in Lab 37-564.

3. Prerequisites

N/A

4. Procedure

Upon Entering the Lab:

1. Ensure hood exhaust is ON
2. Turn LEL meter ON
3. Ensure wall-mounted CO and O₂ sensors are ON
 - a. CO sensor should read below 25 ppm
 - b. O₂ sensor should read between 19.5 % – 23.5 %
4. Leave door open for increased air circulation

To Run an Experiment:

1. Conduct a vacuum system checkout:
 - a. Open valve on lid of vacuum chamber to allow ambient air to flow into the chamber. Keep open for minimum of 10 seconds
 - i. If running a cold temperature trial, use freeze spray on the tip of the thermocouple to cool it
 - b. Close valve on lid
 - c. Tighten clamps around vacuum chamber to secure lid into place
 - d. Plug vacuum pump and vacuum pump controller into wall outlet
 - e. Turn vacuum pump and vacuum pump controller ON
 - f. Ensure all appropriate valves are open and connections are secure to allow air to flow from inside the vacuum chamber through the vacuum pump and into the exhaust vent
 - g. Turn knob on vacuum pump controller to change the pressure setpoint to 500 mbar
 - h. Click “Start” on the vacuum pump controller screen to begin the pumping process
 - i. When chamber reaches 500 mbar, turn ball valve on lid of chamber to isolate the chamber from the rest of the tubing and pumping system
 - j. Allow chamber to sit for one minute, and listen for leaks
 - k. If no leaks are detected, open ball valve on lid of vacuum chamber that was previously closed
 - i. If leaks ARE detected, stop and correct the issue. Then repeat the vacuum system checkout
 - l. Click “Stop” on the vacuum pump controller and allow the chamber to fill back to ambient pressure by bleeding air in through one of the ball valves on top of the chamber
 - m. Vacuum chamber checkout is complete!
2. Fill the Vacuum Chamber with Gas
 - a. Isolate the chamber from the ambient air by closing the appropriate inlet ball valve on top of the chamber
 - b. Open all valves in the pump recirculation line to allow air to flow freely from the chamber and through the recirculation line
 - c. Open the ball and needle valves leading from the gas cylinders that will be used for the experiment to the chamber

- d. Fill the lines leading to the chamber with the appropriate gases by bleeding the regulator valves for a few seconds
 - e. Isolate the chamber from the gas cylinders by closing the appropriate inlet ball valve on top of the chamber. Quickly after, close the regulator valves to stop the bleeding of the gases
 - f. Turn the pump controller dial to a lower value than the desired pressure setpoint for the experimental run
 - g. Click “Start” on the pump controller
 - h. When setpoint is achieved, isolate the chamber from the pumping system by closing the appropriate ball valves on top of the chamber lid
 - i. Open valves for the first applicable gas to flow into the chamber
 - j. Continue to feed gas into the chamber in the appropriate proportions until the chamber reaches atmospheric pressure (1 bar)
 - k. When the chamber reaches atmospheric pressure, stop the flow of gases into the chamber by closing the regulator valves on the gas cylinders
 - l. Close the ball valve on top of the chamber that connects the gas cylinders to the chamber
 - m. Set the vacuum pump controller to the appropriate setpoint for the experiment and click “Start”
 - n. Open the ball valve on top of the chamber that connects the chamber to the vacuum controller
 - o. When the pressure setpoint is reached, click “stop” on the pump controller, and isolate the chamber from the pump by closing the appropriate ball valve on top of the chamber

Note: You should now have an isolated vacuum chamber that is filled with the appropriate ratio of gases and at the appropriate experimental pressure.
 - p. Heat or cool the chamber, using either heating tape or dry ice inside a cooler, to the desired experimental temperature
3. Run an Experiment
 - a. Now that the vacuum chamber is at the right temperature, pressure, and flow rate, it is time to run an experiment on the sensors.
 - b. Begin by plugging in the appropriate wires to the computer
 - c. Open the appropriate LabView VIs and prepare to run
 - d. Turn on the recirculation pump to pull flow through the sensor(s) that is(are) being tested
 - e. Click “Run” on the LabView VI to activate the sensor
 - f. Record data as needed
 - g. Between each pressurization cycle (if stepping up the pressure sequentially), wait 90 seconds for the air to become well mixed.
 4. Adjusting to a New Experiment
 - a. It may be possible to keep the chamber at the same concentration and pressure and vary the temperature to achieve multiple experimental trials with the same gas.

Note: the chamber should start out cooled and should increase in temperature over time, as opposed to vice-versa. The thermocouple responds much faster to heating than it does to cooling.

- b. Similarly, it may be possible to keep the chamber at the same concentration and temperature and lower the pressure sequentially to achieve multiple experimental trials with the same gas.
 - i. Note that the chamber should start out at the highest pressure required and dropped between trials by pulling additional vacuum.
 - c. If the pressure needs to be increased or the gas concentration needs to be changed, then all steps in #2 above will need to be repeated.
5. Shutting Down for the Day
- a. Remove any heating or cooling source from the chamber
 - b. Close all regulator valves from gases that may have been previously feeding the vacuum chamber
 - c. Open the ball valve that separates the chamber from the vacuum pump controller to allow a clear path from the chamber to the vent
 - d. Set the vacuum pump controller to 5 mbar setting and click “Start” to begin the flow from the chamber into the vent
 - e. When the vacuum chamber reaches its setpoint, open the filtered ball valve on top of the chamber lid to allow air to bring the chamber back to atmospheric pressure
 - f. Close the valve and pump the chamber down to 5 mbar once more
 - g. Open the valve to fill the chamber with air and bring it back to atmospheric pressure
 - h. Click “Stop” on the vacuum pump controller and turn off the vacuum pump and vacuum pump controller
 - i. Close the bleeder valve on top of the vacuum chamber lid
 - j. Close the ball valve on top of the vacuum chamber lid that leads to the vacuum pump controller.
 - k. Leave hood exhaust ON
 - l. Close and lock door when leaving the room

Any properly trained student or employee who is cleared to operate the sensors vacuum chamber can use this SOP as a guide for his or her experimental run.

5.3.2 Experimental Testing Plan

With an SOP prepared and approved, it was possible to begin the testing process. In order to do so in an efficient manner, a testing plan was prepared that encompassed a variety of tests for the sensors. The goal of the testing plan was to calibrate and characterize CS1, CS2, and CS3, the 0 – 100% CO, 0 – 5% CO₂, and 0 – 100% CO₂ sensors, respectively. This would be done by taking several readings for each sensor in the chamber across a range of parameters. Ultimately, three variables are planned to be altered in the chamber: composition of gas, pressure of chamber, and temperature of chamber.

The composition of gas inside the chamber can be changed by adding different amounts of each desired gas to the chamber sequentially. If a 50/50 mix of CO and CO₂ at 1 bar is desired, the chamber will be evacuated to near vacuum, filled to 500 mbar pressure with CO, and then filled to 1 bar of pressure with CO₂. Each gas can be added to the chamber independently, so custom mixes of the gases at various pressures are relatively straightforward to obtain. In order to ensure the gases

mix properly in the chamber, the recirculation pump will be turned on to cycle the air within the chamber for a minimum of 90 seconds after each gas addition.

The pressure is the main driving force behind these experiments. Since SmartGas built these sensors for Earth applications, they are meant to be operated at atmospheric pressure, around 1 bar. The engineers at SmartGas are unsure how the sensors will operate at different pressures. MOXIE is expected to run at an average pressure of 0.7 bar but will experience a range of pressures from as low as 0.005 bar at the start of each MOXIE run (Mars ambient pressure) to potentially as high as 1.2 bar (if MOXIE is operated at a higher flow rate than currently planned). Therefore, the motivation for testing these sensors is to compare the concentrations they read at a range of pressures to the known concentrations in the chamber. With all this in mind, the experimental testing plan calls for a range of pressure tests at various compositions from 0.005 bar to 1.2 bar.

The temperature is also a potentially important factor in characterizing the SmartGas sensors. Therefore, it is intended that the chamber will be cooled with dry ice or warmed with heat strips to test under a variety of temperatures. Whether or not these tests will actually take place at MIT, as opposed to JPL, is a decision yet to be made, and is therefore not reflected in the testing plan presented below. It is very likely that they will take place at MIT, either as a redundancy check with JPL or as a stand-alone set of experiments.

With the motivation for altering composition, pressure, and temperature in mind, the experimental plan is shown below. The experimental plan to mimic the cathode-side gas flow in MOXIE is shown in Table 4. The experimental plan to test a mix of CO₂ and N₂ gas in order to check for cross-coupling between the CO and CO₂ sensors is shown in Table 5. Note that all three sensors – CS1, CS2, and CS3 – will be in the chamber collecting data for the majority of these runs.

Table 4: Cathode testing plan; covers a range of compositions and pressures that may be seen by the cathode sensors on MOXIE.

Sensors C&C Test Plan
March 2018

Total Tests	74
--------------------	-----------

CO2 - CO Tests

*Test CO, CO2, and O2 0-100% sensors together

Test #	Test Name	CO2 Concentration	CO Concentration	O2 Concentration	Pressure (bar)	Temperature (C)
1	CO2, P Sweep	100%	0%	0%	0.01	20
2		100%	0%	0%	0.1	20
3		100%	0%	0%	0.2	20
4	V	100%	0%	0%	0.3	20
5		100%	0%	0%	0.4	20
6		100%	0%	0%	0.5	20
7		100%	0%	0%	0.6	20
8		100%	0%	0%	0.7	20
9		100%	0%	0%	0.8	20
10		100%	0%	0%	0.9	20
11		100%	0%	0%	1	20
12		100%	0%	0%	1.1	20
13		100%	0%	0%	1.2	20
14	CO2 [0.2] + CO (add CO in 1/10 bar)	100%	0%	0%	0.2	20
15		67%	33%	0%	0.3	20
16		50%	50%	0%	0.4	20
17	V	40%	60%	0%	0.5	20
18		33%	67%	0%	0.6	20
19		29%	71%	0%	0.7	20
20		25%	75%	0%	0.8	20
21		22%	78%	0%	0.9	20
22		20%	80%	0%	1	20
23	CO2 [0.4] + CO (add CO in 1/10 bar)	100%	0%	0%	0.4	20
24		80%	20%	0%	0.5	20
25		67%	33%	0%	0.6	20
26	V	57%	43%	0%	0.7	20
27		50%	50%	0%	0.8	20
28		44%	56%	0%	0.9	20
29		40%	60%	0%	1	20
30	CO2 [0.6] + CO (add CO in 1/10 bar)	100%	0%	0%	0.6	20
31		86%	14%	0%	0.7	20
32		75%	25%	0%	0.8	20
33	V	67%	33%	0%	0.9	20
34		60%	40%	0%	1	20
35	CO2 [0.8] + CO (add CO in 1/10 bar)	100%	0%	0%	0.8	20
36		89%	11%	0%	0.9	20
37		80%	20%	0%	1	20
38	CO, P Sweep	0%	100%	0%	0.01	20
39		0%	100%	0%	0.1	20
40		0%	100%	0%	0.2	20
41	V	0%	100%	0%	0.3	20
42		0%	100%	0%	0.4	20
43		0%	100%	0%	0.5	20
44		0%	100%	0%	0.6	20
45		0%	100%	0%	0.7	20
46		0%	100%	0%	0.8	20
47		0%	100%	0%	0.9	20
48		0%	100%	0%	1	20
49		0%	100%	0%	1.1	20
50		0%	100%	0%	1.2	20
Range Covered		0-100%	0-100%	0%	0.01-1.2 bar	20 C

Table 5: CO₂ and N₂ mix tests that will provide a control that enables the quantification cross-talk between CO and CO₂

CO₂ - N₂ Tests

Test #	Test Name	CO ₂ Concentration	N ₂ Concentration	O ₂ Concentration	Pressure (bar)	Temperature (C)
1	CO ₂ [0.2] + N ₂ (add N ₂ in 1/10 bar)	100%	0%	0%	0.2	20
2		67%	33%	0%	0.3	20
3		50%	50%	0%	0.4	20
4	V	40%	60%	0%	0.5	20
5		33%	67%	0%	0.6	20
6		29%	71%	0%	0.7	20
7		25%	75%	0%	0.8	20
8		22%	78%	0%	0.9	20
9		20%	80%	0%	1	20
10	CO ₂ [0.4] + N ₂ (add N ₂ in 1/10 bar)	100%	0%	0%	0.4	20
11		80%	20%	0%	0.5	20
12		67%	33%	0%	0.6	20
13	V	57%	43%	0%	0.7	20
14		50%	50%	0%	0.8	20
15		44%	56%	0%	0.9	20
16		40%	60%	0%	1	20
17	CO ₂ [0.6] + N ₂ (add N ₂ in 1/10 bar)	100%	0%	0%	0.6	20
18		86%	14%	0%	0.7	20
19		75%	25%	0%	0.8	20
20	V	67%	33%	0%	0.9	20
21		60%	40%	0%	1	20
22	CO ₂ [0.8] + N ₂ (add N ₂ in 1/10 bar)	100%	0%	0%	0.8	20
23		89%	11%	0%	0.9	20
24		80%	20%	0%	1	20
Range Covered		0-100%	0-100%	0%	0.01-1 bar	20 C

As a clarification, the purpose of running the same compositions of CO₂ + CO as CO₂ + N₂, as seen by comparing Table 4 with Table 5, is to enable the quantification of cross-talk between the CO₂ and CO sensors. Earlier in this thesis, it was shown how a CO sensor could “detect” CO in a pure CO₂ stream by giving a false positive. The opposite is true with a CO₂ sensor “detecting” CO₂ in a pure CO stream. By taking readings of various compositions of CO₂ + CO and then repeating them with the same compositions of CO₂ + N₂, it will be possible to compare the data and determine the extent of crosstalk at various pressures and compositions.

5.4 Path Forward

As of May, 2018, the experiments have commenced. However, the data will not be fully captured or analyzed prior to the submission of this thesis and therefore will not be included; they will be saved for the Ph.D. dissertation. It is expected that all of the tests requiring only CO₂ or CO₂ with N₂ will be completed in the next month. Those requiring CO will be completed during the coming fall semester, as there is a very long lead time on CO gas cylinders and they will not arrive before the summer. Once completed, it is possible that the team will begin designing test procedures to test the oxygen sensor on MOXIE. Additionally, it is likely that the team will begin running tests at different temperatures to determine a temperature dependence correction factor for the sensors.

References

- [1] Howell, E. (2012). First Spacecraft to Mars. Retrieved from <https://www.space.com/18787-mariner-4.html>
- [2] Blasius, K. R., Cutts, J. A., Guest, J. E., & Masursky, H. (1977). Geology of the Valles Marineris: First analysis of imaging from the Viking 1 Orbiter Primary Mission. *Journal of Geophysical Research* 82(28) 4067-4091. <https://agupubs.onlinelibrary.wiley.com/doi/full/10.1029/JS082i028p04067>
- [3] Smith, P. H., Tamppari, L. K., Arvidson, R. E., Bass, D., Blaney, D., Boynton, W. V...Zent, A. P. (2009). H₂O at the Phoenix Landing Site. *Science*, 325(5936) 58-61. <http://science.sciencemag.org/content/325/5936/58>
- [4] Squyres, S. W., Knoll, A. H., Arvidson, R. E., Clark, B. C., Grotzinger, J. P., Jolliff, B. L...Yen, A. S. (2006). Two Years at Meridiani Planum: Results from the Opportunity Rover. *Science*, 313(5792) 1403-1407. <http://science.sciencemag.org/content/313/5792/1403>
- [5] Webster, C. R., Mahaffy, P. R., Atreya, S. K., Flesch, G. J., Mischna, M. A., Meslin, P...Lemmon, M. T. (2015). Mars methane detection and variability at Gale crater. *Science*, 347(6220) 415-417. <http://science.sciencemag.org/content/347/6220/415.full>
- [6] Williams, R. M., Grotzinger, J. P., Dietrich, W. E., Gupta, S., Sumner, D. Y., Wiens, R. C...Deen, R. G. (2013). Martian Fluvial Conglomerates at Gale Crater. *Science* 340(6136) 1068-1072. <http://science.sciencemag.org/content/340/6136/1068.full>
- [7] Ming, D. W., Archer, P. D., Glavin, D. P., Eigenbrode, J. L., Franz, H. B., Sutter, B...Yingst, R. A. (2014). Volatile and Organic Compositions of Sedimentary Rocks in Yellowknife Bay, Gale Crater, Mars. *Science* 343(6169). <http://science.sciencemag.org/content/343/6169/1245267.full>
- [8] Williams, D. R. (2018). Viking Mission to Mars. Retrieved from <https://nssdc.gsfc.nasa.gov/planetary/viking.html>
- [9] Ash, R. L., Dowler, W. L., & Varsi, G. (1978). Feasibility of rocket propellant production on Mars. *Acta Astronautica* 5(9) 705-724. <http://www.sciencedirect.com/science/article/pii/0094576578900498>
- [10] Hill, P.G. & Peterson, C. R. (1965). *Mechanics and thermodynamics of propulsion*. https://books.google.com/books/about/Mechanics_and_thermodynamics_of_propulsi.html?id=gHITAAAAMAAJ
- [11] Falcon 9 & Falcon Heavy. (2017). Retrieved from <http://www.spaceflightinsider.com/hangar/falcon/>
- [12] Romohalli, K., Lawton, Emil., & Ash, R. (1989). Recent Concepts in Missions to Mars: Extraterrestrial Processes. *Journal of Propulsion and Power* 5(2) 181-187. <https://arc.aiaa.org/doi/pdfplus/10.2514/3.23134>
- [13] Zubrin, R. (1996). *The Case for Mars*. New York City, NY: Simon & Schuster. Pages 16, 157, 165.
- [14] Ashe et al.
- [15] O'Brien, J. E., Stoots, C. M., Herring, J. S., & Hawkes, G. L. (2006). Hydrogen Production from Nuclear Energy via High Temperature Electrolysis. *The 1st Energy Center Hydrogen*

Initiative Symposium, Purdue University.

https://digital.library.unt.edu/ark:/67531/metadc877829/m2/1/high_res_d/911703.pdf

- [16] Chromium alloys – Chromium. (2017). Retrieved from <https://www.plansee.com/en/materials/chromium.html>
- [17] Meyen, F. (2017). *System Modeling, Design, and Control of the Mars Oxygen In-Situ Resource Utilization Experiment (MOXIE) and Implications for Atmospheric ISRU Processing Plants*. Diss. Massachusetts Institute of Technology. Pages 139-140.
- [18] Hua, J., and A. Aboobaker (2017). SOXE Thermal Constants, NASA Jet Propulsion Laboratory.
- [19] Aboobaker, A. (2017). SOXE Cell Temperature Testing, NASA Jet Propulsion Laboratory.
- [20] Aboobaker, A. (2016). SOXE Thermal Testing, NASA Jet Propulsion Laboratory.
- [21] Digi-Key Electronics. (2018). Retrieved from <https://www.digikey.com/products/en?keywords=1-1776293-2-ND>
- [22] Nissen, J. (2018). Gas Sensor Calibration, NASA Jet Propulsion Laboratory.